| | |
|---|---|
| Title | Study on the Turbulent Shear Flow Past a Circular Cylinder |
| Author(s) | Kiya, Masaru |
| Citation | 北海道大學工學部研究報告, 50, 1-101 |
| Issue Date | 1968-12-20 |
| Doc URL | https://hdl.handle.net/2115/40903 |
| Type | departmental bulletin paper |
| File Information | 50_1-102.pdf |

# Study on the Turbulent Shear Flow Past a Circular Cylinder[*]

Masaru KIYA[**]

(Received August 31, 1968)

## Abstract

A two-dimensional flow past a circular cylinder placed in a turbulent boundary layer was described, with special reference to the lift and drag forces acting on the cylinder. A theoretical analysis of the flow was made for the hypothetical inviscid shear flow with a linearly varying velocity profile, and experiments were performed with a circular cylinder placed in an artificially produced shear flow and in a turbulent boundary layer, respectively.

An explicit solution for the stream function that describes a uniform shear flow past a circular cylinder subjected to an interference of a plane wall was obtained. It was found from detailed numerical calculations that stagnation pressure decreases as the distance between the cylinder and the plane wall decreases, while in the case of uniform flow the stagnation pressure coefficient remains in unity. The lift force acting on the cylinder calculated by numerically integrating the pressure on the surface of the cylinder was found to be positive when there exists a certain amount of velocity gadient in the transverse direction of flow, which is similar to the case of a practical boundary layer that develops along a stationary boundary wall.

From the experiment performed in a uniform shear flow artificially produced by arranging a grid of rods in a wind tunnel, it was verified that an acceptable agreement between the theory and the experiment was found concerning the stagnation pressure and the position of stagnation point, respectively, provided that the clearance between the cylinder and the plane wall is not too small. It was also found that the experimental value of lift coefficient increases as the cylinder approaches the boundary wall, as qualitatively predicted by the theory.

The pressure distribution on the surface of the cylinder placed in an artificially thickened turbulent boundary layer of 60 mm in thickness was measured and was found to be integrated in the evaluation of the lift and drag forces. It was found that the drag and lift coefficients plotted against the ratio $\Delta/(2a)$, where $\Delta$ is the clearance between the cylinder and the boundary wall and $a$ is the radius of the cylinder, were represented respectively by a single curve within an acceptable experimental error, the Reynolds number being in a range of $(0.99\text{–}3.78)\times 10^4$. With $\Delta/(2a)$ decreasing, the lift coefficient was found to increase monotonically from zero to the maximum

---

[*] Some parts of this paper were presented at the Japan-U.S. Seminar on Similitude in Fluid Mechanics at the Iowa Institute of Hydraulics Research, University of Iowa, Iowa City on September 25, 1967.

[**] Fluid Mechanics I, Department of Mechanical Engineering.

value of about 0.8 at $\Delta/(2a)=0$, and on the contrary the drag coefficient decreases from 1.2 to the minimum value of 0.95 after passing the maximum value of about 1.3 in the vicinity of $\Delta/(2a)=0.16$.

Thin circular cylinders were placed in the same turbulent boundary layer 30 mm apart from the boundary wall to measure the variations of mean velocity, turbulence and the static pressure in the wake. A complex interaction between the turbulence in the boundary layer and that generated in the wake was suggested. A drag coefficient computed from the momentum principle was found, within the limit of experimental errors, to be the same as that of a cylinder placed in an unbounded uniform flow. This fact suggests that the normal velocity gradient of the boundary layer exerts little effect on the drag coefficient of a thin circular cylinder, when the cylinder is not in the immediate vicinity of the boundary wall. It also becomes evident that the spread of the wake is greater towards the side of the smaller velocity than on the side of the larger one.

These experimental results were satisfactorily interpreted by the theoretical analysis that assumes the approaching flow of a constant vertical velocity gradient.

## Contents

Appendix

## List of symbols

| | |
|---|---|
| $a$ . . . . . . | radius of cylinder |
| $g$ . . . . . . | acceleration of gravity |
| $h$ . . . . . . | height of air-tunnel |
| $h_1$ . . . . . . | distance between $x$-axis and the center of cylinder |
| $i$ . . . . . . | imaginary unit |
| $p$ . . . . . . | pressure, $k\pi$ |
| $\bar{p}$ . . . . . . | mean pressure |
| $p'$ . . . . . . | fluctuating pressure |
| $q_1$ . . . . . . | velocity-defect |
| $q_2$ . . . . . . | $U_2$ |
| $r, \theta$ . . . . . | polar coordinates |
| $s$ . . . . . . | complex plane |

| | |
|---|---|
| $t$ | time |
| $u, v, w$ | velocity components in the $x$, $y$ and $z$ direction, respectively |
| $u', v', w'$ | fluctuating components of velocity |
| $u_\tau$ | shear velocity |
| $x, y, z$ | cartesian coordinates |
| $x_c, y_c$ | coordinates of the center of cylinder |
| $z$ | complex plane |
| $A$ | $C_D/\sqrt{4\pi\varepsilon_0}$ |
| $C_p$ | pressure coefficient |
| $C_D$ | drag coefficient |
| $C_L$ | lift coefficient |
| $D$ | drag force |
| $H$ | shape factor |
| $K$ | shape parameter |
| $L$ | lift force |
| $M_s$ | torque |
| $R_e, R$ | Reynolds number |
| $R_\delta, R_{\delta^*}, R_\theta$ | Reynolds number |
| $R_{12}$ | correlation coefficient |
| $U_0$ | approaching velocity at the center of cylinder |
| $U$ | velocity at the edge of laminar boundary layer |
| $U_\infty$ | velocity at the edge of turbulent boundary layer |
| $W$ | complex flow potential |
| $Z$ | shape factor |
| $\gamma$ | specific gravity of air |
| $\delta$ | boundary layer thickness |
| $\delta^*$ | displacement thickness of boundary layer |
| $\varepsilon$ | nondimensional velocity gradient, eddy viscosity |
| $\zeta$ | vorticity |
| $\eta$ | $y\sqrt{\bar{u}_1/\nu}$ , $\xi_2/\sqrt{\xi_1}$ |
| $\lambda$ | $\varepsilon \cosh \alpha$, $\omega d/U_0$ |
| $\mu$ | dynamic viscosity |
| $\nu$ | kinematic viscosity |
| $\rho$ | density of air |
| $\tau_w$ | viscous shear stress at the wall |
| $\tau_0$ | viscous shear stress on the cylinder |
| $\phi$ | velocity potential |
| $\psi$ | stream function |
| $\omega$ | transverse velocity gradient of approaching flow |
| $\Delta$ | clearance between the cylinder and the boundary wall |
| $\Theta$ | angle |
| $\Psi$ | stream function |
| $\Im$ | imaginary part |
| $\Re$ | real part |

## 1. Introduction

The uniform flow of fluid around a body submerged in it has long been a problem in fluid mechanics. Especially the prediction of the drag and lift forces acting on the body concerned is of great importance for practical purposes, and a considerable amount of effort has been devoted on this subject.

However, there are many examples in practice where a parallel flow of fluid is non-uniform to the extent that the velocity of the stream parallel to the flow varies in magnitude according to the position measured transversely to the stream. Such a flow exhibits shear characteristics, a typical example being the flow in the presence of a plane boundary where the velocity increases with the distance from the boundary. Other examples of shear flow appear in the wake of a body, in jets and in the free mixing layer of two streams with different velocities.

In developing the theory of shear flow, an undisturbed velocity profile must be desribed at first. Since actual shear flows usually have a somewhat complex velocity profiles, some simplifications are necessary in order to make the problem analytically tractable. One of the simplest models for the general shear flow may be an inviscid uniform shear flow in which the velocity increases linearly in a transverse direction to the stream of a non-viscous fluid. Most theoretical studies fall under this category.

This paper describes theoretical and experimental investigations on the flow about a circular cylinder placed in a turbulent boundary layer. The plane boundary wall placed near the cylinder parallel to the undisturbed stream out of necessity comes into the question. The flow fields near the surface and in the far wake of the cylinder are considered by analytical and experimental means, hence it becomes possible to determine the lift and drag forces and the moment acting on the cylinder concerned.

The knowledge of the lift and drag forces experienced by a body or bodies located in a shear flow is believed to be indispensable when the behavior of particles in it is treated, a practical example being the transportotion of small particles through a pipe by means of air or water flow. The experimental study (Welschof [1]) concerning the flow of air containing numerous solid particles shows clearly the existence of a region of large transverse velocity gradient.

On the other hand, the diffusion process in the turbulent shear flow is an important phenomenon in air polution by smoke and in chemical engineering, and several investigations have been performed in these fields. Skramstad [2] measured the temperature distribution behind a heated thin wire placed in a turbulent boundary layer. Corrin & Uberoi [3] and Hinze & van der Hegge Zijnen [4] made the same kind of measurement in the turbulent mixing zone of a round free jet and a plane free jet, respectively. They obtained an interesting result in which the diffusion of heat energy is greater towards the side of a larger velocity than on the side of the smaller one, while the spread of wake of a body placed in a turbulent boundary layer may be greater towards the side of smaller velocity, as will be shown in section 5 of Chapter 5.

The natural wind near the ground has a comparatively large vertical velocity gradient up to a height of a few hundred meters. The wings of an aircraft which takes off into the wind will then be affected by the existing shear in the approaching stream. The effect of shear must also be considered on the aerodynamic forces experienced by the high architechtural structures, such as skyscrapers, towers, stacks, etc. Some theoretical investigations of this category have so far been made by several authors. V. Sanden [5] obtained a numerical solution of shear flow past a wedge-shaped airfoil. Tsien [6] determined analytically the flow field around a two-dimensional symmetrical Joukowsky airfoil placed in a uniform shear flow, the velocity increasing linearly in the transverse direction to the stream. He clarifed the effect of shear on the aerodynamic properties of the airfoil concerned, by obtaining the lift force and the moment acting on it. Jones [7] studied the characteristics of thin airfoils placed in a slightly parabolic shear flow. More recently, Kotansky [8] made an experimental study on an airfoil placed in an artificially produced shear flow. The analytical treatment given in Chapter 2 of this paper will give a clue for the determination of the combined effect of both the shear and the neighboring ground on the aerodynamic characteristics of the airfoils.

In conjunction with the measurements of velocity distribution in the turbulent shear flows, several efforts have been made to obtain the so-called Pitot tube displacement effect. Arie [9] showed that a considerable amount of correction of the velocity profile might be necessary when measurements are performed in a shear flow by means of a circular Pitot tube, describing how the location of the stagnation point and the stagnation pressure would be shifted by the presence of a uniform shear in the approaching flow. A three dimensional version of this study was made by Hall [10] and Lighthill [11], concerning a sphere in a uniform shear flow. Young & Maas [12] and Davies [13] performed some experimental studies on this subject.

The dynamics of small particles suspended in a slow shear flow is of great importance, for example, in chemical engineering. The behavior of red corpuscles in blood may be another example. Bretherton [14], Saffman [15] and Kiya [16] obtained a theoretical formulae for the drag and lift forces exerted on a circular cylinder and a sphere, respectively, placed in a uniform shear flow. Segre & Silberberg [17] made extensive experimental investigations on the concentration distribution of small particles suspended in a pipe Poiseuille flow. Eichhorn & Small [18] determined experimentally the lift force acting on a sphere under the same flow condition.

In Chapter 2 of this paper, an inviscid uniform shear flow about a circular cylinder placed near an infinite boundary plane is treated analytically. The comparisons of the theory with experiment are described in Chapter 3, confirming that the cylider is subjected to a lift force which tends to move the cylinder away from the boundary plane.

Chapter 4 is the description of the experimental investigations of the flow near the surface of the circular cylinder placed in the turbulent boundary layer that develops along the tunnel wall. The lift and drag forces acting on the cylinder are obtained from the pressure distribution as the functions of the spacing between the cylinder and the boundary wall. The laminar boundary layers on the cylinder surface are computed in detail by means of the Pohlhausen-Walz method, which permits an estimation of the viscous correction to the lift and drag forces. Some remarks on the comparison between the theory and the experiment are given.

The flow in the far wake of the cylinder placed in a turbulent boundary layer is described in Chapter 5. Measurements of the mean velocity, the turbulence intensities and the Reynolds stress are made. The theoretical derivation of the velocity profile in the wake of the cylinder in a uniform shear flow was performed with the object of interpreting the experimental results. The theoretical results show that the effect of shear on the drag coefficient of the cylinder is of a higher order of magnitude than the first power of the shear and this fact is confirmed by the experimental results.

## 2. Simple Shear Flow past a Circular Cylinder Subjected to an Interference of a Plane Wall

In this chapter, a simple shear flow about a circular cylinder is described analytically, together with the interference of a neighbouring bounday plane. This may be the simplified model of the flow across a circular cylinder placed in a turbulent byundary layer. A steady flow of an inviscid and incompressible fluid is assumed throughout.

The analytical method thus developed can also be applied to the analysis of shear flow across two cylinders, and the results coincide with the solutions given by Lagally [19] and Müller [20] when the oncoming flow is uniform. A proper technique of conformal transformation of a circle near a plane boundary may give a clue to the analysis of the flow across an airfoil in the vicinity of a ground surface, and the flow pattern around the cylinder would reveal an aspect of the limit of the workability of a Pitot-cylinder in the vicinity of a stationary boundary frequently encountered in the measurement of a two-dimensional shear flow. Furthermore, the lift force of a cylinder in shear flow exerted by the existence of a boundary should not be overlooked in the practical engineering of an efficient hydraulic and pneumatic transportation of matters.

### 2.1 Stream Function

It is widely known that the straight lines $\xi=$ a constant and $\eta=$ a constant on a $s$-plane correspond to the two families of circles that intersect at right angles with each other on a $z$-plane when the relation

$$s=i\log_e\frac{z+ic}{z-ic} \tag{2. 1}$$

exists between $z$ and $s$-planes, where $s=\xi+i\eta$ and $z=x+iy$. If $\eta$ is designated to have a constant positive value of $\alpha$, the equation of the circle on the $z$-plane that corresponds to $\eta=\alpha(>0)$ becomes

$$x^2+(y-c\coth\alpha)^2=(c/\sinh\alpha)^2 \tag{2. 2}$$

The radius of this circle $a$ and the distance between its center and $x$-axis $h_1$ are respectively

$$a=c/\sinh\alpha\,,\qquad h_1=c\coth\alpha \tag{2. 3}$$

In the same manner, the straight line $\eta=-\beta(\beta>0)$ on the $s$-plane gives

$$x^2+(y+c\coth\beta)^2=(c/\sinh\beta)^2 \tag{2. 4}$$

$$b=c/\sinh\beta\,,\qquad h_2=c\coth\beta \tag{2. 5}$$

on the $z$-plane. Further, $x$ and $y$ can be written in the following forms in terms of $\xi$ and $\eta$ by means of Eq. (2. 1):

$$x=\frac{-c\sin\xi}{\cosh\eta-\cos\xi} \tag{2. 6 a}$$

$$y=\frac{c\sinh\eta}{\cosh\eta-\cos\xi} \tag{2. 6 b}$$

Therefore, it can be seen that the $x$-axis on the $z$-plane corresponds to the straight line $\eta=0$ on the $s$-plane, and the origin on the $s$-plane goes to the point at infinity on the $z$-plane. The two circles on the $z$-plane given by Eqs. (2. 2) and (2. 4) are shown in Fig. 2. 1.

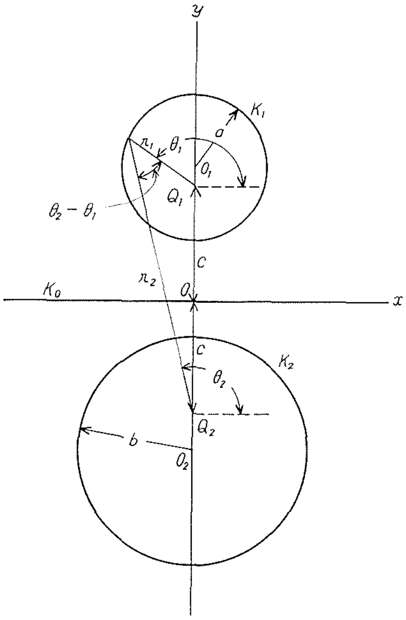

**Fig. 2. 1.** Definition sketch of two circular cylinders.

When the oncoming flow has a constant velocity gradient, the velocity distribution of the approaching flow sufficiently upstream of the cylinder can be expressed by

$$u_\infty=u_0+\omega y\,,\qquad v_\infty=0 \tag{2. 7}$$

Then, the stream function to describe the undisturbed flow field must be

$$\psi_\infty=\int u_\infty dy=u_0 y+\frac{\omega y^2}{2} \tag{2. 8}$$

Any arbitrary constant may of course be added as a constant of integration to the right-hand side of Eq. (2. 8), but this constant may be made zero without missing the generality of the present consideration, because it simply indicates the relative level of the stream functions. The vorticity included in the present flow field can easily be obtained from Eq. (2. 7):

$$\zeta_\infty=\frac{\partial v_\infty}{\partial x}-\frac{\partial u_\infty}{\partial y}=-\omega \tag{2. 9}$$

So for as a two-dimensional uniform shear flow of an inviscid fluid is assumed, the vorticity given by this equation must be constant everywhere in the flow field now considered. When the stream function $\psi$ at any point in the flow field is written, for convenience, as

$$\begin{aligned}\psi &= \psi_\infty + \Psi_0 + \Psi_1 \\ &= (u_0 y + \Psi_0) + \left(\frac{\omega y^2}{2} + \Psi_1\right)\end{aligned} \tag{2. 10}$$

the velocity components and the vorticity at this point are respectively

$$u = \frac{\partial \psi}{\partial y}, \qquad v = -\frac{\partial \psi}{\partial x} \tag{2. 11}$$

$$\zeta = \frac{\partial v}{\partial x} - \frac{\partial u}{\partial y} = -\left(\frac{\partial^2 \psi}{\partial x^2} + \frac{\partial^2 \psi}{\partial y^2}\right) \tag{2. 12}$$

Since $\zeta = \zeta_\infty \equiv -\omega$ (a constant), one can obtain the following relation by substituting Eq. (2. 10) into Eq. (2. 12):

$$\left(\frac{\partial^2 \Psi_0}{\partial x^2} + \frac{\partial^2 \Psi_0}{\partial y^2}\right) + \left(\frac{\partial^2 \Psi_1}{\partial x^2} + \frac{\partial^2 \Psi_1}{\partial y^2}\right) = 0 \tag{2. 13}$$

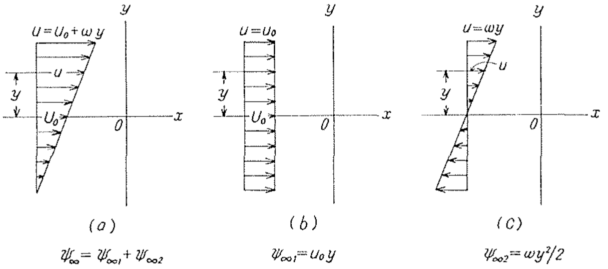

**Fig. 2. 2.** Configuration of shear flow across a circular cylinder.

Fig. 2. 2 shows a schematic physical view of the flow field expressed by Eq. (2. 10). Fig. 2. 2 (b) is the case of the first term in the right-hand side of Eq. (2. 10), which is the case of a uniform flow across a circle. Fig. 2. 2 (c) indicates, in the same manner, a pure shear flow across a circle to be introduced by the second term of Eq. (2. 10). These two cases of flow can be superposed to realize the flow field of a shear flow across a circle shown in Fig. 2. 2 (a) which is the case to be solved. Therefore, the relation of Eq. (2. 13) that was deirved by substituting Eq. (2. 10) into Eq. (2. 12) leads to the Laplace equations:

$$\frac{\partial^2 \Psi_0}{\partial x^2} + \frac{\partial^2 \Psi_0}{\partial y^2} = 0 \tag{2. 14}$$

$$\frac{\partial^2 \Psi_1}{\partial x^2} + \frac{\partial^2 \Psi_1}{\partial y^2} = 0 \tag{2. 15}$$

that can be solved independently for superposition. A definition sketch of a two-dimensional shear flow across a cylinder in the vicinity of a plane wall is shown in Fig. 2.3. The boundary conditions to be introduced in this case are:

(i) When $z \to \infty$, namely when $s \to 0$,

$$\Psi_0 \to 0 \qquad (2.16\,\mathrm{a})$$

$$\Psi_1 \to 0 \qquad (2.16\,\mathrm{b})$$

because there should be no effect of the cylinder there.

(ii) When $\eta = \alpha$, namely on the surface of the cylinder,

$$\Psi_0 = -u_0[y]_{\eta=\alpha} + \gamma_0 = -\frac{u_0 c \sinh\alpha}{\cosh\alpha - \cos\xi} + \gamma_0 \qquad (2.17\,\mathrm{a})$$

$$\Psi_1 = -\frac{\omega}{2}[y]^2_{\eta=\alpha} + \gamma_1 = -\frac{\omega c^2}{2}\left(\frac{\sinh\alpha}{\cosh\alpha - \cos\xi}\right)^2 + \gamma_1 \qquad (2.17\,\mathrm{b})$$

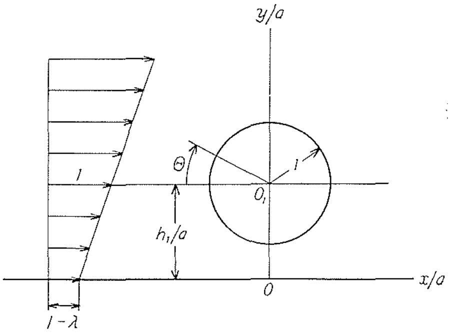

**Fig. 2. 3.** Definition sketch of shear flow across a cylinder in the vicinity of a plane wall.

(iii) When $\eta = 0$, namely along $x$-axis in the $z$-plane that corresponds to the plane wall, there should be no effect of the cylinder on the stream function, because the wall is a solid boundary:

$$\Psi_0 = 0 \qquad (2.18\,\mathrm{a})$$

$$\Psi_1 = 0 \qquad (2.18\,\mathrm{b})$$

$\gamma_0$ and $\gamma_1$ in Eqs. (2.17 a) and (2.17 b) are respectively the values of stream functions that form a cylinder in shear flow and pure shear flow. The terms $[y]_{\eta=\alpha}$ and $[y]^2_{\eta=\alpha}$ can be expanded in Fourier series:

$$[y]_{\eta=\alpha} = c\left[1 + 2\sum_{n=1}^{\infty} e^{-n\alpha}\cos n\xi\right] \qquad (2.19\,\mathrm{a})$$

$$[y]^2_{\eta=\alpha} = c^2\left[\coth\alpha + 2\sum_{n=1}^{\infty} e^{-n\alpha}(\coth\alpha + n)\cos n\xi\right] \qquad (2.19\,\mathrm{b})$$

The boundary conditions given by Eqs. (2.16) and (2.18) and the Fourier series expansions of $[y]_{\eta=\alpha}$ and $[y]^2_{\eta=\alpha}$ suggest a transformation of the independent variables $x$, $y$ to $\xi$, $\eta$ in Eqs. (2.14) and (2.15). From the general theory of the curvilinear orthogonal coordinates, we have the relation

$$\frac{\partial^2\phi}{\partial x^2} + \frac{\partial^2\phi}{\partial y^2} = \frac{1}{g_1 g_2}\left[\frac{\partial}{\partial\xi}\left(\frac{g_2}{g_1}\frac{\partial\phi}{\partial\xi}\right) + \frac{\partial}{\partial\eta}\left(\frac{g_1}{g_2}\frac{\partial\phi}{\partial\eta}\right)\right] \qquad (2.19\,\mathrm{c})$$

where $\phi$ is an arbitrary continuous function and

$$g_1 = \left[\left(\frac{\partial x}{\partial\xi}\right)^2 + \left(\frac{\partial y}{\partial\xi}\right)^2\right]^{\frac{1}{2}}, \qquad g_2 = \left[\left(\frac{\partial x}{\partial\eta}\right)^2 + \left(\frac{\partial y}{\partial\eta}\right)^2\right]^{\frac{1}{2}} \qquad (2.19\,\mathrm{d})$$

Substitution of Eqs. (2.6) into Eqs. (2.19 c) and (2.19 d) gives

$$g_1 = g_2 = \frac{c}{\cosh\eta - \cos\xi}$$

$$\frac{\partial^2\phi}{\partial x^2} + \frac{\partial^2\phi}{\partial y^2} = \frac{(\cosh\eta - \cos\xi)^2}{c^2}\left(\frac{\partial^2\phi}{\partial\xi^2} + \frac{\partial^2\phi}{\partial\eta^2}\right)$$

Accordingly, the governing equations (2. 14) and (2. 15) take the form

$$\frac{\partial^2\Psi_0}{\partial\xi^2} + \frac{\partial^2\Psi_0}{\partial\eta^2} = 0 \tag{2. 14 a}$$

$$\frac{\partial^2\Psi_1}{\partial\xi^2} + \frac{\partial^2\Psi_1}{\partial\eta^2} = 0 \tag{2. 15 a}$$

which are again the Laplace equations.

The general solution of Eq. (2. 14 a) can be written by the technique of separation of variables:

$$\begin{aligned}\Psi_0 = A_0 + \sum_{n=1}^{\infty} (&A_n \cosh n\eta \cos n\xi + B_n \sinh n\eta \cos n\xi \\ &+ C_n \cosh n\eta \sin n\xi + D_n \sinh n\eta \sin n\xi)\end{aligned} \tag{2. 20}$$

The solution for $\Psi_1$, to be obtained from Eq. (2. 15 a), also takes the same form. When the boundary condition on the surface of the cylinder given by Eq. (2. 17 a) and the relation given by Eq. (2. 19 a) are inspected, it will easily be seen that $\xi$ is contained in Eqs. (2. 19) in the form of $\cos n\xi$. Therefore, the comparison between Eqs. (2. 17 a) and (2. 20) gives

$$C_n = 0\,, \qquad D_n = 0 \qquad\qquad (n = 1, 2, 3, \cdots) \tag{2. 21}$$

Further, when the boundary condition of $\Psi_0 = 0$ at $\eta = 0$ given by Eq. (2. 18 a) is substituted into Eq. (2.20) together with Eq. (2. 21), one obtains

$$A_0 + \sum_{n=1}^{\infty} A_n \cos n\xi = 0$$

Namely,

$$A_0 = 0\,, \qquad A_n = 0 \qquad\qquad (n = 1, 2, 3, \cdots) \tag{2. 22}$$

Then, on the surface of the cylinder ($\eta = \alpha$) the equation of $\Psi_0$ given by Eq. (2. 20) becomes

$$\Psi_0 = \sum_{n=1}^{\infty} B_n \sinh n\alpha \cos n\xi \tag{2. 23}$$

On the other hand, the condition given by Eq. (2. 17 a) is

$$\Psi_0 = -u_0 c\left[1 + 2\sum_{n=1}^{\infty} e^{-n\alpha} \cos n\xi\right] + \gamma_0 \tag{2. 24}$$

when Eq. (2. 19 a) is introduced. Therefore, the comparison of coefficients in Eqs. (2. 23) and (2. 24) gives

$$\gamma_0 = u_0 c\,, \qquad B_n = -\frac{4u_0 c}{e^{2n\alpha} - 1} \tag{2. 25}$$

Now, the stream function $\Psi_0$ given by Eq. (2. 20) is reduced to the following form when all of the values of coefficients thus determined by Eqs. (2. 21), (2. 22) and (2. 25) are substituted:

$$\Psi_0 = -4u_0 c \sum_{n=1}^{\infty} \frac{\sinh n\eta \cos n\xi}{e^{2n\alpha}-1} \tag{2. 26}$$

In the same manner as $\Psi_0$, $\Psi_1$ can be written as

$$\begin{aligned}\Psi_1 = A_0' + \sum_{n=1}^{\infty} (A_n' \cosh n\eta \cos n\xi + B_n' \sinh n\eta \cos n\xi \\ + C_n' \cosh n\eta \sin n\xi + D_n' \sinh n\eta \sin n\xi)\end{aligned} \tag{2. 27}$$

and the boundary conditions given by Eqs. (2. 16 b), (2. 17 b) and (2. 18 b) determine the values of coefficients:

$$A_0' = 0\,, \quad A_n' = 0\,, \quad C_n' = 0\,, \quad D_n' = 0\,, \quad \Gamma_1 = \frac{\omega c^2}{2} \coth \alpha\,, \tag{2. 28 a}$$

$$B_n' = -2\omega c^2 \frac{\coth \alpha + n}{e^{2n\alpha}-1} \tag{2. 28 b}$$

Therefore, Eq. (27) becomes

$$\Psi_1 = -2\omega c^2 \sum_{n=1}^{\infty} \frac{\coth \alpha + n}{e^{2n\alpha}-1} \sinh n\eta \cos n\xi \tag{2. 29}$$

As a result, the stream function given by Eq. (2. 10) to describe the flow field around a cylinder in the vicinity of a plane wall could be determined:

$$\begin{aligned}\phi &= (u_0 y + \Psi_0) + \left(\frac{\omega y^2}{2} + \Psi_1\right) \\ &= u_0 c \phi^{(0)} + \frac{\omega c^2}{2} \phi^{(1)}\end{aligned} \tag{2. 30}$$

where the symbols $\phi^{(0)}$ and $\phi^{(1)}$ are respectively

$$\phi^{(0)} = \left(\frac{\sinh \eta}{\cosh \eta - \cos \xi}\right) - 4\sum_{n=1}^{\infty} \frac{\sinh n\eta}{e^{2n\alpha}-1} \cos n\xi \tag{2. 31}$$

$$\phi^{(1)} = \left(\frac{\sinh \eta}{\cosh \eta - \cos \xi}\right)^2 - 4\sum_{n=1}^{\infty} \frac{\coth \alpha + n}{e^{2n\alpha}-1} \sinh n\eta \cos n\xi \tag{2. 32}$$

Since $\Gamma_0 = u_0 c$ and $\Gamma_1 = (\omega c^2/2) \coth \alpha$, the quantity of fluid that flows through the clearance between the cylinder and the plane wall can easily be evaluated when the stream function along the wall is taken as the reference value of zero:

$$\phi_c = \Gamma_0 + \Gamma_1 = u_0 c + \frac{\omega c^2}{2} \coth \alpha \tag{2. 33}$$

When the velocity $u_0$ in Eq. (2. 8) is replaced by $U_0 - \omega h_1$, $U_0$ being the velocity of approach at $y = h_1$, the stream function given by Eq. (2. 30) can be reduced to the following dimensionless form:

$$\frac{\phi}{U_0 a} = (1-\lambda)\, \phi^{(0)} \sinh \alpha + \frac{\lambda}{2} \phi^{(1)} \sinh \alpha \tanh \alpha \tag{2. 34}$$

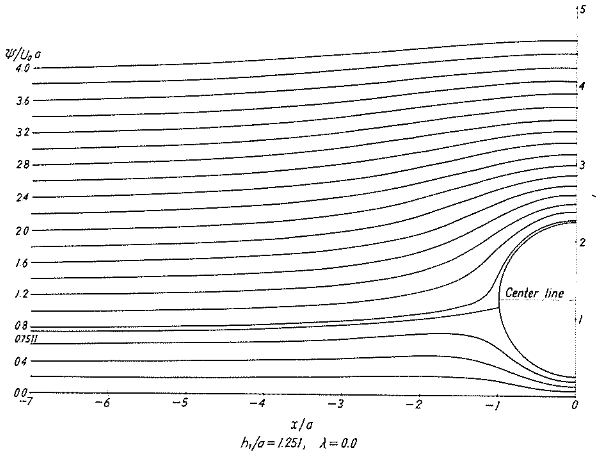

**Fig. 2. 4.** Streamlines around a cylinder in a uniform flow: $h_1/a=1.251$, $\lambda=0.0$.

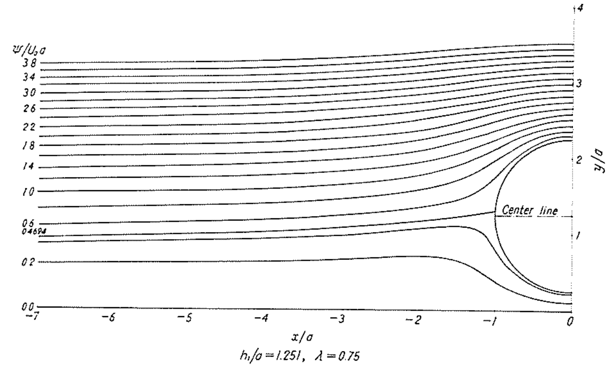

**Fig. 2. 5.** Streamlines around a cylinder in a uniform shear flow: $h_1/a=1.251$, $\lambda=0.75$

where

$$\lambda=\varepsilon \cosh \alpha\,, \qquad \varepsilon=\omega a/U_0$$

Obviously, $U_0(1-\lambda)$ means the velocity of approach at the $x$ axis as will be seen in Fig. 2. 3. Figs. 2. 4 and 2. 5 are the examples of streamlines computed after Eq. (2. 34).

Attention may momentarily be diverted to the writing of the first term of Eq. (2. 34) by means of the elliptic functions. Since the two terms appearing in $\phi^{(0)}$ are written in the form

$$\frac{\sinh \eta}{\cosh \eta-\cos \xi}=\Im\left(-\cot \frac{s}{2}\right)$$

$$4\sum_{n=1}^{\infty} \frac{1}{e^{2n\alpha}-1} \sinh n\eta \cos n\xi=\Im\left(4\sum_{n=1}^{\infty} \frac{q^n}{1-q^n} \sin ns\right)$$

$$q=e^{-\alpha}$$

$\Im(z)$ meaning "the imaginary part of $z$," the first term $u_0 c\phi^{(0)}$ of Eq. (2. 30) can be defined as the imaginary part of the following complex flow potential:

$$\Omega(s) = -u_0 c\left[\cot\frac{s}{2} + 4\sum_{n=1}^{\infty}\frac{q^n}{1-q^n}\sin ns\right]$$

The right-hand side of this equation may be rewritten as

$$\Omega(s) = -u_0 c\left[\cot\frac{s}{2} + 4\sum_{n=1}^{\infty}\frac{q^n}{1-q^n}\sin ns + 4\sum_{n=1}^{\infty}\frac{q^{2n}}{1-q^{2n}}\sin ns\right] \tag{2. 34 a}$$

On the other hand, the trigonometric series expansions of the elliptic $\zeta$ function of Weierstrass with the real period $2\omega_1 = 2\pi$ and the imaginary period $2\omega_3 = 4i\alpha$ assume the forms

$$\zeta(s) = \frac{\eta_1 s}{\pi} + \frac{1}{2}\cot\frac{s}{2} + 2\sum_{n=1}^{\infty}\frac{q^{2n}}{1-q^{2n}}\sin ns \tag{2. 34 b}$$

$$\zeta(s+\omega_3) = \frac{\eta_1 s}{\pi} + \eta_3 + 2\sum_{n=1}^{\infty}\frac{q^n}{1-q^{2n}}\sin ns \tag{2. 34 c}$$

where

$$\eta_1 = \zeta(\omega_1), \qquad \eta_3 = \zeta(\omega_3)$$

The substitution of Eqs. (2. 34 b) and (2. 34 c) into Eq. (2. 34 a) yields

$$\Omega(s) = -2u_0 c\left[\zeta(s) + \zeta(s+\omega_3) - \frac{2\eta_1 s}{\pi}\right]$$

omitting a constant without loss of generality. This is equivalent to the result obtained by Lagally who considered the potential flow past two circles of arbitrary radii and arbitrary relative distance.

### 2. 2 Velocity distribution

The velocity components $u$ and $v$ can be computed from Eq. (2. 11):

$$u = \frac{\partial\psi}{\partial y} = h^2\left(\frac{\partial y}{\partial\xi}\frac{\partial\psi}{\partial\xi} + \frac{\partial y}{\partial\eta}\frac{\partial\psi}{\partial\eta}\right)$$

$$v = -\frac{\partial\psi}{\partial x} = -h^2\left(\frac{\partial x}{\partial\xi}\frac{\partial\psi}{\partial\xi} + \frac{\partial x}{\partial\eta}\frac{\partial\psi}{\partial\eta}\right)$$

where

$$h = \frac{\cosh\eta - \cos\xi}{c}$$

The terms $\partial y/\partial\xi$, $\partial y/\partial\eta$, $\partial x/\partial\xi$ and $\partial x/\partial\eta$ can easily be computed with Eqs. (2. 6 a) and (2. 6 b), and the velocity components expressed above become

$$u = \frac{1}{c}\left[\sinh\eta\sin\xi\frac{\partial\psi}{\partial\xi} + (1-\cosh\eta\cos\xi)\frac{\partial\psi}{\partial\eta}\right] \tag{2. 35 a}$$

$$v = -\frac{1}{c}\left[(1-\cosh\eta\cos\xi)\frac{\partial\psi}{\partial\xi} + \sinh\eta\sin\xi\frac{\partial\psi}{\partial\eta}\right] \tag{2. 35 b}$$

Still, the terms $\partial\psi/\partial\xi$ and $\partial\psi/\partial\eta$ must further be computed with Eq. (2. 30):

$$\frac{\partial\psi}{\partial\xi} = u_0 c f_1(\xi, \eta) + \frac{\omega c^2}{2} f_2(\xi, \eta)$$

$$\frac{\partial \phi}{\partial \eta} = u_0 c g_1(\xi, \eta) + \frac{\omega c^2}{2} g_2(\xi, \eta)$$

where $f_1$, $f_2$, $g_1$ and $g_2$ imply

$$f_1(\xi, \eta) = \frac{-\sinh \eta \sin \xi}{(\cosh \eta - \cos \xi)^2} + 4 \sum_{n=1}^{\infty} \frac{n}{e^{2n\alpha} - 1} \sinh n\eta \sin n\xi$$

$$f_2(\xi, \eta) = \frac{-\sinh^2 \eta \sin \xi}{(\cosh \eta - \cos \xi)^3} + 4 \sum_{n=1}^{\infty} \frac{n(\coth \alpha + n)}{e^{2n\alpha} - 1} \sinh n\eta \sin n\xi$$

$$g_1(\xi, \eta) = \frac{1 - \cosh \eta \cos \xi}{(\cosh \eta - \cos \xi)^2} - 4 \sum_{n=1}^{\infty} \frac{n}{e^{2n\alpha} - 1} \cosh n\eta \cos n\xi$$

$$g_2(\xi, \eta) = \frac{2 \sinh \eta (1 - \cosh \eta \cos \xi)}{(\cosh \eta - \cos \xi)^3} - 4 \sum_{n=1}^{\infty} \frac{n(\coth \alpha + n)}{e^{2n\alpha} - 1} \cosh n\eta \cos n\xi$$

Accordingly, by introducing new forms of function

$$F_1(\xi, \eta) = (1 - \cosh \eta \cos \xi) f_1(\xi, \eta) + \sinh \eta \sin \xi g_1(\xi, \eta)$$

$$F_2(\xi, \eta) = (1 - \cosh \eta \cos \xi) f_2(\xi, \eta) + \sinh \eta \sin \xi g_2(\xi, \eta)$$

$$G_1(\xi, \eta) = -\sinh \eta \sin \xi f_1(\xi, \eta) + (1 - \cosh \eta \cos \xi) g_1(\xi, \eta)$$

$$G_2(\xi, \eta) = -\sinh \eta \sin \xi f_2(\xi, \eta) + (1 - \cosh \eta \cos \xi) g_2(\xi, \eta)$$

one can write the velocity components as

$$u = u_0 G_1(\xi, \eta) + \frac{\omega c}{2} G_2(\xi, \eta) \tag{2. 36 a}$$

$$v = -\left[ u_0 F_1(\xi, \eta) + \frac{\omega c}{2} F_2(\xi, \eta) \right] \tag{2. 36 b}$$

Hence, these velocity components can be expressed in the following dimensionless form when the reference velocity is taken as $U_0$ shown in Fig. 2. 3.

$$\frac{u}{U_0} = (1 - \lambda) G_1(\xi, \eta) + \frac{\lambda}{2} \tanh \alpha \, G_2(\xi, \eta) \tag{2. 37 a}$$

$$\frac{v}{U_0} = -\left[ (1 - \lambda) F_1(\xi, \eta) + \frac{\lambda}{2} \tanh \alpha \, F_2(\xi, \eta) \right] \tag{2. 37 b}$$

### 2. 3 Pressure distribution

When the body force is absent, the equations of motion to describe a two-dimensional flow of an inviscid fluid are

$$u \frac{\partial u}{\partial x} + v \frac{\partial u}{\partial y} = -\frac{1}{\rho} \frac{\partial p}{\partial x} \tag{2. 38 a}$$

$$u \frac{\partial v}{\partial x} + v \frac{\partial v}{\partial y} = -\frac{1}{\rho} \frac{\partial p}{\partial y} \tag{2. 38 b}$$

Since the vorticity is

$$\zeta = \frac{\partial v}{\partial x} - \frac{\partial u}{\partial y}$$

Eqs. (2. 38 a) and (2. 38 b) become

$$u\frac{\partial u}{\partial x}+v\frac{\partial v}{\partial x}-v\zeta=-\frac{1}{\rho}\frac{\partial p}{\partial x} \tag{2.39 a}$$

$$u\frac{\partial u}{\partial y}+v\frac{\partial v}{\partial y}+u\zeta=-\frac{1}{\rho}\frac{\partial p}{\partial y} \tag{2.39 b}$$

Further, the definition of stream function is

$$d\psi=\frac{\partial\psi}{\partial x}dx+\frac{\partial\psi}{\partial y}dy=udy-vdx$$

Accordingly, the sum of the two equations (2.39 a) and (2.39 b) after being multiplied respectively by $dx$ and $dy$ gives

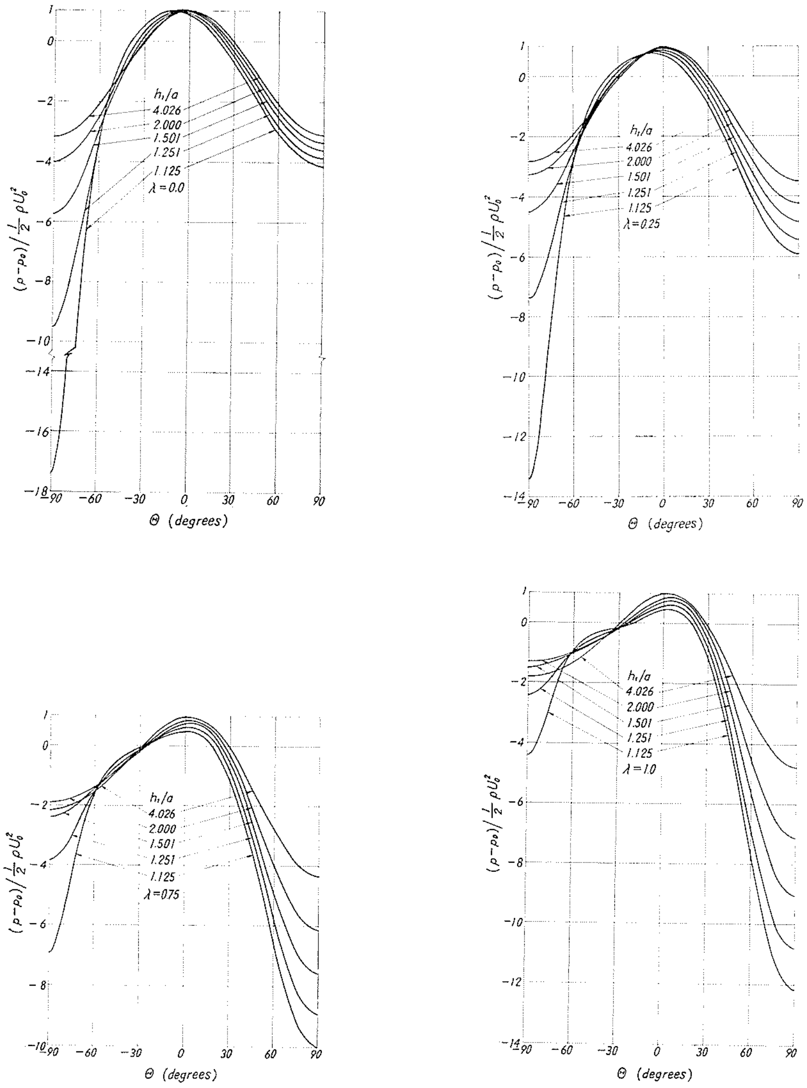

**Fig. 2. 6.** Pressure distribution around a cylinder in a uniform shear flow: (a) $\lambda=0.0$, (b) 0.25, (c) 0.75, (d) 1.0.

$$d\left(\frac{1}{2}q^2+\frac{p}{\rho}-\omega\psi\right)=0$$

whence

$$\frac{1}{2}q^2+\frac{p}{\rho}-\omega\psi=\text{constant} \tag{2.40}$$

where

$$q=(u^2+v^2)^{\frac{1}{2}}$$

Eq. (2.40) is a form of energy equation for the shear flow now considered. Since the velocity components are already obtained, the pressure distribution in the flow field can easily be computed. If the values at a reference point are denoted by subscription $s$, the dimensionless form of pressure at any point is

$$\frac{p-p_s}{\frac{1}{2}\rho q_s^2}=1-\left(\frac{q}{q_s}\right)^2+\frac{2\omega}{q_s^2}(\psi-\psi_s) \tag{2.41}$$

When the point of reference is taken at $(\infty, h_1)$,

$$q_s=U_0, \qquad p_s=p_0, \qquad \psi_s=(U_0-\omega h_1)h_1+\frac{\omega h_1^2}{2}$$

Therefore, the pressure coefficient $C_p$ expressed by Eq. (2.41) becomes

$$C_p\equiv\frac{p-p_0}{\frac{1}{2}\rho U_0^2}=1-\left(\frac{q}{U_0}\right)^2+\frac{2\omega}{U_0^2}\left[\psi-\left\{(U_0-\omega h_1)h_1+\frac{\omega h_1^2}{2}\right\}\right]$$

Then, the pressure coefficient $C_{pc}$ along the surface of the cylinder can be obtained by the use of Eq. (2.33):

$$C_{pc}=1+\lambda(\lambda-2)(1-\tanh\alpha)-\left(\frac{q_c}{U_0}\right)^2 \tag{2.42}$$

where $q_c$ is the velocity along the surface of the cylinder. Examples of pressure distribution on the surface of the cylinder in the vicinity of a plane wall are shown in Fig. 2.6 in terms of pressure coefficient and the distance between the cylinder and the wall in dimensionless form. The lift exerted upon the cylinder is then obtainable in terms of lift coefficient $C_L$ by integrating the pressure distribution given by Eq. (2.42):

$$C_L\equiv\frac{L}{\rho U_0^2 a}=-\int_{-\pi/2}^{\pi/2}C_{pc}\sin\Theta\, d\Theta \tag{2.43}$$

where $\Theta$ is the angle shown in Fig. 2.3. The results of this integration are shown in Fig. 2.7. As will be seen in this figure, the lift is negative in the vicinity of plane wall so far as $\lambda=0$ namely in the case of

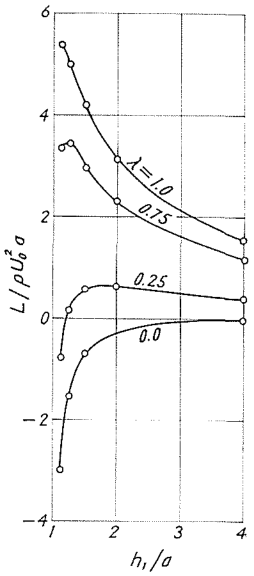

**Fig. 2.7.** Lift coefficient of a cylinder in a uniform shear flow.

a uniform flow. But the lift becomes positive when there exists a certain amount of velocity gradient in the vertical direction of flow which is similar to the case of a practical boundary layer that develops along a stationary boundary of a wall.

### 2.4 Shear Flow across two cylinders

This problem can be solved in the same way as the previous case by slightly changing the boundary conditions in solving the Laplace equations given by Eqs. (2.14a) and (2.15a). The definition sketch of the two cylinders is given in Fig. 2.1. The boundary conditions to be replaced for Eqs. (2.16), (2.17) and (2.18) are

(i) $\Psi_0 \to 0$ and $\Psi_1 \to 0$ at $s \to 0$ $(z \to \infty)$

(ii) Since $\eta = \alpha$ on the surface of circle $0_1$,

$$\begin{aligned}\Psi_0 &= -u_0[y]_{\eta=\alpha} + \gamma_0' \\ &= -u_0 c\left[1 + 2\sum_{n=1}^{\infty} e^{-n\alpha}\cos n\xi\right] + \gamma_0'\end{aligned}$$

$$\begin{aligned}\Psi_1 &= -\frac{\omega}{2}[y]^2_{\eta=\alpha} + \gamma_1' \\ &= -\frac{\omega c^2}{2}\left[\coth\alpha + 2\sum_{n=1}^{\infty} e^{-n\alpha}(\coth\alpha + n)\cos n\xi\right] + \gamma_1'\end{aligned}$$

(iii) $\eta = -\beta$ on the surface of circle $0_2$, whence

$$\begin{aligned}\Psi_0 &= -u_0[y]_{\eta=-\beta} + \delta_0' \\ &= u_0 c\left[1 + 2\sum_{n=1}^{\infty} e^{-n\beta}\cos n\xi\right] + \delta_0'\end{aligned}$$

$$\begin{aligned}\Psi_1 &= -\frac{\omega}{2}[y]^2_{\eta=-\beta} + \delta_1' \\ &= -\frac{\omega c^2}{2}\left[\coth\beta + 2\sum_{n=1}^{\infty} e^{-n\beta}(\coth\beta + n)\cos n\xi\right] + \delta_1'\end{aligned}$$

The stream functions $\Psi_0$ and $\Psi_1$ can be obtained by taking the following forms that correspond to Eqs. (2.20) and (2.27):

$$\begin{aligned}\Psi_0 = A_{00} + \sum_{n=1}^{\infty}(&A_{n0}\cosh n\eta\cos n\xi + B_{n0}\sinh n\eta\cos n\xi \\ &+ C_{n0}\cosh n\eta\sin n\xi + D_{n0}\sinh n\eta\sin n\xi)\end{aligned}$$

$$\begin{aligned}\Psi_1 = A_{01} + \sum_{n=1}^{\infty}(&A_{n1}\cosh n\eta\cos n\xi + B_{n1}\sinh n\eta\cos n\xi \\ &+ C_{n1}\cosh n\eta\sin n\xi + D_{n1}\sinh n\eta\sin n\xi)\end{aligned}$$

The coefficients can now be determined by the boundary condition stated above, and the results are

$$A_{n0} = 2u_0 c\frac{\sinh n(\alpha-\beta)}{\sinh n(\alpha+\beta)}$$

$$B_{n0} = 2u_0 c\left[1 - 2\frac{\cosh n\alpha\cosh n\beta}{\sinh n(\alpha+\beta)}\right]$$

$$C_{n0} = 0, \qquad D_{n0} = 0$$

$$A_{00} = -u_0 c + \gamma_0' = u_0 c + \delta_0' = -\sum_{n=1}^{\infty} A_{n0} \tag{2. 44 a}$$

$$A_{01} = -\sum_{n=1}^{\infty} A_{n1} = -\frac{\omega c^2}{2} \coth\alpha + \gamma_1' = -\frac{\omega c^2}{2} \coth\beta + \delta_1' \tag{2. 44 b}$$

$$A_{n1} = -\omega c^2 \frac{e^{-n\alpha}(\coth\alpha + n)\sinh n\beta + e^{-n\beta}(\coth\beta + n)\sinh n\alpha}{\sinh n(\alpha+\beta)}$$

$$B_{n1} = -\omega c^2 \frac{e^{-n\alpha}(\coth\alpha + n)\cosh n\beta - e^{-n\beta}(\coth\beta + n)\cosh n\alpha}{\sinh n(\alpha+\beta)}$$

$$C_{n1} = 0\,, \qquad D_{n1} = 0$$

The relations (2. 44 a) and (2. 44 b) yield

$$\gamma_0' - \delta_0' = 2u_0 c \tag{2. 45 a}$$

$$\gamma_1' - \delta_1' = \frac{\omega c^2}{2}(\coth\alpha - \coth\beta) \tag{2. 45 b}$$

Obviously, Eqs. (2. 45 a) and (2. 45 b) give the quantity of flow between two cylinders in uniform flow and in pure shear flow, respectively. Eq. (2. 45 a) is equivalent to the result obtained by Lagally [19].

Finally the stream function becomes

$$\psi = u_0 c \psi^{(2)} + \frac{\omega c^2}{2} \psi^{(3)}$$

where

$$\psi^{(2)} = \frac{\sinh\eta}{\cosh\eta - \cos\xi} + 2\sum_{n=1}^{\infty} \frac{\sinh n(\alpha-\beta)}{\sinh n(\alpha+\beta)} (\cosh n\eta \cos n\xi - 1)$$
$$-2\sum_{n=1}^{\infty} \left[\frac{2\cosh n\alpha \cosh n\beta}{\sinh n(\alpha+\beta)} - 1\right] \sinh n\eta \cos n\xi$$

$$\psi^{(3)} = \left(\frac{\sinh\eta}{\cosh\eta - \cos\xi}\right)^2$$
$$-2\sum_{n=1}^{\infty} \frac{e^{-n\alpha}(\coth\alpha + n)\sinh n\beta + e^{-n\beta}(\coth\beta + n)\sinh n\alpha}{\sinh n(\alpha+\beta)} (\cosh n\eta \cos n\xi - 1)$$
$$-2\sum_{n=1}^{\infty} \frac{e^{-n\alpha}(\coth\alpha + n)\cosh n\beta - e^{-n\beta}(\coth\beta + n)\cosh n\alpha}{\sinh n(\alpha+\beta)} \sinh n\eta \cos n\xi$$

## 3. Experiments on the Uniform Shear Flow past a Circular Cylinder

The experiments were conducted for the purpose of verifying the trend of change in the lift coefficient of a circular cylinder in a uniform shear flow developed in an air tunnel installed at the Fluid Mechanics Laboratory of the Faculty of Engineering, Hokkaido University. The air tunnel is of a blow-off type, the flow being produced by a centrifugal blower driven by a 100 kW electric motor. The velocity of air flow can be adjusted in three ways ; by changing the revolution of the blower and by changing the valve and gate opening installed respectively at the suction tower of the blower and at the exit of the tunnel. The cross section of the test section is 50 cm × 50 cm, and the side walls over the entire length of 5 m are transparent.

The experiments were made in a uniform shear flow artificially generated by arranging a grid of rods of 3.2 mm diameter over an entire section of the approaching flow after Owen and Zienkiewicz's [21] theory.

### 3.1 Theory of Grid Design

The test section of the wind tunnel may be treated as a long channel, as sketched in Fig. 3.1, with walls $y=0$, $y=h$, in which a grid is placed in the plane $x=0$. At great distances upstream the velocity is uniform and has the value $U$; far downstream the velocity is again parallel to the walls and its magnitude is given by

$$u = U + \omega\left(y - \frac{h}{2}\right) \tag{3.1}$$

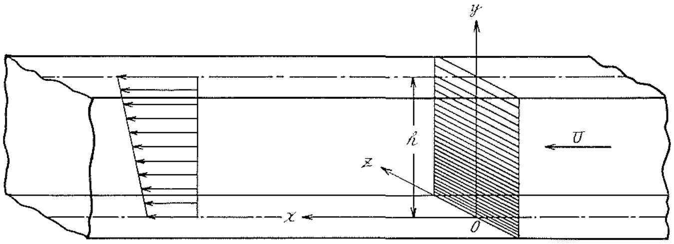

**Fig. 3.1.** Arrangement of the grid and the coordinate system.

One assumes that the fluid is inviscid and that $\omega h/U$ is of a smaller order of magnitude than unity, and consequently the departure of any streamline from a straight line is small. Accordingly, the stream function which describes the entire flow field may be written as

$$\psi = Uy + \psi' \quad \text{for} \quad x < 0 \tag{3.2 a}$$

$$= Uy + \frac{\omega}{2}(y^2 - hy) + \psi' \quad \text{for} \quad x > 0 \tag{3.2 b}$$

$\psi'$ is the perturbation stream function which represents the effect of the grid, and satisfies the Laplace equation

$$\frac{\partial^2 \psi'}{\partial x^2} + \frac{\partial^2 \psi'}{\partial y^2} = 0 \tag{3.3}$$

owing to the constancy of vorticity throughout the flow field. $\psi'$ is everywhere small compared with $Uh$. Appropriate solutions satisfying the boundary conditions

$$\frac{\partial \psi'(x, 0)}{\partial x} = \frac{\partial \psi'(x, h)}{\partial x} = 0$$

for all $x$ are

$$\frac{\psi'}{Uh} = \sum_{n=1}^{\infty} A_n e^{\frac{n\pi x}{h}} \sin \frac{n\pi y}{h}, \qquad x < 0 \tag{3.4 a}$$

$$= \sum_{n=1}^{\infty} B_n e^{-\frac{n\pi x}{h}} \sin \frac{n\pi y}{h}, \qquad x > 0 \tag{3. 4 b}$$

where the constants $A_n$ and $B_n$ may be determined by the condition of flow at the grid.

The presence of the grid requires that (i) $\partial\phi/\partial y$ is continuous through $x=0$ (continuity), (ii) the velocity component $\partial\phi/\partial x$ obeys a certain refraction condition across $x=0$, and (iii) the difference between the total pressures on a given streamline for large positive and negative values of $x$ must be equal to the resistance per unit area imposed by the grid. To these may be added the condition that the static pressures far upstream and far downstream of the grid are independent of $y$.

Condition (i) leads to

$$\pi \sum_{n=1}^{\infty} nA_n \cos \frac{n\pi y}{h} - \pi \sum_{n=1}^{\infty} nB_n \cos \frac{n\pi y}{h} = \left(\frac{y}{h} - \frac{1}{2}\right) \frac{\omega h}{U}$$

or, setting

$$\frac{1}{2}\, y(y-h) = h^2 \sum_{n=1}^{\infty} C_n \sin \frac{n\pi y}{h}$$

$$A_n - B_n = C_n \frac{\omega h}{U} \tag{3. 5}$$

The refraction condition (ii) requires the $y$-component of the velocity to change by a factor $\alpha$ in passing through the grid. $\alpha$ for a grid of uniform resistance is known to be $1.1(1+K)^{-1/2}$, where $K$ is the resistance coefficient

$$K = (p_- - p_+) \Big/ \left(\frac{1}{2}\, \rho [u(0)]^2\right)$$

$p_-$ and $p_+$ being the pressures far upstream and far downstream of the grid. It is unlikely that this value will be seriously in error for a grid with slightly graded resistance provided that $K$ is given its local value. If the resistance grading is reprented by

$$K = K_0 \Big[1 + \varepsilon(y)\Big] \tag{3. 6}$$

such that $\varepsilon(y)$ is small and

$$\int_0^h \varepsilon(y)\, dy = 0$$

it follows that

$$\alpha = \frac{1.1}{(1+K_0)^{1/2}} \left[1 - \frac{K_0 \varepsilon}{2(1+K_0)}\right] + O(\varepsilon^2) \tag{3. 7}$$

With $\alpha$ given by Eq. (3. 7), the refraction condition is

$$\sum_{n=1}^{\infty} nB_n \sin \frac{n\pi y}{h} + (a + b\varepsilon) \sum_{n=1}^{\infty} nA_n \sin \frac{n\pi y}{h} = 0$$

which, noting that $A_n$ and $B_n$ are $O(\omega h/U)$, reduces to

$$B_n + aA_n = 0 + O(\omega h \varepsilon / U) \tag{3.8}$$

where

$$a = \frac{1.1}{(1+K_0)^{1/2}}, \qquad b = -\frac{1.1K_0}{2(1+K_0)^{3/2}}$$

Finally, one must consider the change in total pressure along a streamline. According to the assumption of an inviscid fluid, the total pressure remains constant along streamlines upstream and downstream of the grid but, at the grid itself, there is a decrease in total pressure amounting to $K(1/2)\rho[u(0)]^2$. Hence

$$p_0 + \frac{1}{2}\rho U^2 - p_1 - \frac{1}{2}\left[U + \omega\left(y_1 - \frac{1}{2}h\right)\right]^2 = K\frac{1}{2}\rho[u(0)]^2 \tag{3.9}$$

where $p_0$ and $p_1$ are respectively the static pressuses far upstream and far downstream of the grid. The streamline which has the ordinate $y_1$ for large $x$ meets the grid at $y = y_0$, and the relation between $y_0$ and $y_1$ follows from Eqs. (3.2);

$$y_1 = y_0 + \frac{\psi'(0, y_0)}{U} + O\left(\frac{\omega\psi'}{U^2}\right) \tag{3.10}$$

Eq. (3.10) implies that, to the first order in $\omega h/U$ and $\psi'/Uh$, the $x$ component of the velocity at the grid is given by

$$u(0) = U + \omega\left(y_0 - \frac{1}{2}h\right) + \frac{\partial\psi'(0, y_0)}{\partial y} \tag{3.11}$$

which, together with Eq. (3.9), leads to

$$\frac{p_0 - p_1}{\frac{1}{2}\rho U^2} = K_0(1+\varepsilon) + 2\frac{\omega h}{U}(1+K_0)\left(\frac{y_0}{h} - \frac{1}{2}\right) + \frac{2K_0}{U}\frac{\partial\psi'(0, y_0)}{\partial y} \tag{3.12}$$

Since $(p_0 - p_1)$ is independent of $y$, Eq. (3.12) resolves into

$$\frac{p_0 - p_1}{\frac{1}{2}\rho U^2} = K_0 \tag{3.13}$$

and

$$K_0\varepsilon + 2\frac{\omega h}{U}(1+K_0)\left(\frac{y_0}{h} - \frac{1}{2}\right) + 2\frac{K_0}{U}\frac{\partial\psi'(0, y_0)}{\partial y} = 0 \tag{3.14}$$

The distribution $\varepsilon(y_0)$ follows directly from Eq. (3.14) if one notes from Eqs. (3.4), (3.5) and (3.9) that

$$\frac{\partial\psi'(0, y_0)}{\partial y} = -\pi\omega h^2\left(\frac{a}{1+a}\right)\sum_{n=1}^{\infty} nC_n \cos\frac{n\pi y}{h} = -\omega h\left(\frac{a}{1+a}\right)\left(\frac{y_0}{h} - \frac{1}{2}\right) \tag{3.15}$$

hence,

$$\varepsilon(y_0) = -2\frac{\omega h}{U}\left(\frac{1}{K_0} + \frac{1}{1+a}\right)\left(\frac{y_0}{h} - \frac{1}{2}\right) \tag{3.16}$$

At large Reynolds numbers the resistance of a grid of rods in a uniform stream can be predicted with good accuracy if the drag coefficient based on the blocked area and the average interstitial velocity is taken to be unity (Wieghardt [22]). For the present purpose it will be assumed permissible to adopt the same procedure for each portion of the grid, with the possible exception of places where the spacing changes rapidly with $y$, since the scale of variation in the $y$-direction of the velocity through the plane of the grid, $u(0)$, is much larger than the greatest spacing between adjacent rods. Accordingly,

$$K_0(1+\varepsilon)=\frac{\xi}{(1-\xi)^2}$$

where

$$\xi=d/s\,;$$

$d$ is the diameter of each rod and the spacing is $s(y)$. With $\varepsilon$ given by Eq. (3.16), one obtains

$$\frac{\xi}{(1-\xi)^2}=K_0\left[1-2\frac{\omega h}{U}\left(\frac{1}{K_0}+\frac{1}{1+a}\right)\left(\frac{y}{h}-\frac{1}{2}\right)\right] \qquad (3.17)$$

### 3.2 Production of Uniform Shear Flow.

A grid composed of parallel rods of 3.2 mm diameter was constructed according to Eq. (3.17) with $\omega h/U=0.45$ and $K_0=1.15$. The appropriate values of $\xi$ are shown in Fig. 3.2.

The grid was placed at a section 60 cm downstream of the entrance to the working section, 50 cm square, of the wind tunnel at the Fluid Mechanics Laboratory. Fig. 3.3 shows the arrangement of the grid in the air tunnel. Traverses, across the working section in planes parallel to the grid at a number of distances from it were made with N.P.L. type of Pitot tube of 8 mm diameter, Pitot coefficient being unity, at the mean wind speced $U$ of 19.2 m/sec and 22.6 m/sec, respectively.

No variation in static pressure could be detected from the traverses, which were confined to distances greater than approximately one tunnel height from the grid. The grid could not be approached much more closely with a conventional static probe owing to an appreciable inclination and curvature of the streamlines.

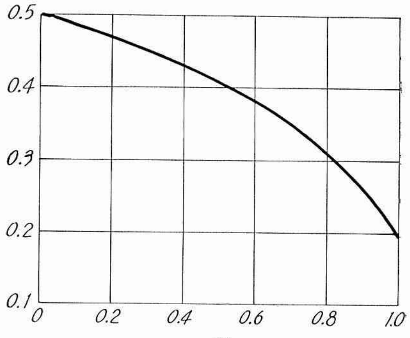

Fig. 3.2. Spacing of rods.

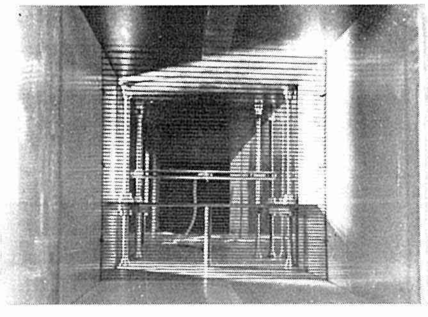

Fig. 3.3. Grid of rods for the production of shear flow.

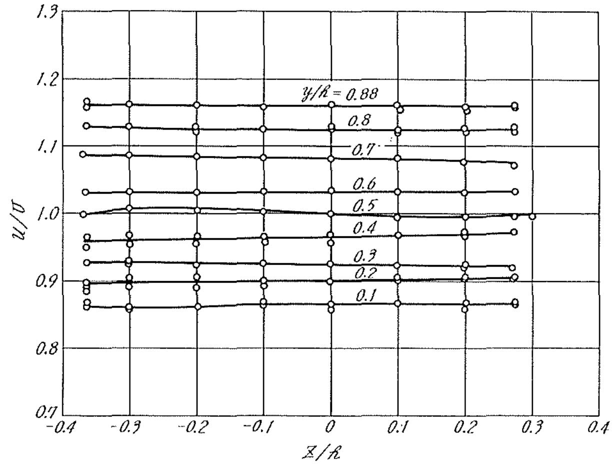

Fig. 3. 4. Velocity contours in the plane $x/h=3.0$.

The contours of $u/U$ as deduced from the Pitot tube traverses in a plane parallel to the grid and 150 cm ($x/h=3.0$) downstream of it are shown in Fig. 3. 4. The absence of any systematic departure from lines parallel to the $z$-axis, together with the previously mentioned fact that the static pressure is constant over the region, suggests that no secondary flow was present on a large scale.

The profile of $u/U$ in the plane of symmetry of the tunnel, $z=0$, at distances of 59.5 cm and 150 cm from the grid ($x/h=1.19$ and 3.0) are presented in Fig. 3. 5. The agreement between the measured velocity distribution and that predicted by the theory is tolerable.

Ostensibly there is no systematic change in the rate of shear between $x/h=1.19$ and $x/h=3.0$, and even small irregularities in the velocity profile appear to suffer no appreciable decay. The small scale irregularities in the velocity profile, which were found to be repeatable in the experiments, can be attributed to inaccuracies in the manufacture of the grid.

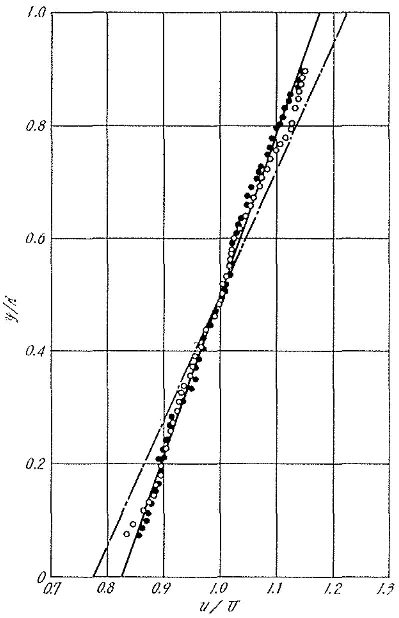

Fig. 3. 5. Velocity profiles measured in the plane of symmetry of the tunnel: $x/h=3.0$, $z/h=0.0$; ●, $U=$ 22.6 m/sec, ○, $U=19.2$ m/sec, —— most probable curve, — — — theory.

### 3. 3 Uniform Shear Flow past a Circular Cylinder: Experiment

The plane wall that would be located in the neighborhood of a circular cylinder was represented by placing a polyvynil chloride plate, 5 mm in thickness, parallel to the flow, the leading edge being given 26.5° bevel on the other side of

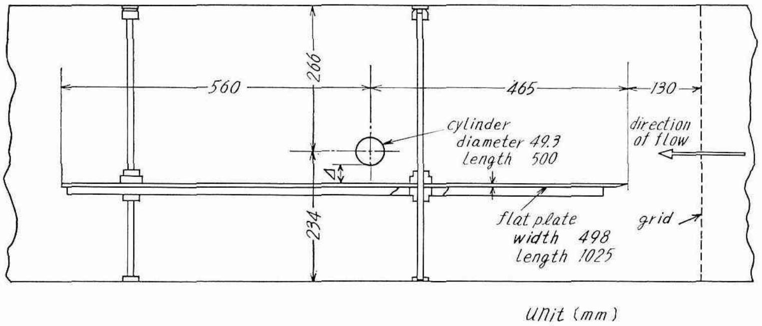

**Fig. 3. 6.** Schematic view of the experimental installation.

the test flow as will be seen in Fig. 3. 6. The test cylinder was made of a brass tube, the diameter being 49.3 mm. Fig. 3. 7 is given to supplement Fig. 3. 6 in order to show the features of the test. The velocity distributions of the shear flow at the three sections are shown in Fig. 3. 8. The distance between the test cylinder and the plate was adjusted by a screw device and a static pressure hole of 1 mm diameter in the central section of the cylinder was connected to a Göttingen type manometer. The angular position of the pressure hole, read on a protractor, gave the pressure distribution around the surface of the cylinder, which was integrated to evaluate the lift and drag forces acting on the cylinder.

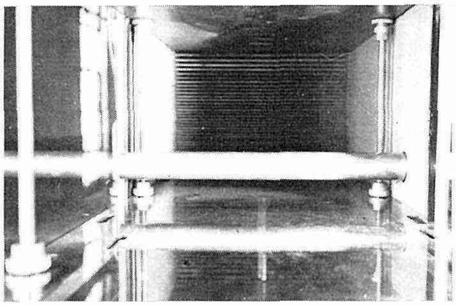

**Fig. 3. 7.** Experimental installation.

The measured pressure distributions around the test cylinder are shown in Fig. 3.9 in terms of the pressure coefficient and the angle measured from the straight line parallel to the approaching flow, the parameter being the ratio of the clearance between the cylinder and the plane wall to the diameter of the cylinder. The pressure coefficient is defined by

$$C_p=\frac{p-p_0}{\frac{1}{2}\rho U^2}$$

where $U_0$ is the approaching velocity at the center of the cylinder and $p_0$ is the static prassure of the approaching flow. Since the upstream velocity profile and the configuration of the test cylinedr yield the values of $\lambda$ and $\alpha$ which appeared in

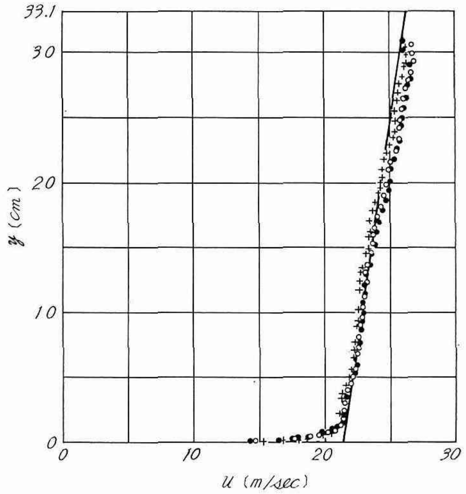

**Fig. 3. 8.** Velocity profiles of the artificially produced shear flow: +, 25 cm, ○, 41 cm and ●, 59 cm from the leading edge.

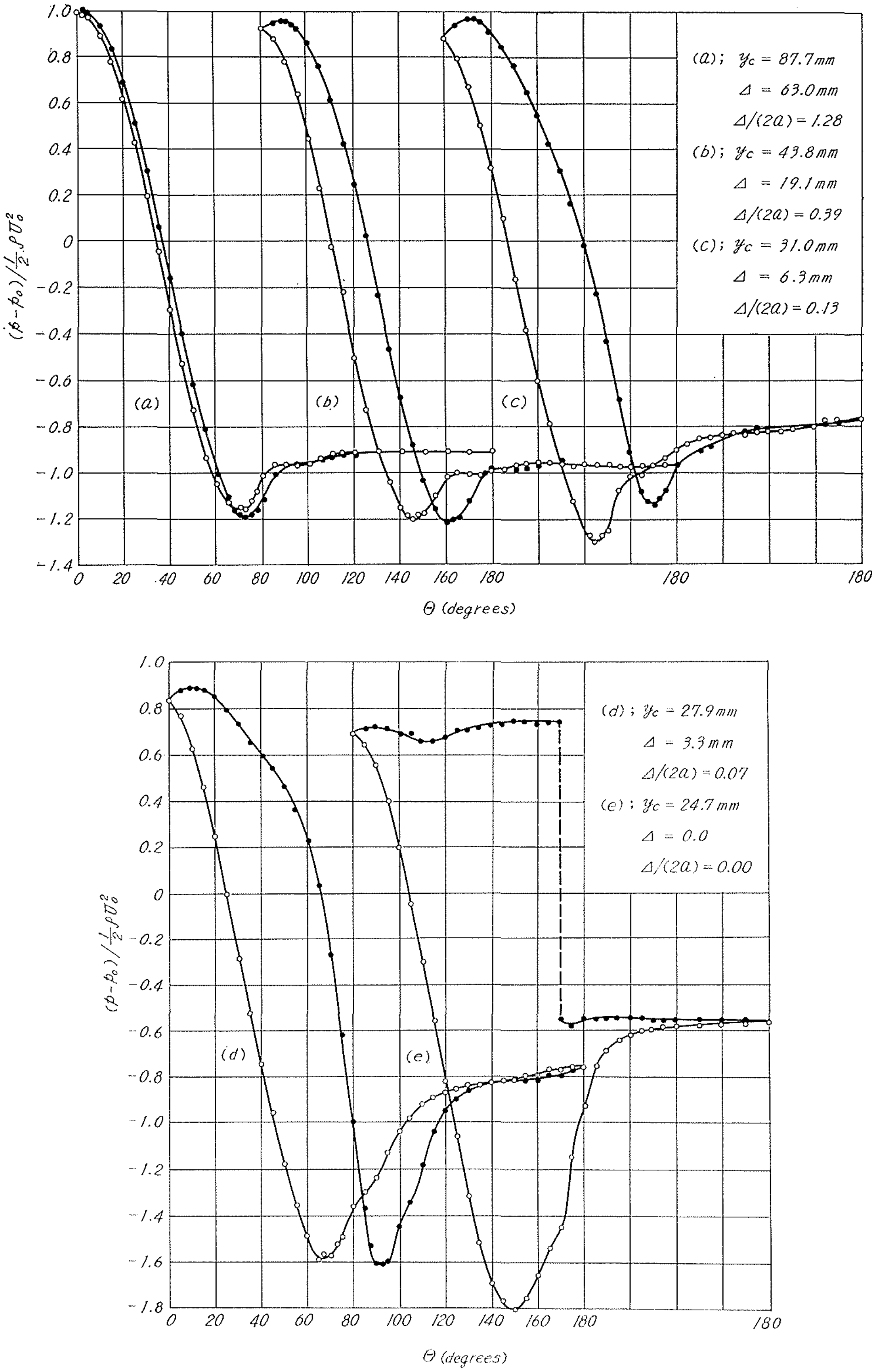

Fig. 3. 9. Pressure distribution around the cylinder.

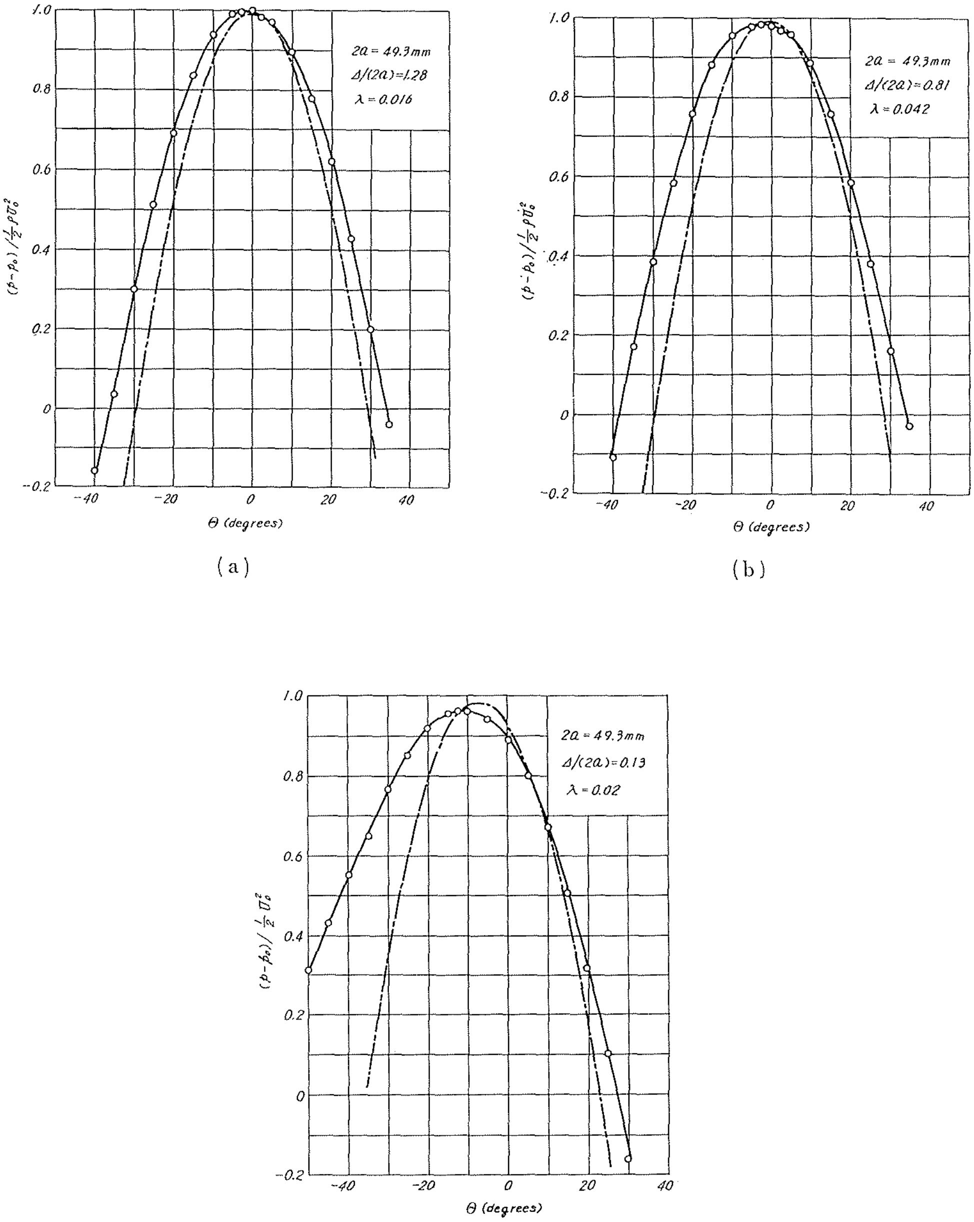

(a)

(b)

(c)

**Fig. 3. 10.** Pressure distribution around the test cylinder: (a) $\Delta/(2a)=1.28$, (b) 0.81 and (c) 0.02; —— experiment, ——— theory.

the theoretical treatment, it becomes possible to compared the theoretical results with the experiments. The theory is believed to be valid on the surface of the cylinder near the stagnation point, so a comparison is made concerning the pressure distribution in the neighbourhood of the stagnation point. Fig. 3. 10 (a), (b) and (c) show that a tolerable agreement is obtained for both the stagnation pressure and the position of stagnation point, provided that the clearance between the cylinder and the plane wall is not too small. The turbulent boundary layer which develops along the surface of the plate, as will be seen in Fig. 3. 8, may be responsible for the large discrepancy between the theory and the experiment, because the velocity gradient is much larger in the boundary layer than in the uniform shear flow of the outside layer. Morever, it should be noted that the pressure distribution predicted by the theory deviates increasingly from the measured one with the increase in angle from the stagnation point. This fact may be interpreted as the development of a laminar or turbulent boundary layer along the surface of the cylinder, the displacement effect of which produces an effect akin to the increase in the radius of curvature of the surface.

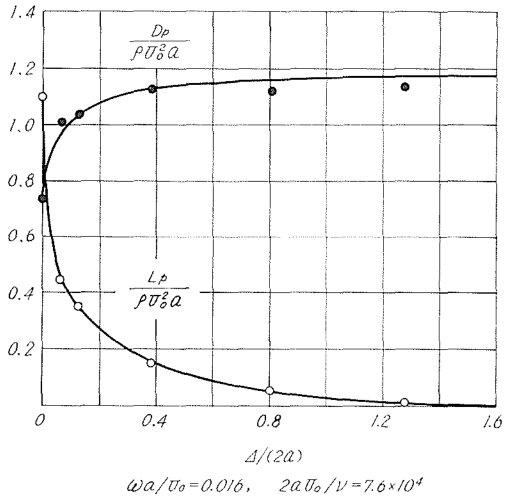

**Fig. 3. 11.** Lift and drag coefficients of the cylinder in a uniform shear flow.

The lift and drag forces acting on the cylinder are obtained by integrating numerically the pressure distribution on the surface of the test cylinder. The results are shown in Fig. 3.11 in terms of the lift and drag coefficients $C_{Lp}$, $C_{Dp}$ and the distance between the cylinder and the plane wall in dimensionless form. $C_{Lp}$ and $C_{Dp}$ are defined by

$$C_{Lp}=\frac{L_p}{\rho U_0^2 a}=\frac{1}{2}\int_0^{\pi}\frac{p_l-p_u}{\frac{1}{2}\rho U_0^2}\sin\Theta\, d\Theta$$

$$C_{Dp}=\frac{D_p}{\rho U_0^2 a}=\frac{1}{2}\int_0^{\pi}\frac{p_l+p_u}{\frac{1}{2}\rho U_0^2}\cos\Theta\,d\Theta$$

where $L_p$ and $D_p$ and the lift and drag forces, and $p_l$ and $p_u$ are the pressures on the lower $(-180°\leqq\Theta\leqq 0°)$ and upper $(0°\leqq\Theta\leqq 180°)$ surfaces of the cylinder, respectively. A suffix of $p$ is given to the lift $L$ and drag $D$, because computations were made only from the pressure distribution without evaluating the shear force on the cylinder. As will be evident in this figure, the value of lift coefficient increases when the cylinder approaches the plane wall, again confirming another qualitative agreement with the theoretical result.

Finally, it is of some interest to point out that the boundary layers on the cylinder seem to separate from the surface after the transition from laminar to turbulent flows, for three values of $\Delta/(2a)$, namely, 0.128, 0.066 and 0.0. The Reynolds number $2aU_0/\nu$ for these cases is $7.6\times 10^4$, while the ordinary uniform flow of the same Reynolds number past a circular cylinder is found not to exhibit the transition of the boundary layer on its surface. Fig. 3.12 shows the relation between the pressure and shear stress distributions around the circular cylinder in the uniform flow obtained experimentally by Fage and Faldner [23] for both several

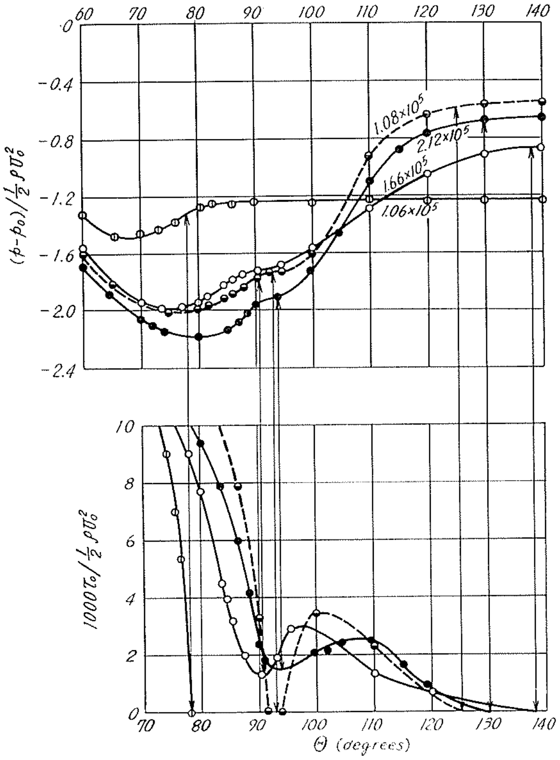

**Fig. 3. 12.** Relation between the pressure distribution and the shear stress distribution around a circular cylinder in a uniform flow (Fage and Falkner [23]).

Reynolds numbers and oncoming flow conditions. It is obvious from this figure that the point of inflexion of the pressure curve near $\Theta=90°$ implies the transition point from laminar to turbulent flows, if the Reynolds number is more than $1.08\times10^5$. Also, the point where the pressure becomes almost constant corresponds to the separation point of the boundary layer. The pressure curve for $R=1.06\times10^5$ implies the laminar separation.

Upon considering the striking resemblance between the pressure distributions around the cylinder for $\Delta/(2a)=1.128$, 0.66 and 0.0 and those obtained by Fage and Falkner, togethether with the fact that the pressure recoveries at the rear side of the cylinder are almost the same for both cases, one may say that the transition of the boundary layer occured even for the subcritical Reynolds numbers when the cylinder apporached sufficiently to the plane wall in a uniform shear flow. The increase in the turbulence level near the plane wall may be responsible for the transition, although the true mechanisms of the transition from laminar to turbulent flows are as yet unknown.

## 4. Flow around a Circular Cylinder in a Turbulent Boundary Layer

Since the velocity gradient in a turbulent boundary layer is several times greater than that in the artificially generated uniform shear flow, more effective comparisons of the theory with experiments may become possible. Thus, experimental studies of the flow around a circular cylinder placed in a turbulent boundary layer which develops along the tunnel wall were performed in some detail.

### 4.1 Experimental Equipments

*a) Air tunnel*

All experiments were carried out in the air tunnel of the Fluid Mechanics Laboratory of the Faculty of Engineering, Hokkaido University.

Pressure taps of 1 mm diameter installed at intervals of 30 cm, in the upper and lower boundaries of the test section over its entire length of 5 m permit the measuremeut of the static pressure distribution along the tunnel walls. Smooth poly-vynil chloride plates, 10 mm in thickness, are attached to the floor of the tunnel with wood screws in order to eliminate the effect of roughness of the wooden floor, because use is made of the turbulent bondary layer which develops along the lower tunnel wall. Accordingly, the effective area of the test section becomes 50 cm × 49 cm.

The velocity of the undisturbed flow in the test section was determined by calibration in terms of the pressure difference between two piezometer holes, one of which was located about 5 cm downstream from the entrance of the test section and the other was located at the end of the plenum chamber. The longitudinal turbulence level $\sqrt{\overline{u'^2}}/U_\infty$ is about 0.5% at an air speed of $U_\infty=20$ m/sec.

Other dimensions and characteristics of this tunnel are explained in Chapter 3.

*b*) *Velocity Measurements.*

The air velocities are measured by means of both standard Prandtl-type Pitot tube of 8 mm diameter and the total head tube of rectangular cross section 0.57 mm × 1.5 mm. The total head tube is mainly utilized to obtain the velocity distributions in the turbulent boundary layer and in the wake of the circular cylinder. Each of these tubes is mounted on a traversing mechanism which can be adjusted to the measuring position with an accuracy of 0.1 mm.

The total and static pressures are connected to a Göttingen type manometer (1/20 mm) or a Betz type manometer (1/10 mm) to obtain the dynamic pressure.

Allowance must be made for the transverse gradient of velocity, for proximity to the wall, and (strictly, although this is often neglected in practice) for the velocity fluctuations in a turbulent layer.

The transverse velocity gradient gives rise to a highly complex flow pattern in the mouth of the Pitot tube, where the viscosity of fluid produces a marked effect. As a result, the reading of the tube is not clearly related to the total pressure of any of the approaching stream filaments and the observed total pressure differs from that of the filament occupying the position of the axis of the tube before its introduction into the flow. The effect can alternatively be represented by a displacement of the effective center of the tube. According to Young and Maas [12] the effective displacement $\Delta y$ for a square-cut head in turbulent flow is towards the region of a higher velocity and is given by the equation

$$\frac{\Delta y}{D} = 0.13 + 0.08\,\frac{d}{D} \tag{4.1}$$

where $d$ and $D$ are the internal and external diameters of tube. For want of the corresponding formula for the total head tube of rectangular cross section, the effective displacement was tentatively estimated by means of Eq. (4. 1) to obtain the reasonable results, as will be seen in Section 4. 4. Since $d = 0.35$ mm and $D = 0.56$ mm, one obtains $\Delta y/D = 0.18$. In the case of turbulent boundary layers, the corrections were restricted up to the distance $4D = 2.2$ mm from the plane boundary.

When the tube is closer to the surface than twice its diameter, the effect of wall proximity act in the opposite direction to the effects of velocity gradient and a further correction may be required. For turbulent pipe flow MacMillan [24] finds that the correction may conveniently be expressed as an increment $\Delta V$ to be added to the measured velocity, and indicates that a correction of the same order is applicable in turbulent boundary layer flow as well. Davies's [13] results, however, suggest that his negligible correction in boundary layer flow is maintained right to the wall for all sizes of the tube. The reason for these discrepancies is somewhat obscure, thus no correction for proximity to the wall is made in the present experiments.

*c*) *Turbulence measurements.*

The values of $\sqrt{\overline{u'^2}}$, $\sqrt{\overline{v'^2}}$ and $\overline{u'v'}$ are measured with a constant temperature type of hot-wire anemometer using a single-hot-wire technique. Tungsten wire of 5 $\mu$ diameter was copper plated with $CuSO_4$ before soldering onto a probe. When the copper is removed by etching with $HNO_3$ to produce about 5 ohms of electric resistance, the length of the acting part of the wire is about 1.5 mm and the total length of the wire is approximately 2 mm. The calibration of this hot wire was made in a uniform flow in the air tunnel by comparing with a standard Prandtl-type Pitot tube and the change of voltage necessary to keep the temperature of the wire constant for various speeds of air is obtained. Through calibration the characteristics of this hot wire is found to be linear as intended. One example of the results of calibration is shown in Fig. 4.1.

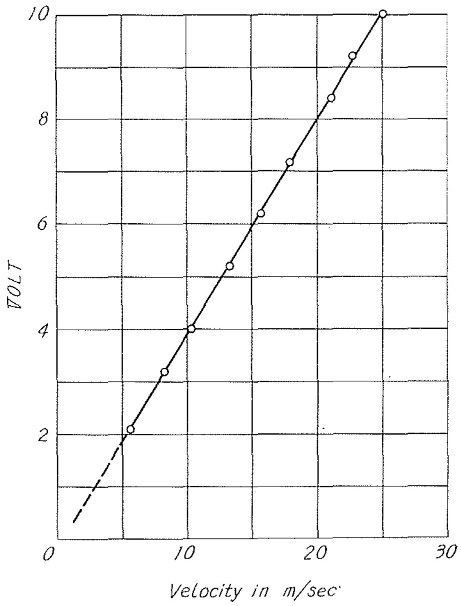

**Fig. 4. 1.** An example of the hot-wire calibration.

*d*) *Static pressure measurements*

If it is assumed that the static pressure in a turbulent boundary layer is constant and equal to that at the outer edge of the layer, the static pressure becomes constant over each cross-section normal to the main flow, and consequently may be estimated as the static pressure at the walls of the test section. The results of measurement of the static pressure using static pressure holes of a standard Prandtl-type Pitot tube show that the above assumption is reasonably satisfied.

## 4.2 Turbulent boundary layer along the floor of the test section

*a*) *Coordinate system*

In the following descriptions of the experimental results, the Cartesian coordinate system $x$, $y$ and $z$ will be used. The origin of the coordinate system is located at the mid-point of the tunnel floor at the entrance to the test section, as shown in Fig. 4.2. The $x$ axis is in the downstream direction, the $y$ axis is vertically upwards and the $z$ axis is taken normal to both $x$ and $y$ so as to form the right-hand system of coordinates.

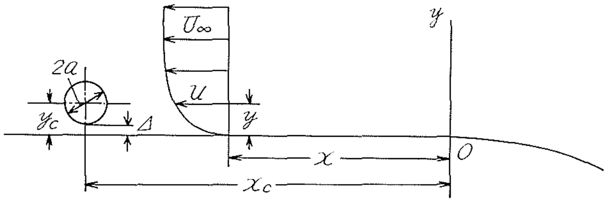

**Fig. 4. 2.** Illustration of the coordinate system.

### *b*) *Static pressure distribution*

Owing to the development of the turbulent boundary layer along the tunnel walls, the main flow velocity increases in a downstream direction, and at the same time the static pressure decreases in view of Bernoulli theorem. The measured static pressure distribution is shown in Fig. 4.3, together with the best fit curve obtained by the method of least squares;

$$p_{st} = -0.0050(x-28.3)\ \mathrm{mmAq} \qquad (4.2)$$

where $x$ must needs be measured in cm. Eq. (4.2) may be used to compute the static pressure at any desired position. The corresponding velocity distribution is given in Fig. 4.4.

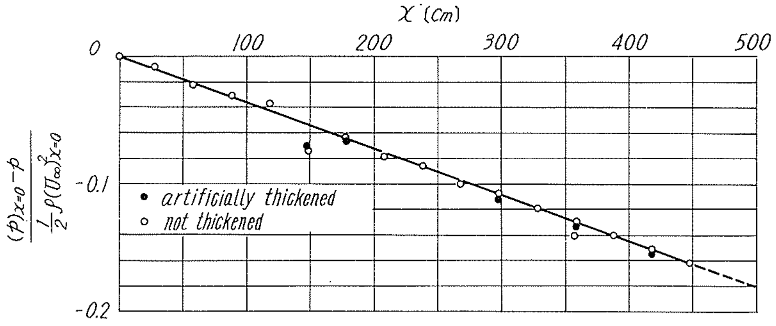

**Fig. 4.3.** Static pressure distribution along the tunnel.

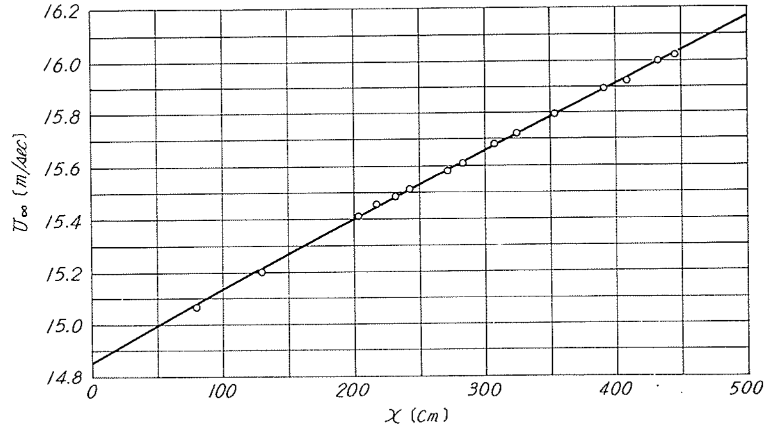

**Fig. 4.4.** Velocity distribution along the tunnel.

### *c*) *Two-dimensionality of the velocity field.*

In the experiments to be described in this chapter, the turbulent boundary layer along the tunnel floor is used as the approaching shear flow to the circular cylinders, then one must examine the two-dimensionality of the velocity field. Since the air tunnel has a rectangular cross section with the right-angled corners, secondary flows necessarily occur in any section normal to the main flow. The

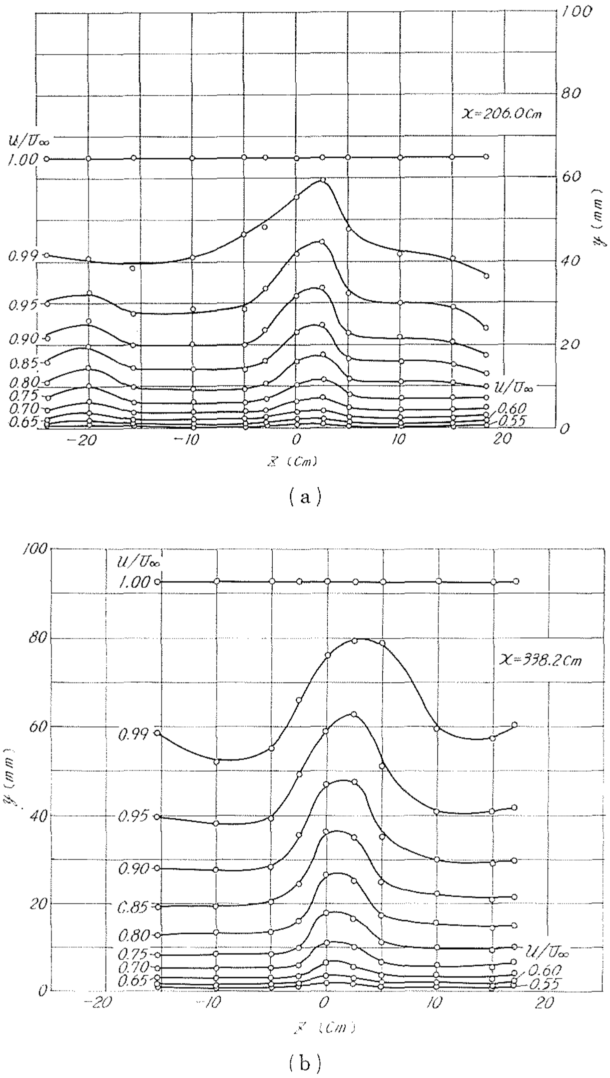

(a)

(b)

**Fig. 4.5.** Velocity contours in the $yz$-plane: (a) $x=206.0$ cm, (b) 338.2 cm.

longitudinal velocity distributions measured at the two sections $x=206.0$ cm and $x=338.2$ cm, respectively, are shown in Fig. 4.5 (a) and (b) in terms of $u/U_\infty$, $y$ and $z$. Although the velocity distributions outside the boundary layer are seen to be exactly two-dimensional, those within the boundary layer are somewhat distorted, the velocity near the center line $z=0$ being highly decreased. However, the velocity field in the vicinity of $z=-8$ cm may be said to be nearly two-dimensional, then the developments of the turbulent boundary layer are measured at this section.

### d) *Characteristics of the turbulent boundary layer*

Fig. 4.6 shows the mean velocity distributions in the turbulent boundary layer measured at the section $z=-8$ cm in terms of $u/U_\infty(x)$ and $y$. The displacement and momentum thicknesses, $\delta^*$ and $\theta$, defined by the equations

$$\delta^* = \int_0^\infty \left(1-\frac{u}{U_\infty}\right)dy\,, \qquad \theta = \int_0^\infty \frac{u}{U_\infty}\left(1-\frac{u}{U_\infty}\right)dy$$

are shown in Fig. 4.7 as functions of $x$. The viscous shear stress at the wall $\tau_w$ and the shear velocity $u_\tau$

$$\tau_w = \mu\left(\frac{\partial u}{\partial y}\right)_{y=0}, \qquad u_\tau = \left(\frac{\tau_w}{\rho}\right)^{1/2}$$

may be computed from the measured velocity profiles by means of the well-known momentum integral equation originally derived by Kármán:

$$\frac{\tau_w}{\rho U_\infty^2} = \frac{d\theta}{dx} + (H+2)\frac{\theta}{U_\infty}\frac{dU_\infty}{dx} \tag{4.3 a}$$

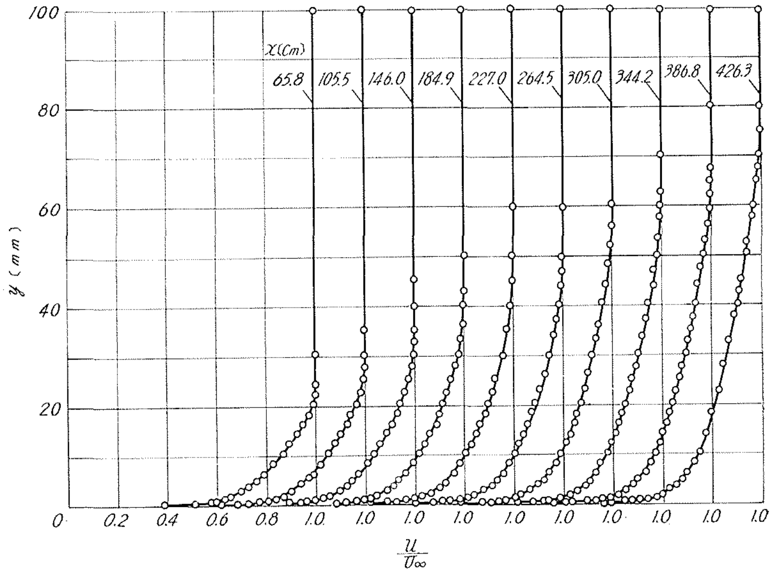

**Fig. 4. 6.** Mean velocity distribution in the turbulent boundary layer along the tunnel wall.

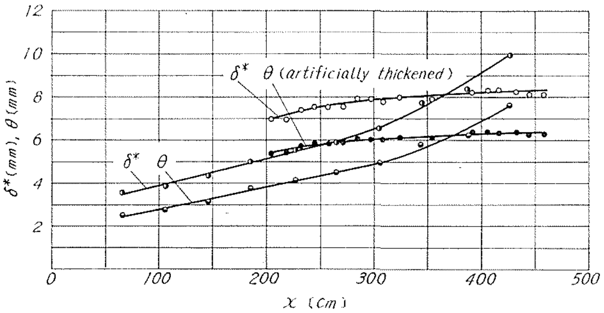

**Fig. 4. 7.** Distribution of displacement and momentum thicknesses.

or

$$\frac{u_\tau^2}{U_\infty^2}=\frac{d\theta}{dx}+(H+2)\frac{\theta}{\rho U_\infty^2}\left(-\frac{dp}{dx}\right) \tag{4. 3 b}$$

$H$ is called the shape factor of bonudary layers and defined by

$$H=\frac{\delta^*}{\theta} \tag{4. 4}$$

The values of $u_\tau/U_\infty$ thus determined are shown in Fig. 4. 8.

Fig. 4. 9 shows the same velocity profiles on a non-dimensional basis. In order to avoid the arbitrariness of $\delta$ (boundary layer thickness), the nondimensional distance from the wall $y/\delta^*$ is used. It is seen from Fig. 4. 9 that the nondimensional velocity profiles exhibit a similarity downstream from the section $x=65.8$ cm.

These profiles, together with the values of $H$ and $R_\theta$ $(=U_\infty\theta/\nu)$ computed at each section, may be compared with the data obtained by Klebanoff and Diehl [25] which are included in Fig. 4. 9.

The wall proximity law and the velocity-defect law for the velocity distribu-

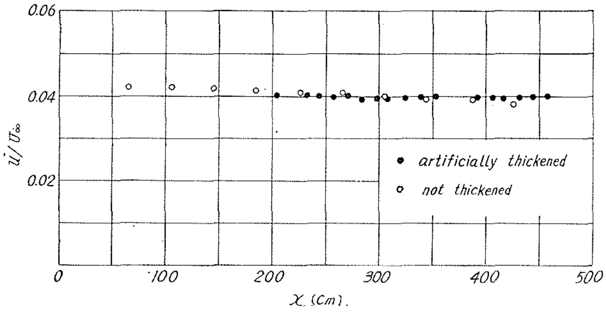

**Fig. 4. 8.** Distribution of shear velocity.

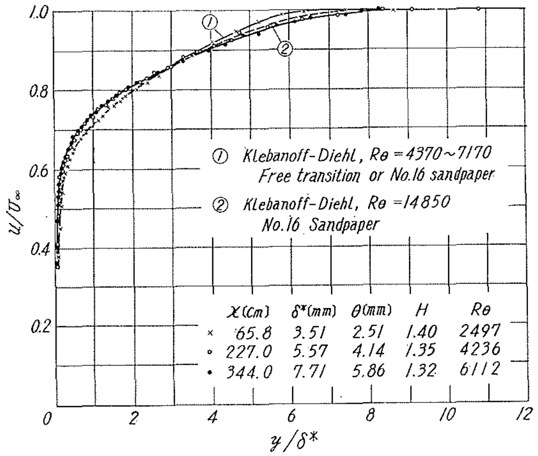

| | $x$(cm) | $\delta^*$(mm) | $\theta$(mm) | $H$ | $R_\theta$ |
|---|---|---|---|---|---|
| × | 65.8 | 3.51 | 2.51 | 1.40 | 2497 |
| ○ | 227.0 | 5.57 | 4.14 | 1.35 | 4236 |
| • | 344.0 | 7.71 | 5.86 | 1.32 | 6112 |

**Fig. 4. 9.** Nondimensional mean velocity distribution in the turbulent boundary layer.

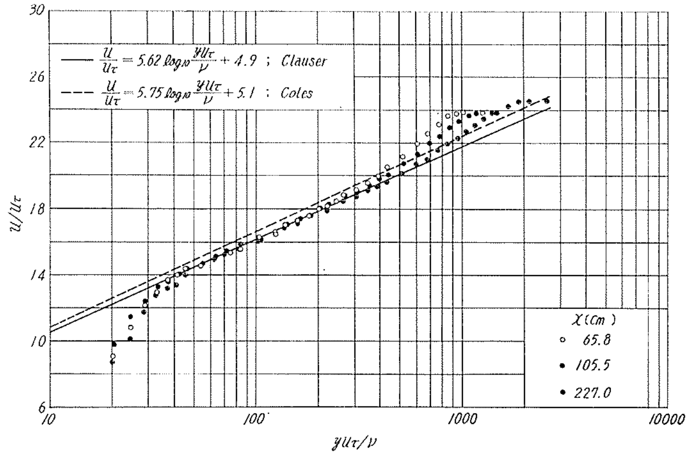

**Fig. 4. 10.** Comparison of experimental results with the logarithmic law.

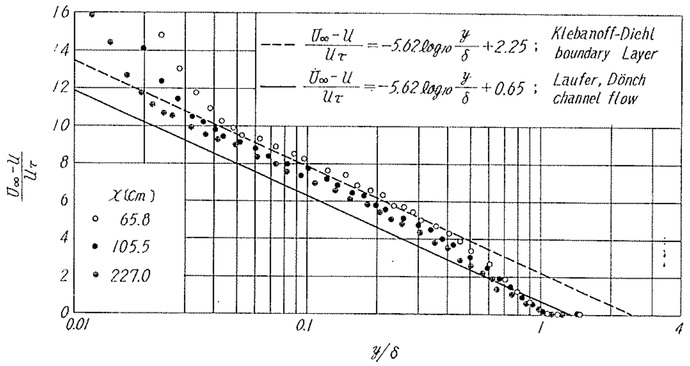

**Fig. 4. 11.** Comparison of experimental results with the velocity-defect law.

tion are compared with experimental results in Figs. 4. 10 and 4. 11. The mean velocity distributions for the turbulent boundary layer along the tunnel floor, together with the law of the wall suggested by Clauser [26] and Coles [27], are plotted in the form of $u/u_\tau$ against $yu_\tau/\nu$ in Fig. 4. 10. The law of the wall takes the form

$$\frac{u}{u_\tau} = 5.62 \log_{10} \frac{yu_\tau}{\nu} + 4.9 \qquad \text{(Clauser)} \tag{4. 5 a}$$

or

$$\frac{u}{u_\tau} = 5.75 \log_{10} \frac{yu_\tau}{\nu} + 5.1 \qquad \text{(Coles)} \tag{4. 5 b}$$

In contrast with the measurements for pipes and channels, it is seen that there is a systematic increase in the deviation from the logarithmic law as the Reynolds number decreases.

In Fig. 4. 11, the boundary layer results are plotted in the form suggested by the velocity-defect law, together with the channel results. It is seen that the present experiments give the velocity-defect law between the boundary layer with zero pressure gradient and the channel results. The velocity-defect law for each case is given respectively by

$$\frac{U_\infty - u}{u_\tau} = -5.62 \log_{10} \frac{y}{\delta} + 2.25 \tag{4. 6 a}$$

(Boundary layer, Klebanoff-Diehl [25])

$$\frac{U_\infty - u}{u_\tau} = -5.62 \log_{10} \frac{y}{\delta} + 0.65 \tag{4. 6 b}$$

(Channel, Laufer [28] and Dönch [29])

## 4. 3 Artificially thickened Turbulent Boundary Layer

As seen in Fig. 4. 6, the boundary layer thickness, $\delta$, is about 40 mm at the position $x=219.8$ cm where one intends to set the test cylinders. In order to carry out accurate measurements, it is desirable to use test cylinders of as large diameter as possible. However, for very large diameters, the finite cross-sectional area of the tunnel test section necessarily introduces complicated wall interference effects on the flow past the test cylinder, then the maximum diameter of the cylinder must be limited to one-tenth of the height of the test section at most. Since, as a compromise, the maximum diameter is selected to be 36.2 mm, it is better to have a thicker boundary layer than that described in section 4. 2. This need leads one to artificially thicken the boundary layer along the tunnel floor by means of some tripping devices.

### *a) Method of Artificial Thickening of Boundary Layer*

It is at once obvious that the objects protruding outward from a surface create a larger drag than that of the surface, and hence offer a means of producing a layer of de-energized flow in a comparatively short distance in a streamwise direction. The energy of the main flow is diverted into eddy motion in wakes, and, while the flow is turbulent, it does not have the same dynamic structure as a fully-developed turbulent boundary layer over a smooth surface. The question is, after leaving drag-producing objects, what length of smooth surface is needed for the layer to become the same as a smooth surface generated layer. It would seem that the length would be less than that required to generate a layer of the same thickness, but this is by no means a foregone conclusion.

An attempt of artificial thickening of the turbulent boundary layer with zero pressure gradient was made by Klebanoff and Diehl [25], for the purpose of facilitating the use of multi-wire hot-wire probes and minimizing errors due to wire length. Their measurements were performed with regard to the boundary layer on a flat plate mounted vertically along the center line of the tunnel test section. In one attempt to thicken the layer rods of several diameters were placed singly in the otherwise laminar layer and in contact with the surface at 4 feet from the leading edge. Another method consisted of cementing sand-paper to the surface beginning at the leading edge and extending to distances up to 2 feet downstream. By measuring the distributions of the mean velocity $u$, the intensity of longitudinal velocity fictuations $\sqrt{\overline{u'^2}}$ and one-dimensional spectrum of $u$-fluctuations across the layer, they found that, of these three criterions, the mean velocity distribution appeared to afford a simple means of identifying a fully-developed turbulent boundary layer. Each of the above methods was found to produce a turbulent boundary layer of desired thickness, namely, about two times of the original layer, at a specified section.

The turbulent boundary layer thus formed was found to become characteristic of that developed from the beginning on a smooth flat plate after passing over the required length of smooth surface. For a given boundary layer thickness, artificial thickening made possible a saving in length provided that there was enough length for the layer to become free from distortions.

However, in the present experiment, unsuccessful was an attempt to thicken the original turbulent boundary layer by cementing rough sand-paper onto the surface beginning at the entrance of the tunnel test section and extending up to 70 cm downstream. Another method was to place a circular rod of 3.2mm diameter on the surface at the entrance of the test section, but this also yielded no change in the mean velocity profile. This was not unexpected, because the boundary layer was already turbulent at the entrance of the test section, contrary to the case treated by Klebanoff and Diehl. Although a much larger rod of 19 mm diameter arranged in the same manner could thicken the boundary layer appreciably, the non-dimensional velocity profiles not only were distorted in excess, but did not attain a similarity even at the far downstream position of $x=250$ cm.

Finally, an appropriate position to place this rod was found by trial and error. Fig. 4. 12 shows the final configuration of the tripping rod.

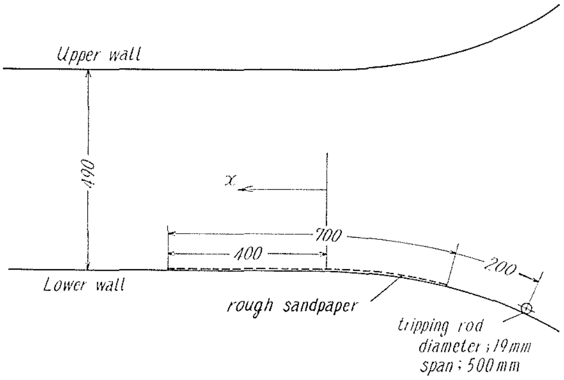

**Fig. 4. 12.** Configuration of the tripping rod.

*b*) *Static pressure distribution*

In order to examine the characteristics of the artificially thickened turbulent boundary layer, the static pressure distribution at the tunnel wall was measured at first. The results are shown in Fig. 4. 3. It will be seen from this figure that

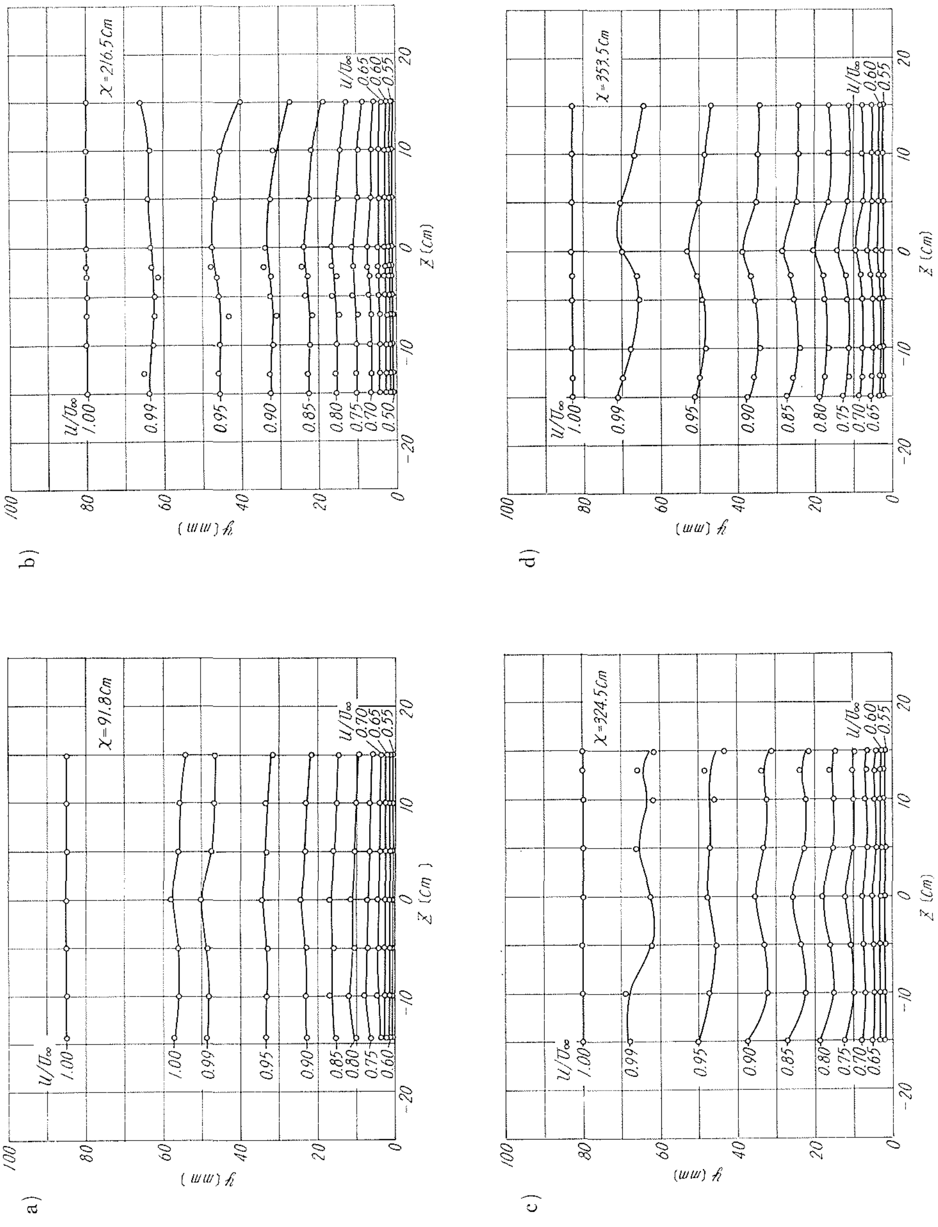

**Fig. 4. 13.** Two-dimensionality of the artificially thickened turbulent boundary layer: (a) $x$=91.8 cm, (b) 216.5 cm, (c) 324.5 cm and (d) 353.5 cm.

the static pressure is identical with that along the original boundary layer, and Eq. (4.2) may also be applied to the thickened boundary layer. This is because the increase in the displacement thickness due to articifical thickening is not so large, namely, 3 mm at the most, corresponding to the increase of 0.6% of the main flow velocity, that the extra decrease of the static pressure will be submerged in the pressure fluctuations and experimental errors.

### c) *Two-Dimensionality of the Artificially Thickened Boundary Layer*

Mean velocity distributions in the artificially thickened boundary layer are measured at four sections, that is, $x=91.8$ cm, 216.5 cm, 324.5 cm and 353.5 cm, in order to examine the two-dimensionality of the flow. These are shown in Fig. 4.13. Comparing these figures with Figs. 4.5 (a) and (b), one can see that the two-dimensionality of the flow is remarkably improved by the introduction of the tripping rod. Especially, the flow fields in the sections $x=91.8$ cm and $x=216.5$ cm may be said to be almost completely two-dimensional. The equi-velocity lines at further downstream sections $x=324.5$ cm and $x=353.5$ cm are somewhat distorted, and are believed to demonstrate the development of the secondary flow. However, since the two-dimensionality of the flow is satisfactory as a whole, the development of the boundary layer is measured at the section $z=-8$ cm, as was done for the boundary layer without the tripping rod.

### d) *Characteristics of the Artificially Thickened Boundary Layer.*

#### (1) Mean Velocity

The mean velocity profiles in the artificially thickened boundary layer are shown in Fig. 4.14, at a number of sections downstream from $x=203.7$ cm. From a comparison of this figure with Fig. 4.6, it will be seen that the boundary layer

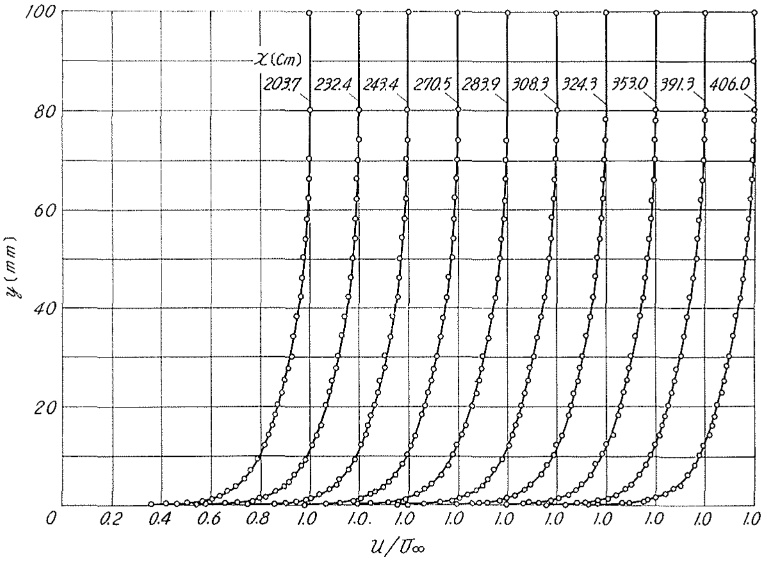

**Fig. 4. 14.** Mean velocity distribution in the artificially thickened turbulent boundary layer.

is increased by about 20 mm in thickness at the section $x=219.8$ cm where the test cylinders are to be arranged. The values of the displacement and momentum thicknesses are shown in Fig. 4.7. The shear velocity is also shown in Fig. 4.8 in terms of $u_\tau/U_\infty$ and $x$. The values of $u_\tau/U_\infty$ are almost identical with those for the original boundary layer.

(2) Turbulence Distribution

The values of $\sqrt{\overline{u'^2}}$, $\sqrt{\overline{v'^2}}$ and $\overline{u'v'}$ were measured with a single hot wire (Arie [30]) in order to clarify the characteristics of turbulence of the thickened boundary layer.

Measurement of $\sqrt{\overline{u'^2}}$ : The single hot wire was supported vertically in $xy$ plane. In this case, the hot wire is sensitive to $u'$ and $w'$, but when $u$ is large, the error for $u'$ which will be caused by $w'$ is negligible. With the hot wire supported in this manner, the mean horizontal velocity $u$ is also measurable. The measurement of this component of velocity agreed fairly well with the results previously obtained with the total head tube. The quantity $\sqrt{\overline{u'^2}}$ can be computed from

$$\sqrt{\overline{u'^2}}=A\times V_{\mathrm{RMS}} \tag{4.7}$$

in which $V_{\mathrm{RMS}}$ is the root-mean-square value of the fluctuating voltage and $A$ is the slope of the voltage-velocity characteristics of the hot wire.

Measurement of $\sqrt{\overline{v'^2}}$ and $\overline{u'v'}$ : When the single hot wire is supported at an angle of 60° against the $x$ axis in the $xy$ plane, the root-mean-square of the fluctuating voltage gives a clue for obtaining $\sqrt{\overline{v'^2}}$ and $\overline{u'v'}$. In this case,

$$(A\times V_{\mathrm{RMS}})_1=(\overline{(u'\sin 60^\circ+v'\sin 30^\circ)^2}\,)^{1/2}$$

or

$$(A\times V_{\mathrm{RMS}})_1^2=(0.866\sqrt{\overline{u'^2}})^2+(0.5\sqrt{\overline{v'^2}})^2+0.866\,\overline{u'v'} \tag{4.8}$$

In the same way, when the hot wire is supported at an angle of 120° to the $x$ axis in the $xy$ plane, one obtains

$$(A\times V_{\mathrm{RMS}})_2^2=(0.866\sqrt{\overline{u'^2}})^2+(0.5\sqrt{\overline{v'^2}})^2-0.866\,\overline{u'v'} \tag{4.9}$$

The sum of Eqs. (4.8) and (4.9) gives

$$(A\times V_{\mathrm{RMS}})_1^2+(A\times V_{\mathrm{RMS}})_2^2=1.5(\sqrt{\overline{u'^2}})^2+0.5\,(\sqrt{\overline{v'^2}})^2$$

or

$$\sqrt{\overline{v'^2}}=\sqrt{2}\left[(A\times V_{\mathrm{RMS}})_1^2+(A\times V_{\mathrm{RMS}})_2^2-1.5\,(\sqrt{\overline{u'^2}})^2\right]^{1/2} \tag{4.10}$$

Since $\sqrt{\overline{u'^2}}$ is obtainable with Eq. (4.7), $\sqrt{\overline{v'^2}}$ can be obtained with Eq. (4.10). When Eq. (4.9) is subtracted from Eq. (4.8), $\overline{u'v'}$ is obtained as

$$\overline{u'v'}=\frac{1}{1.732}\left[(A\times V_{\mathrm{RMS}})_1^2-(A\times V_{\mathrm{RMS}})_2^2\right] \tag{4.11}$$

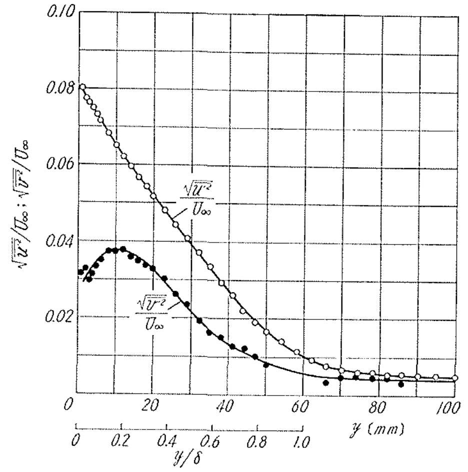

**Fig. 4. 15.** Variation of the fluctuating turbulent velocity components.

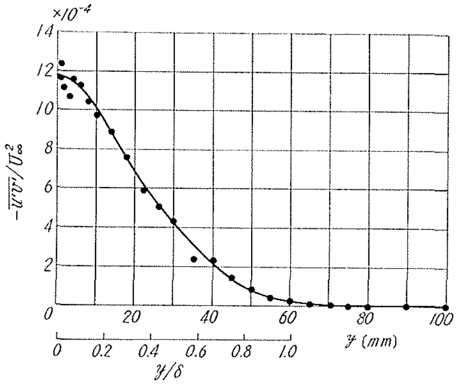

**Fig. 4. 16.** Variation of the turbulent Reynolds stress.

The results of measurements at the section $x=221.3$ cm are plotted on Figs. 4.15 and 4.16.

(3) Non-Dimensional Plot of Mean Velocity and Turbulence

The non-dimensional mean velocity $u/U_\infty$ at various sections are shown in Fig. 4. 17, the abscissa being the nondimensional distance $y/\delta^*$ from the wall. Since the Reynolds number $R_\theta$ does not differ so much for each section, the measured velocities fall on the same curve. In this figure, the non-dimensional mean velocity distributions for free transition and for a 0.25 in. cylindrical tripping rod proposed by Klebanoff and Diehl are included. It should be noted that their results for the 0.25 in. rod coincides with that of the 19 mm rod used in the present experiment. The shape factor of the velocity profile is about 1.3 at each section.

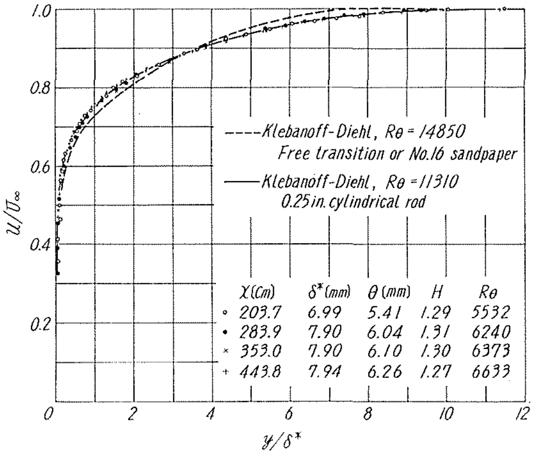

**Fig. 4. 17.** Nondimensional mean velocity distribution.

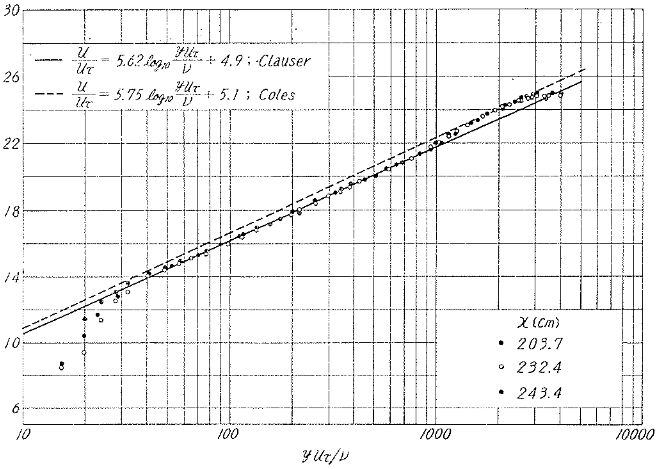

**Fig. 4.18.** Logarithmic velocity distirbution law.

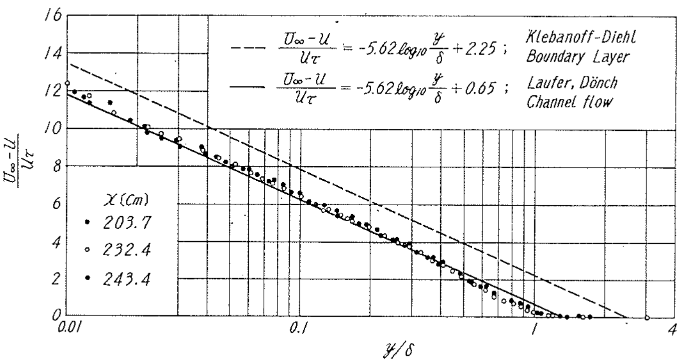

**Fig. 4.19.** Velocity-defect law.

The non-dimensional mean velocities are plotted in Figs. 4.18 and 4.19 in the form of $u/u_\tau$ against $yu_\tau/\nu$ and $(U_\infty - u)/u_\tau$ against $y/\delta$, respectively. In the region where the law of the wall is valid the mean velocities are well represented by Clauser's law of the wall Eq. (4.5 a). However, Fig. 4.19 shows that the artificially thickened boundary layer has the velocity-defect law Eq. (4.6 b) for channel flow rather than that for the boundary layer derived from the data of Schulz-Grunow and Klebanoff and Diehl.

Fig. 4.20 shows the longitudinal turbulence level $\sqrt{\overline{u'^2}}/U_\infty$ against the non-dimensional distance $y/\delta^*$ at various sections, together with the nondimensional mean velocity $u/U_\infty$.

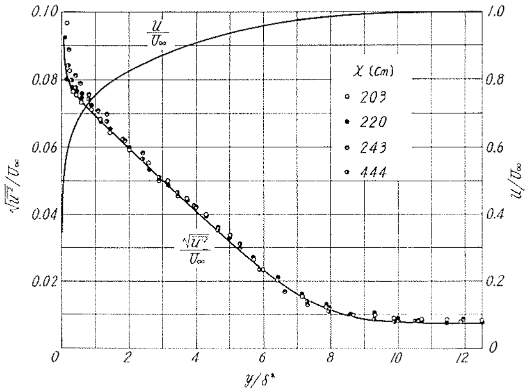

**Fig. 4.20.** Similarity of the longitudinal component of the turbulent velocity.

It will be seen from this figure that a similarity in the turbulent fluctuating velocities exists, which may suggest that the artificially thickened boundary layer has fully developed and thus attained dynamical equilibrium at the sections of measurements.

## 4.4 Experiments on the Flow near a Circular Cylinder in the Turbulent Boundary Layer

### *a) Test Cylinders*

The test cylinders were made of carefully machined brass cylinders and had the diameters of $2a=36.2$ mm, 25.0 mm, 18.5 mm and 9.45 mm, respectively. Each of the cylinders was mounted horizontally with bearings to the side walls of the tunnel so that the span coincided with the width of the tunnel. The cylinders could be rotated abot their axis in order to obtain any angular position of the pressure hole of 0.5 mm diameter. The angular position was read on the protractor attached to the bearing. The distance between the cylinders and the tunnel floor could be changed arbitrarily by adjusting the position of the bearings.

The angular position of the pressure hole was measured from the stagnation point when the cylinder was placed in a uniform flow. The stagnation point was previously determined by measuring the pressure distribution around the test cylinder placed at the outside of the boundary layer.

In order to simulate the flow about a cylinder of an infinite span in a wind tunnel it is necessary to eliminate the end effects. For this purpose, the span of the test cylinders was chosen to coincide with the whole width of the tunnel, and the junction of the test cylinder with the side walls of the tunnel was carefully sealed with oil clay. Another method was to mount two circular baffle plates of various diameters and 1 mm thickness on each side of the pressure hole. The interval between the baffle plates was 20 cm and the pressure hole was located at the mid-point of the baffle pates.

### *b) Static Pressure Distribution around the Test Cylinders*

Fig. 4.21 is the definition sketch of the test cylinder placed in the turbulent boundary layer. $2a$ is the diameter of the test cylinder, $\varDelta$ is the clearance between the test cylinder and the plane boundary wall, and $\theta$ is the angle measured from the stagnation point for uniform flow to the direction of positive $y$. The surface of the test cylinder that corresponds to $0° \leqq \theta \leqq 180°$ will be denoted by the suffix "$u$" (upper), and that for $-180° \leqq \theta \leqq 0°$ by the suffix "$l$" (lower). $U_0$ is the approaching velocity at the center of the test cylinder.

Each test cylinder was mounted at the section $x=219.8$ cm where the artificially thickened boundary layer was fully developed and had the following properties:

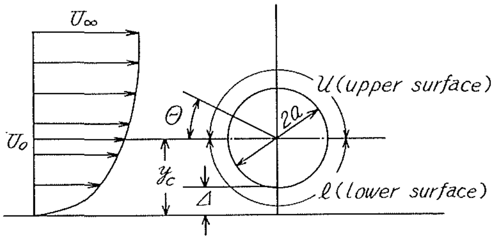

**Fig. 4.21.** Definition sketch of the test cylinder placed in the turbulent boundary layer.

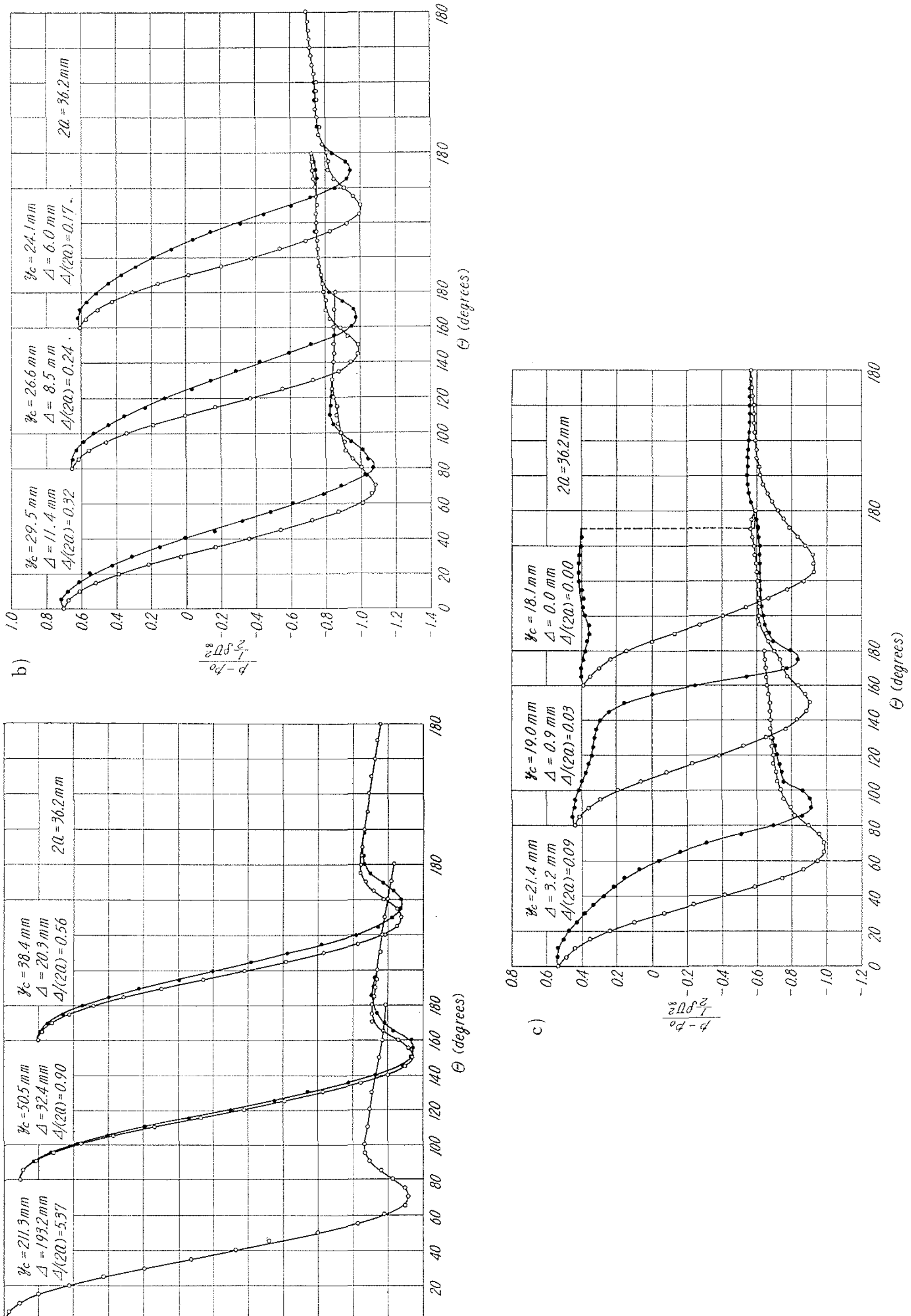

**Fig. 4. 22.** Pressure distribution around a circular cylinder of 36.2 mm diameter placed in the turbulent boundary layer; ○, $p_u$, ●, $p_l$.
]

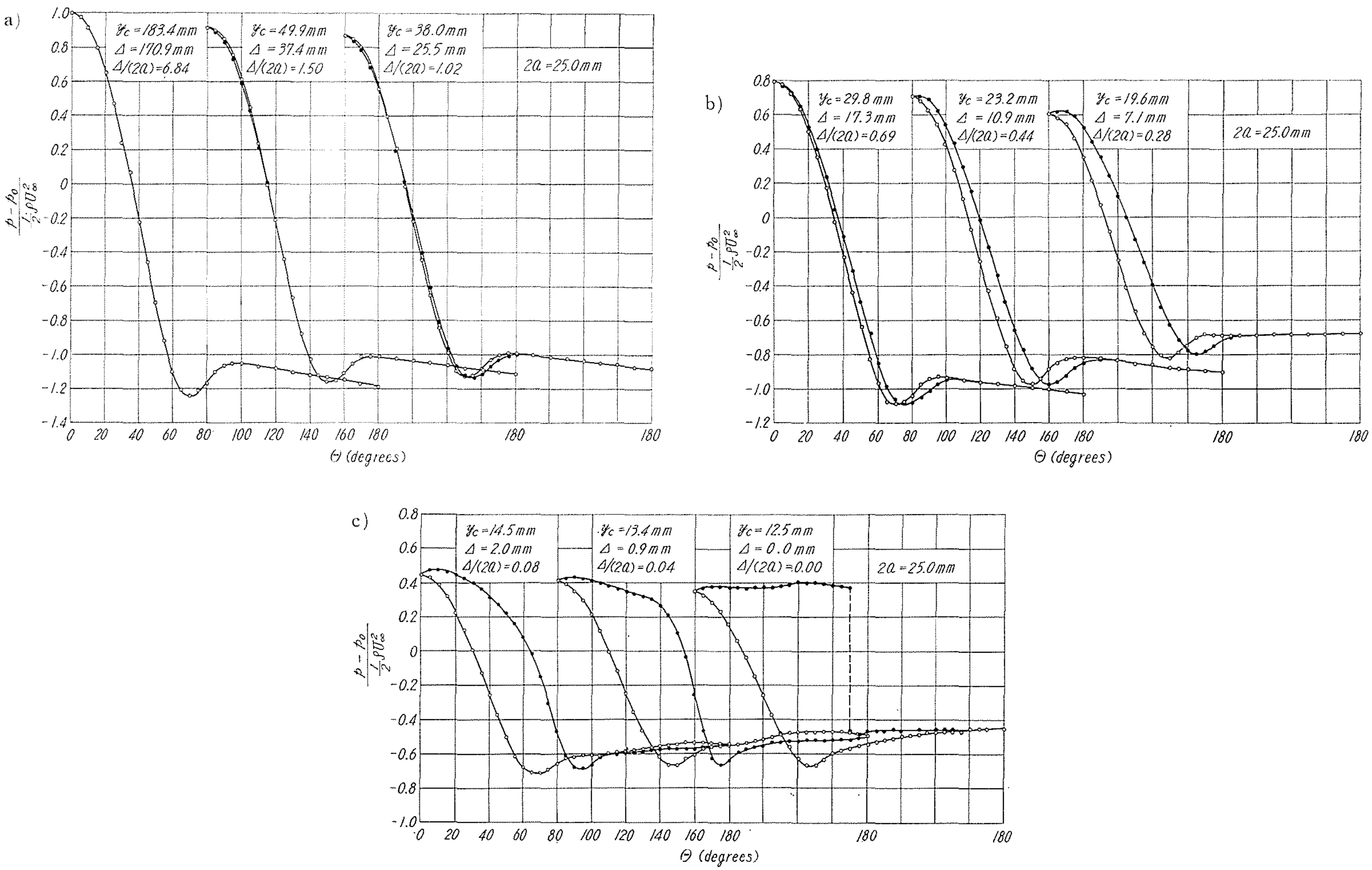

**Fig. 4.23.** Pressure distribution around a circular cylinder of 25.0 mm diameter placed in the turbulent boundary layer; ○, $p_u$, ●, $p_l$.

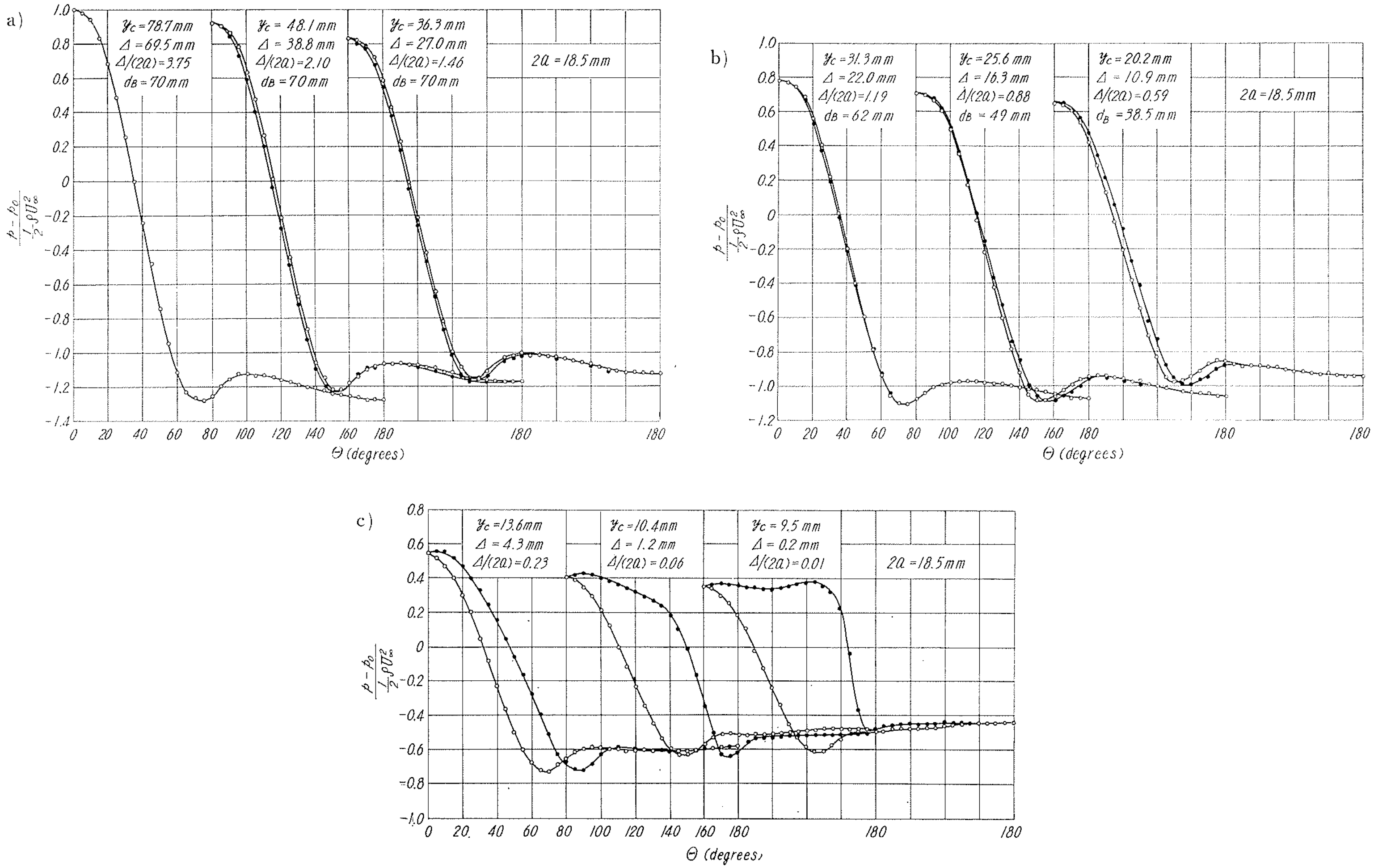

**Fig. 4. 24.** Pressure distribution around a circular cylinder of 25.0 mm diameter placed in the turbulent boundary layer.; ○, $p_u$, ●, $p_l$.

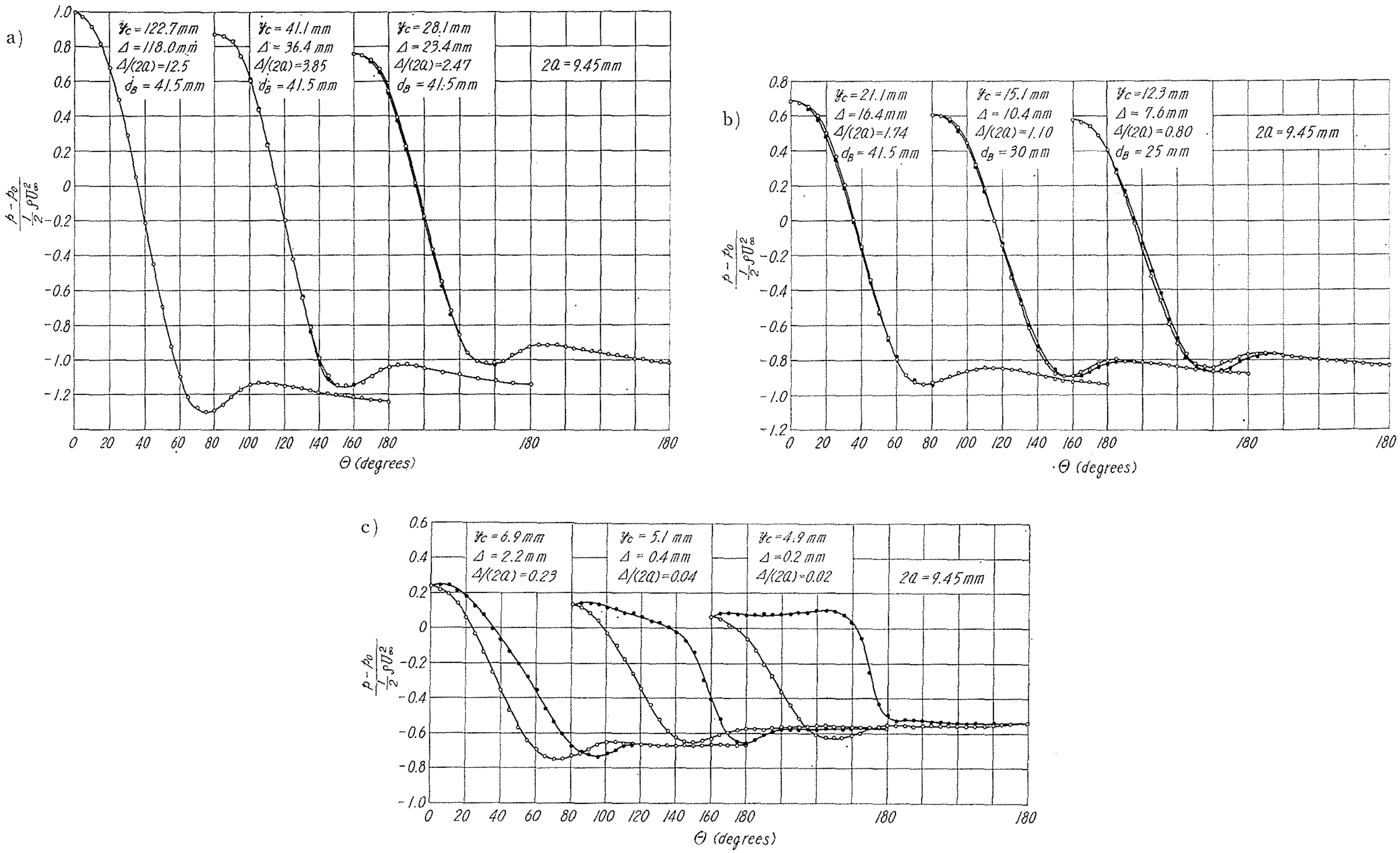

**Fig. 4. 25.** Pressure distribution around a circular cylinder of 9.45 mm diameter placed in the turbulent boundary layer.; ○, $p_u$, ●, $p_l$.

$U_\infty = 15.46$ m/sec , $\delta = 60$ mm , $\delta^* = 7.22$ mm , $\theta = 5.55$ mm

$R_\delta = 61250$ , $R_{\delta^*} = 7382$ , $R_\theta = 5675$

The static pressure distributions were measured for the four test cylinders described in (a), and the results are shown in Figs. 4.22, 4.23, 4.24 and 4.25, respectively. The pressure distributions are given in the form of the pressure coefficient $\frac{p-p_0}{(1/2)\rho U_\infty^2}$ against the angle $\Theta$, the parameter being the ratio $\Delta/(2a)$. It is seen from these figures that there occurs a systematic decrease in the stagnation pressure as the clearance $\Delta$ decreases. At the same time, the pressure distributions around the upper and lower surfaces of the cylinder are found to deviate systematically from the symmetry. It should also be noted that the effects of both the velocity gradient of the approaching flow and the plane boundary wall are clearly seen in the pressure distribution around the front part of the cylinder. Namely, the velocity gradient tends to increase the pressure on the upper surface of the cylinder compared with the pressure on the lower suface, which is seen in Fig. 4.23 (a) and (b), and quite conversely the effect of the plane boundary wall is to increase the pressure on the lower surface. The stagnation point shifts to the lower surface of the cylinder as $\Delta/(2a)$ decreases, and attains the maximum value of about −10°.

The effect of the baffle plates was tested by measuring the pressure on the test cylinders with and without baffle plates. The measurements were made in the central part of the tunnel where the velocity was uniform and the results are shown in Fig. 4.26, together with the results obtained by Fage and Falker [23]. It is seen from this figure that the static pressure at the rear of the test cylinder with the baffle plates decreases still further than that of the cylinder without the baffle plates. It is also seen that the pressure distribution around the cylinders without baffle plates coincides quite well with the data obtained by Fage and

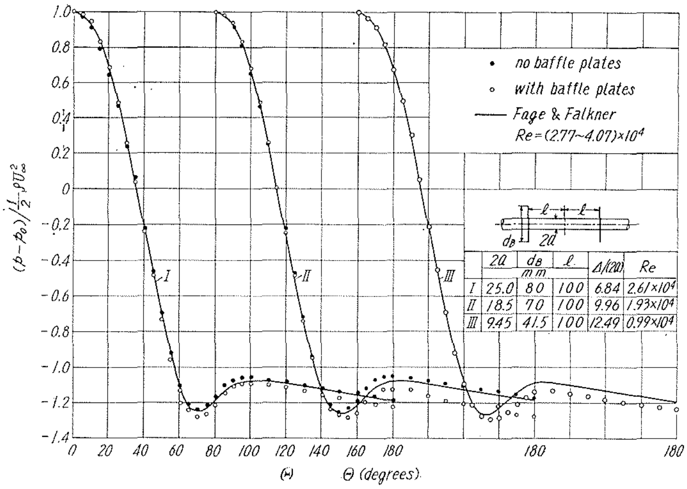

| | 2a | $d_B$ | ℓ | Δ/(2a) | Re |
|---|---|---|---|---|---|
| | mm | | | | |
| I | 25.0 | 80 | 100 | 6.84 | $2.61\times10^4$ |
| II | 18.5 | 70 | 100 | 9.96 | $1.93\times10^4$ |
| III | 9.45 | 41.5 | 100 | 12.49 | $0.99\times10^4$ |

**Fig. 4. 26.** Effect of the baffle plates on the pressure distribution around the circular cylinder.

Falkner. Therefore, the baffle plates overcompensate the pressure at the rear of the cylinder.

Fig. 4.27 shows variation of the stagnation pressure $(p_{\text{stag}}-p_0)\Big/\left(\frac{1}{2}\rho U_\infty^2\right)$ against the distance $y$ from the plane wall. The distribution of the dynamic pressure $\left(\frac{1}{2}\rho u^2\right)\Big/\left(\frac{1}{2}\rho U_\infty^2\right)$ in the undisturbed turbulent boundary layer is also included in this figure. It is clearly seen that the stagnation pressure takes a lower value for larger cylinders than for smaller ones when the distance of the center of the cylinders from the plane wall is the same. This fact reveals that the undisturbed location of the stagnation streamline is nearer to the plane wall with the increase in size of the diameter of the cylinder. This phenomenon may also be suggested by the theoretical analysis described in chapter 2.

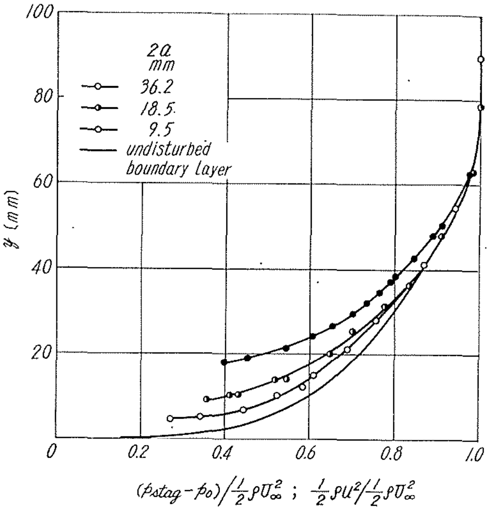

**Fig. 4.27.** Variation of the stagnation pressure of the circular cylinder placed in the turbulent boundary layer.

However, since the velocity gradient is not constant through the boundary layer, it is slightly difficult to define the quantity $\omega$ introduced into the theoretical consideration. A possible choice may be the undisturbed velocity gradient $\partial u/\partial y$ at the center of the cylinder. With the values of $\omega$ thus determined, the stagnation pressure coefficient and the location of the stagnation streamline far upstream of the cylinder are computed from

$$\frac{p_{\text{stag}}-p_0}{\frac{1}{2}\rho U_0^2} = 1+\lambda(\lambda-2)(1-\tanh\alpha) \tag{4.12}$$

$$\frac{y_s}{a} = \frac{\cosh\alpha}{\lambda}\left[\lambda-1+\left\{(\lambda-1)^2+\lambda(2-\lambda)\tanh\alpha\right\}^{1/2}\right] \tag{4.13}$$

The values of $(p_{\text{stag}}-p_0)\Big/\left(\frac{1}{2}\rho U_0^2\right)$ and $y_s/a$ obtained by Eqs. (4.12) and (4.13) were of the same order of magnitude as those determined experimentally, but a precise agreement was not obtained. The reason for this is probably that the choice of $\omega$ is not adequate. Next an attempt was made to use the values of $\omega$ counted backward from Eq. (4.12) with the experimentally determined stagnation pressure coefficient, in order to compute the theoretical pressure distribution. The results are shown in Figs. 4.28 (a), (b) and (c). It should be noted that the position of the stagnation point is well predicted by the theory.

### c) *Lift and Drag Forces of the Circular Cylinder*

The static pressures on the surface of the test cylinders are integrated to

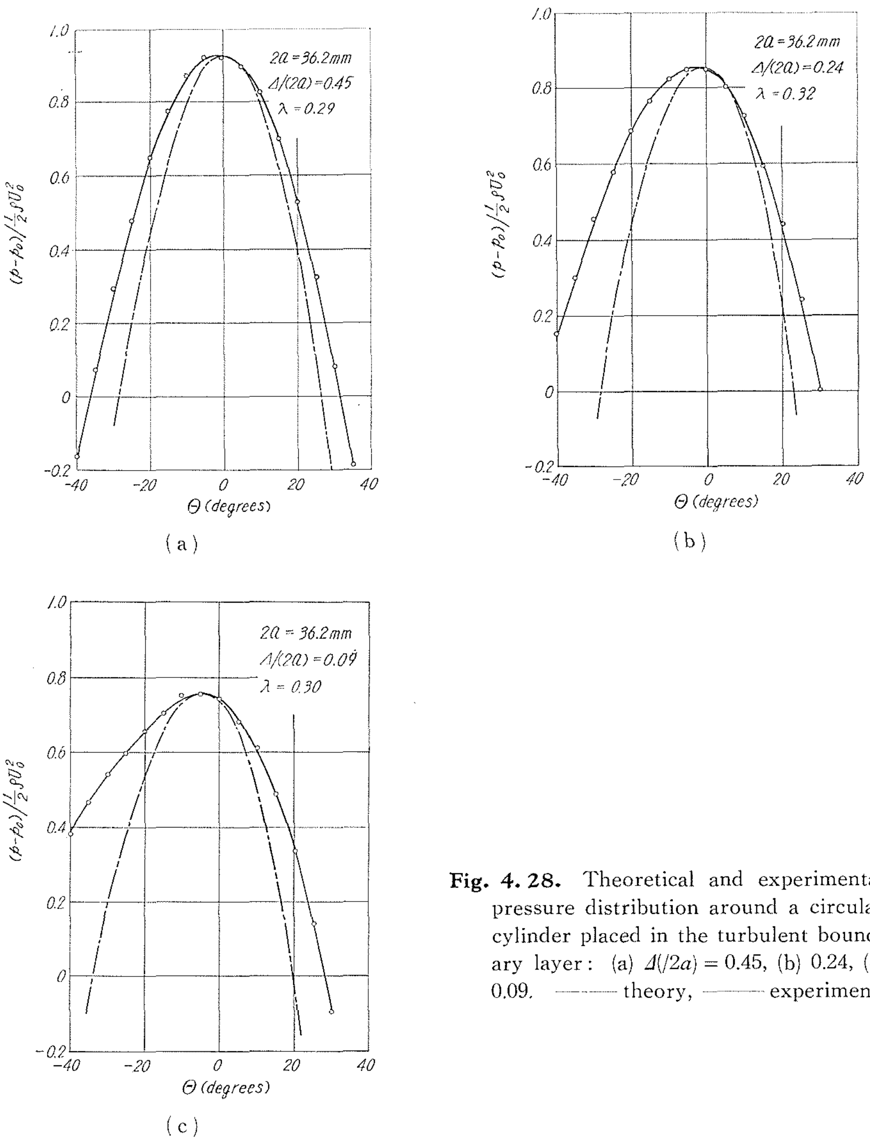

**Fig. 4. 28.** Theoretical and experimental pressure distribution around a circular cylinder placed in the turbulent boundary layer: (a) $\Delta/(2a) = 0.45$, (b) 0.24, (c) 0.09. ——— theory, ——— experiment.

obtain the lift and drag forces acting upon them in the form of lift and drag coefficients, $C_{Lp}$ and $C_{Dp}$:

$$C_{Lp} = \frac{L_p}{\frac{1}{2}\rho U_0^2 \cdot 2a} = \frac{1}{2}\int_0^{\pi} (C_{pl} - C_{pu}) \sin\Theta \, d\Theta$$

$$C_{Dp} = \frac{D_p}{\frac{1}{2}\rho U_0^2 \cdot 2a} = \frac{1}{2}\int_0^{\pi} (C_{pl} + C_{pu}) \cos\Theta \, d\Theta$$

Suffix $p$ given to $C_L$ and $C_D$ means that they are computed from pressure only. The results are shown in Fig. 4. 29, together with the values of Reynolds number.

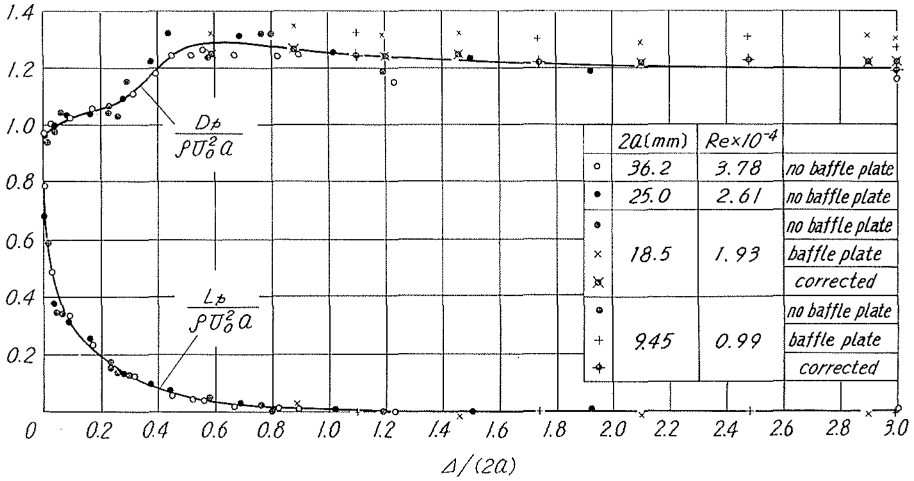

**Fig. 4. 29.** Lift and drag coefficients of the circular cylinder placed in the turbulent boundary layer.

It is seen from this figure that, with $\Delta/(2a)$ decreasing, the lift coefficient increases montonically from 0 to the maximum value of about 0.8 at $\Delta/(2a)=0$, and conversely the drag coefficient decreases from 1.2 to the minimum value of about 0.95 after passing the maximum value of about 1.3 in the vicinity of $\Delta/(2a)=0.6$. The positive value of $C_{Lp}$ implies that a circular cylinder in the turbulent boundary layer acquires a transverse force that tends to move it from the boundary wall, as was previously predicted qualitatively by the theoretical analysis of the uniform shear flow. $C_{Lp}$ vanishes at $\Delta/(2a)=1.0$ approximately.

The value of $C_{Dp}$ is about 1.2 for a large $\Delta/(2a)$, which is equal to the drag coefficient of a circular cylinder in an unbounded uniform flow. The circular cylinders with baffle plates yield somewhat higher values of $C_{Dp}$, i. e. 1.3 for a large $\Delta/2(a)$, which corresponds to a larger decreases in static pressure at the rear. However, it is possible to estimate the effect of the baffle plates on the drag coefficient by making use of the experimentally determined pressure distribution shown in Fig. 4. 26. Since the drag coefficient is almost but not quite detemined by the static pressure at the rear surface of the cylinder, the ratio of $C_{Dp}$ to $(C_{Dp})_b$, the drag coefficient of the cylinder with baffle plates, may be written as

$$\frac{C_{Dp}}{(C_{Dp})_b}=\frac{C_{pcr}}{(C_{pcr})_b}$$

where $(C_{pcr})_b$ and $C_{pcr}$ imply the pressure coefficients at the rear of the cylinder with or without the baffle plates. This ratio is found from Fig. 4. 26 to be approximately 0.95. The corrected values of the drag coefficient are also shown in Fig. 4. 29.

It should be noted in Fig. 4. 29 that the data of $C_{Lp}$ and $C_{Dp}$ fall on the same curves, respectively, with acceptable accuracy. This fact may be of great practical importance when one studies the motion of solid particles located in the turbulent boundary layer. Since the ratio $C_{Lp}/C_{Dp}$ is an important parameter for

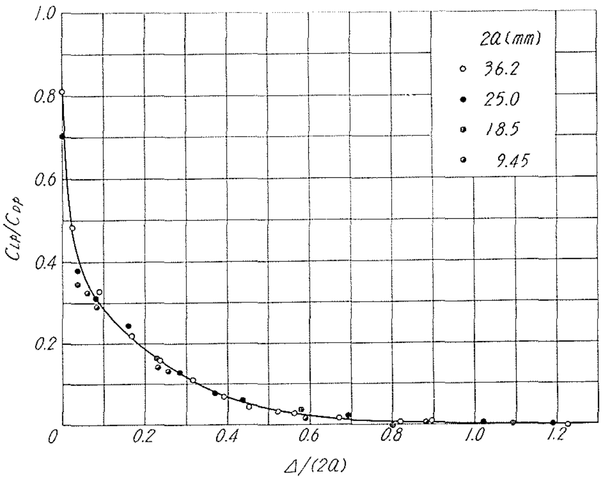

**Fig. 4. 30.** Variation of the ratio $C_{Lp}/C_{Dp}$ with respect to $\Delta/(2a)$.

practical purposes, its distribution with respect to $\Delta/(2a)$ is plotted in Fig. 4. 30. These data also fall on a single curve.

### d) *Estimation of Laminar Boundary Layer on the Circular Cylinder*

In the last section, the lift and drag coefficients were computed only from the static pressure on the circular cylinders, and consequently the effect of viscous skin friction was not included. In this section, the laminar boundary layer developing along the surface of the circular cylinder was considered to some detail for the purpose of estimating the contribution of viscous shear stress to the lift and drag coefficients. In order to calculate the laminar boundary layer, use is made of the Blasius series extended to an asymmetrical case and the approximate method due to Pohlhausen and Walz, respectively.

#### (1) Estimation due to the Blasius series for an Asymmetrical Case

The laminar boundary layer on a flat plate placed parallel to a uniform shear flow has been considered by several authors. Li [31], Ting [32], Murray [33] and Devan [34] treated this problem theoretically on the basis of various procedures and revealed that the effect of shear on the laminar boundary layer is not of great importance near the leading edge, but it becomes dominant as the downstream region is approached. However, an exact analysis of laminar boundary layer on a cylindrical body, such as a circular cylinder, placed in a shear flow has not been made as yet, and this problem remains to be solved.

In the present consideration, it is assumed that Prandtl's boundary layer equations for a two-dimensional steady flow

$$u\frac{\partial u}{\partial x}+v\frac{\partial u}{\partial y}=U\frac{dU}{dx}+\nu\frac{\partial^2 u}{\partial y^2} \tag{4. 14}$$

$$\frac{\partial u}{\partial x}+\frac{\partial v}{\partial y}=0 \tag{4. 15}$$

can be applicable, with the boundary conditions

$$y=0\ :\ u=0\,,\quad v=0\,;\qquad y=\infty\ :\ u=U(x) \tag{4.16}$$

It should be noted that $x$ denotes here the distance from the stagnation point measured along the surface of the cylinder and $y$ is the distance measured at right angles to the surface. $u$ and $v$ are the components of velocity in the $x$ and $y$ directions, respectively. If one defines the non-dimensional variables

$$\bar{x}=x/(2a)\,,\qquad \bar{y}=(y/(2a))\sqrt{R_e}\,,\qquad \bar{u}=u/U_\infty\,,\qquad \bar{v}=(v/U_\infty)\sqrt{R_e}\,,$$
$$\bar{U}=U/U_\infty\,,\qquad \bar{\psi}=\psi/\sqrt{2a\nu U_\infty}\,,\qquad R_e=2aU_\infty/\nu$$

where $a$ is the radius of the circular cylinder and $U_\infty$ is the velocity outside of the turbulent boundary layer in which the cylinder is placed, Eqs. (4.14) and (4.15) may be rewritten as

$$\bar{u}\frac{\partial\bar{u}}{\partial\bar{x}}+\bar{v}\frac{\partial\bar{u}}{\partial\bar{y}}=\bar{U}\frac{d\bar{U}}{d\bar{x}}+\frac{\partial^2\bar{u}}{\partial\bar{y}^2} \tag{4.17}$$

$$\frac{\partial\bar{u}}{\partial\bar{x}}+\frac{\partial\bar{v}}{\partial\bar{y}}=0 \tag{4.18}$$

Now, it is possible to transform these two equations with two unknowns into one equation with one unknown by introducing the stream function $\bar{\psi}$. Putting

$$\bar{u}=\frac{\partial\bar{\psi}}{\partial\bar{y}}\,,\qquad \bar{v}=-\frac{\partial\bar{\psi}}{\partial\bar{x}} \tag{4.19}$$

one sees that the continuity equation is satisfied automatically, and Eq. (4.17) becomes

$$\frac{\partial\bar{\psi}}{\partial\bar{y}}\frac{\partial^2\bar{\psi}}{\partial\bar{x}\partial\bar{y}}-\frac{\partial\bar{\psi}}{\partial\bar{x}}\frac{\partial^2\bar{\psi}}{\partial\bar{y}^2}=\bar{U}\frac{d\bar{U}}{d\bar{x}}+\frac{\partial^3\bar{\psi}}{\partial\bar{y}^3} \tag{4.20}$$

The boundary conditions become from Eq. (4.16)

$$\bar{y}=0\ :\ \frac{\partial\bar{\psi}}{\partial\bar{y}}=0\,,\qquad \frac{\partial\bar{\psi}}{\partial\bar{x}}=0$$
$$\bar{y}=\infty\ :\ \frac{\partial\bar{\psi}}{\partial\bar{y}}=\bar{U}(\bar{x})$$

It should be emphasized here that, although the external shear does not appear explicitly in the mathematical formulation, its effect is treated in the form of an asymmetry of flow on both sides of the stagnation point, in exactly the same manner as the effect of the plane wall that exists in the vicinity of a circular cylinder.

Let the velocity outside the boundary layer be given by the series

$$\bar{U}(\bar{x})=\bar{u}_1\bar{x}+\bar{u}_2\bar{x}^2+\bar{u}_3\bar{x}^3+\cdots \tag{4.21}$$

The coefficients $\bar{u}_1$, $\bar{u}_2$, $\cdots$ depend on the flow about the cylinder and are to be considered known. The normal distance from the surface is made dimensionless by assuming

$$\eta = \bar{y}\sqrt{\frac{\bar{u}_1}{\nu}} \tag{4.22}$$

One adapts the following form for the stream function:

$$\begin{aligned}\bar{\psi} = \sqrt{\frac{1}{\bar{u}_1}}\Big\{&\bar{u}_1\bar{x}f_1(\eta) + 3\bar{u}_2\bar{x}^2 f_2(\eta) + 4\bar{u}_3\bar{x}^3 f_3(\eta)\\ &+ 5\bar{u}_4\bar{x}^4 f_4(\eta) + 6\bar{u}_5\bar{x}^5 f_5(\eta) + 7\bar{u}_6\bar{x}^6 f_6(\eta) + \cdots\Big\}\end{aligned} \tag{4.23}$$

In order to render the functional coefficients $f_1, f_2, \cdots$ independent of the particular properties of the outside flow, i.e. of $\bar{u}_1, \bar{u}_2, \cdots$, it is necessary to split them up as follows:

$$f_3 = g_3 + \frac{\bar{u}_2^2}{\bar{u}_1\bar{u}_3}h_3, \qquad f_4 = g_4 + \frac{\bar{u}_2\bar{u}_3}{\bar{u}_1\bar{u}_4}h_4 + \frac{\bar{u}_2^3}{\bar{u}_1^2\bar{u}_4}k_4,$$

$$f_5 = g_5 + \frac{\bar{u}_2\bar{u}_4}{\bar{u}_1\bar{u}_5}h_5 + \frac{\bar{u}_3^2}{\bar{u}_1\bar{u}_5}k_5 + \frac{\bar{u}_2^3\bar{u}_3}{\bar{u}_1^2\bar{u}_5}j_5 + \frac{\bar{u}_2^4}{\bar{u}_1^3\bar{u}_5}q_5,$$

$$f_6 = g_6 + \frac{\bar{u}_2\bar{u}_5}{\bar{u}_1\bar{u}_6}h_6 + \frac{\bar{u}_3\bar{u}_4}{\bar{u}_1\bar{u}_6}k_6 + \frac{\bar{u}_2^2\bar{u}_4}{\bar{u}_1^2\bar{u}_6}j_6 + \frac{\bar{u}_2\bar{u}_3^2}{\bar{u}_1^2\bar{u}_6}q_6 + \frac{\bar{u}_2^3\bar{u}_3}{\bar{u}_1^3\bar{u}_6}m_6 + \frac{\bar{u}_2^5}{\bar{u}_1^4\bar{u}_6}n_6,$$

$$\cdots\cdots\cdots\cdots\cdots\cdots\cdots\cdots\cdots\cdots\cdots$$

Hence, denoting differentiation with respect to $\eta$ by a prime:

$$\bar{u} = \bar{u}_1\bar{x}f_1' + 3\bar{u}_2\bar{x}^2 f_2' + 4\bar{u}_3\bar{x}^3 f_3' + 5\bar{u}_4\bar{x}^4 f_4' + 6\bar{u}_5\bar{x}^5 f_5' + 7\bar{u}_6\bar{x}^6 f_6' + \cdots \tag{4.24}$$

$$\bar{v} = -\sqrt{\frac{1}{\bar{u}_1}}\Big\{\bar{u}_1 f_1 + 6\bar{u}_2\bar{x}f_2 + 12\bar{u}_3\bar{x}^2 f_3 + 20\bar{u}_4\bar{x}^3 f_4 + 30\bar{u}_5\bar{x}^4 f_5 + 42\bar{u}_6\bar{x}^5 f_6 + \cdots\Big\} \tag{4.25}$$

Inserting expressions (4.21), (4.24) and (4.25) into Eq. (4.17), and comparing terms, one obtains a system of simultaneous ordinary differential equations for the functions $f_1, f_2, g_3, h_3, \cdots$, the first seven of which are:

$$f_1'^2 - f_1 f_1'' = 1 + f_1'''$$

$$3f_1'f_2' - 2f_1''f_2 - f_1 f_2'' = 1 + f_2'''$$

$$4f_1'g_3' - 3f_1''g_3 - f_1 g_3'' = 1 + g_3'''$$

$$4f_1'h_3' - 3f_1''h_3 - f_1 h_3'' = \frac{1}{2} + h_3''' - \frac{9}{2}(f_2'^2 - f_2 f_2'')$$

$$5f_1'g_4' - 4f_1''g_4 - f_1 g_4'' = 1 + g_4'''$$

$$5f_1'h_4' - 4f_1''h_4 - f_1 h_4'' = 1 + h_4''' - \frac{12}{5}(5f_2'g_3' - 2f_2 g_3'' - 3f_2''g_3)$$

$$5f_1'k_4' - 4f_1''k_4 - f_1 k_4'' = k_4''' - \frac{12}{5}(5f_2'h_3' - 2f_2 h_3'' - 3f_2''h_3)$$

The boundary conditions for the functions $f_1, f_2, \cdots$ follow from Eq. (4.16) and are:

$$\eta = 0: f_1 = f_1' = 0, \qquad f_2 = f_2' = 0, \qquad g_3 = g_3' = 0, \qquad h_3 = h_3' = 0, \cdots$$

$$\eta = \infty: f_1' = 1, \qquad f_2' = \frac{1}{3}, \qquad g_3' = \frac{1}{4}, \qquad h_3' = 0, \cdots$$

**Table 4. 1.** Universal functions for the first six terms of the asymmetrical Blasius series.

| | | | |
|---|---|---|---|
| $f_1''(0)$ | 1.232588 | $j_5''(0)$ | −0.033230 |
| $f_2''(0)$ | 0.798742 | $q_5''(0)$ | −0.000840 |
| $g_3''(0)$ | 0.724447 | $g_6''(0)$ | 0.604228 |
| $h_3''(0)$ | 0.164046 | $h_6''(0)$ | 0.237570 |
| $g_4''(0)$ | 0.673188 | $k_6''(0)$ | 0.206131 |
| $h_4''(0)$ | 0.285916 | $j_6''(0)$ | −0.021769 |
| $k_4''(0)$ | −0.017072 | $q_6''(0)$ | −0.009554 |
| $g_5''(0)$ | 0.634702 | $m_6''(0)$ | 0.000190 |
| $h_5''(0)$ | 0.257808 | $n_6''(0)$ | 0.0072072 |
| $k_5''(0)$ | 0.119182 | | |

These equations are solved numerically by means of the Runge-Kutta-Gill method, and the results are tabulated in Table 4. 1 (Arie and Iida [35]).

If one defines the non-dimensional shearing stress $\bar{\tau}_0$, displacement thickness $\bar{\delta}^*$ and momentum thickness $\bar{\theta}$ by

$$\bar{\tau}_0=\frac{\tau_0}{\rho U_\infty^2}\sqrt{R_e}\,,\qquad \bar{\delta}^*=\frac{\delta^*}{2a}\sqrt{R_e}\,,\qquad \bar{\theta}=\frac{\theta}{2a}\sqrt{R_e}$$

they can be evaluated as follows:

$$\bar{\tau}_0=\left(\frac{\partial\bar{u}}{\partial\bar{y}}\right)_{\bar{y}=0}=\bar{u}_1\Big\{\bar{u}_1\bar{x}f_1''(0)+3\bar{u}_2\bar{x}^2f_2''(0)$$
$$+4\bar{u}_3\bar{x}^3f_3''(0)+5\bar{u}_4\bar{x}^4f_4''(0)+6\bar{u}_5\bar{x}^5f_5''(0)+7\bar{u}_6\bar{x}^6f_6''(0)+\cdots\Big\}$$

$$\bar{\delta}^*=\frac{1}{\sqrt{\bar{u}_1}}\int_0^\infty\left(1-\frac{\bar{u}}{\bar{U}}\right)d\eta$$

$$\bar{\theta}=\frac{1}{\sqrt{\bar{u}_1}}\int_0^\infty\frac{\bar{u}}{\bar{U}}\left(1-\frac{\bar{u}}{\bar{U}}\right)d\eta$$

(2) Numerical Calculations.

The numerical calculations of the laminar boundary layer are performed for the circular cylinder of 25.0 mm diameter for the case of $\Delta/(2a)=6.836$, 1.496, 0.692, 0.284, 0.160, 0.080 and 0.036. On the assumption of the Bernoulli theorem

$$\frac{U^2}{2}+\frac{p}{\rho}=\frac{p_{\mathrm{stag}}}{\rho}$$

the measured values of pressure coefficient $C_p$ are used to compute the velocity at the edge of the boundary layer $\bar{U}$:

$$\bar{U}=\frac{U}{U_\infty}=\left[C_{p\mathrm{stag}}-C_{pc}(\bar{x})\right]^{\frac{1}{2}} \tag{4. 26}$$

The distributions of $\bar{U}(\bar{x})$ and $d\bar{U}/d\bar{x}$ calculated from Eq. (4. 26) are shown in Fig. 4. 31 (a) and (b). The best fit curves of the sixth degree were obtained by applying the method of least squares and the coefficients of polynomials are listed

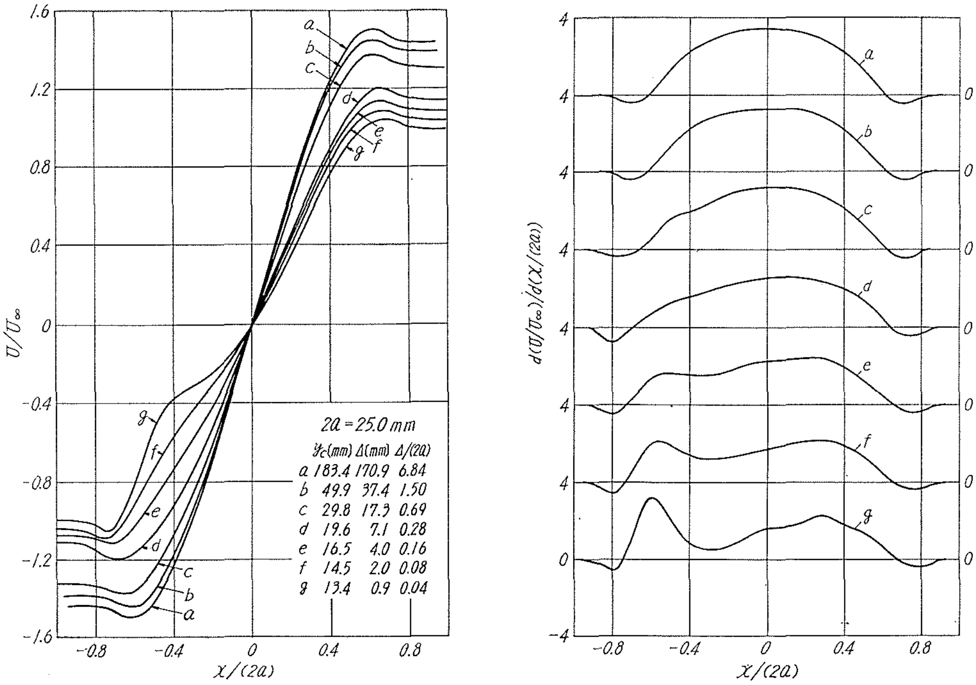

(a) (b)

**Fig. 4.31.** Variation of (a) surface velocity and (b) its derivative with respect to $x$ on the circular cylinder.

**Table 4.2.** Coefficients of the best-fit curves of the sixth degree.

| $\Delta/(2a)$ | 6.836 | 0.692 | 0.080 |
|---|---|---|---|
| $\bar{u}_1$ | 3.4588 | 3.0558 | 1.7120 |
| $\bar{u}_2$ | 0.0000 | 0.4058 | 1.6359 |
| $\bar{u}_3$ | −2.2805 | −1.9182 | 0.4013 |
| $\bar{u}_4$ | 0.0000 | −1.4471 | −5.5902 |
| $\bar{u}_5$ | −1.0450 | −0.6756 | −1.5503 |
| $\bar{u}_6$ | 0.0000 | 1.3076 | 4.7747 |

in Table 4.2. It was found that the measured data were well represented by these polynomials, with the exception of the cases of $\Delta/(2a) = 0.080$ and $0.036$ in which there exists a large asymmetry of $\bar{U}$ on both sides of the stagnation point.

The computation of $\bar{\tau}_0$, $\bar{\delta}^*$ and $\bar{\theta}$ was performed for three cases, i.e. $\Delta/(2a) = 6.836$, $0.692$ and $0.080$, and the results are shown in Figs. 4.32 (a), (b) and (c). The asymmetry of flow is clearly seen in Figs. 4.32 (b) and (c), while the boundary layer is practically symmetrical for the case of $\Delta/(2a) = 6.836$. The calculated velocity profiles $\bar{u}/\bar{U}$ are also shown in Figs. 4.33 (a) and (b). Since, owing to the increased complexity of the differential equations for $f_n$ as $n$ increases, the

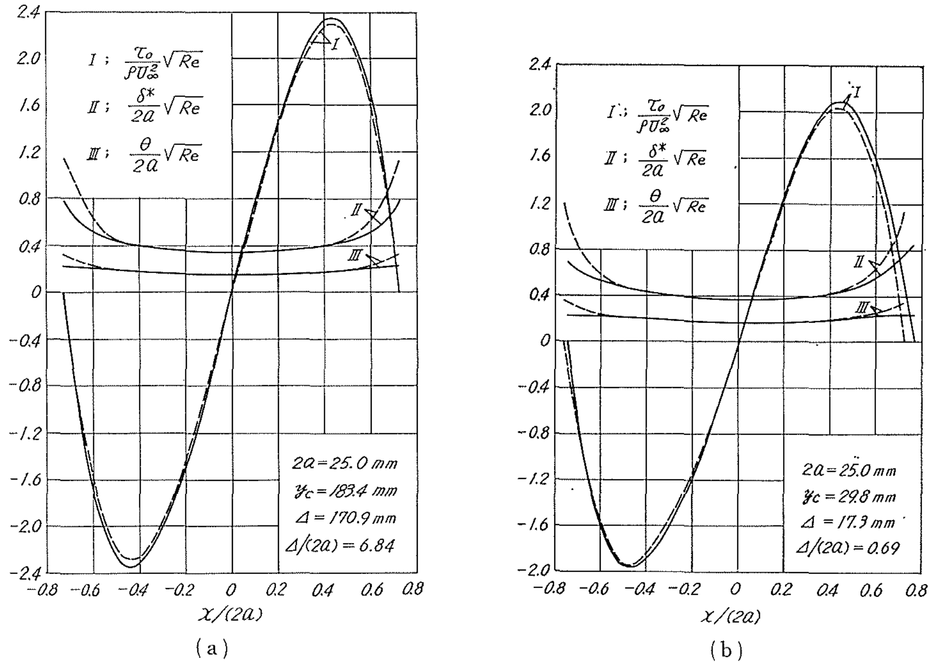

(a)

(b)

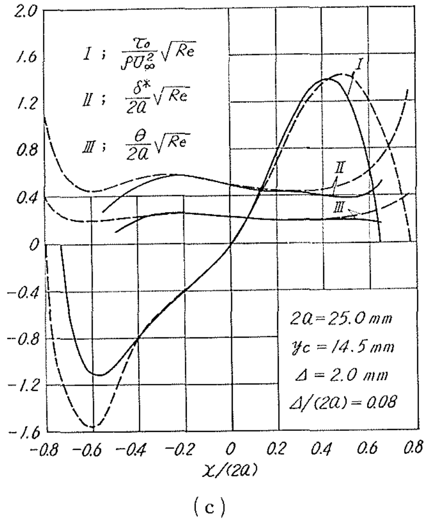

(c)

**Fig. 4. 32.** Variation of shearing stress, displacement and momentum thicknesses on the circular cylinder:
(a) $\Delta/(2a)=6.84$, (b) 0.69, (c) 0.08.
——— Blasius series,
– – – – Pohlhausen's method.

evaluation of the functional coefficients was restricted up to $f_6$, the values of $\bar{\tau}_0$, $\bar{\delta}^*$, $\bar{\theta}$ and $\bar{u}/\bar{U}$ obtained for the case of $\Delta/(2a)=0.080$ may not be accurate especially in the vicinity of the point of separation. This fact was shown by the velocity profiles calculated from Eq. (4. 24), because the velocity in the boundary layer near the point of separation became much larger than that at the edge of the boundary layer, which was not thought acceptable for the case of the steady two-dimensional boundary layers. Consequently, the values of $\bar{\tau}_0$, $\bar{\delta}^*$ and $\bar{\theta}$ for most cases of $\Delta/(2a)$ must be computed by other means, for example, the approximation by Pohlhausen [36] and Walz [37].

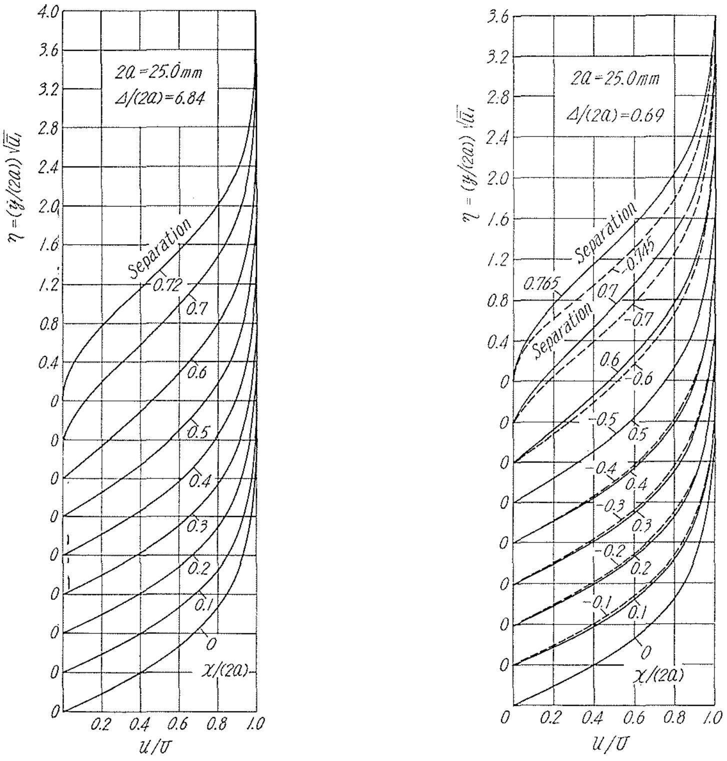

(a) (b)

**Fig. 4. 33.** Tangential velocity distribution in the laminar boundary layer along the surface of the circular cylinder: (a) $\Delta/(2a)=6.84$, (b) 0.69.

(3) Estimation due to the Method of Pohlhausen and Walz

This procedure is based on the momentum integral equation

$$\bar{U}^2\frac{d\bar{\theta}}{d\bar{x}}+(2\bar{\theta}+\bar{\delta}^*)\,\bar{U}\,\frac{d\bar{U}}{d\bar{x}}=\bar{\tau}_0 \tag{4.27}$$

obtained by integrating the equation of motion with respect to $y$ from the surface at $y=0$ to a certain distance outside the boundary layer for all values of $x$. If one assumes a polynomial of the fourth degree for the velocity function in terms of the dimensionless distance from the wall $\eta=y/\delta(x)$ and adapts the necessary boundary conditions, one obtains the relations

$$\frac{\bar{\delta}^*}{\bar{\delta}}=\frac{3}{10}-\frac{\Lambda}{120}, \qquad \frac{\bar{\theta}}{\bar{\delta}}=\frac{37}{317}-\frac{\Lambda}{945}-\frac{\Lambda^2}{9072} \tag{4.28}$$

$$\frac{\bar{\tau}_0\bar{\delta}^*}{\bar{U}}=2+\frac{\Lambda}{6} \tag{4.29}$$

where a shape factor $\Lambda$ is

$$\Lambda=\bar{\delta}^2\frac{d\bar{U}}{d\bar{x}} \tag{4.30}$$

The second shape parameter $K$ is introduced by the equation

$$K=\bar{\theta}^2\frac{d\bar{U}}{d\bar{x}} \tag{4.31}$$

which is connected with the momentum thickness in the same way as the first shape factor, $\Lambda$, was connected with the boundary layer thickness, $\bar{\delta}$, in Eq. (4.30). It isseen from Eqs. (4.28), (4.29), (4.30) and (4.31) that the shape factors $\Lambda$ and $K$ satisfy the universal relation

$$K=\left(\frac{37}{315}-\frac{\Lambda}{945}-\frac{\Lambda^2}{9072}\right)^2\Lambda \tag{4.32}$$

Denoting

$$\frac{\bar{\delta}^*}{\bar{\theta}}=\left(\frac{3}{10}-\frac{\Lambda}{120}\right)\left(\frac{37}{315}-\frac{\Lambda}{945}-\frac{\Lambda^2}{9072}\right)=f_1(K) \tag{4.33}$$

$$\frac{\bar{\tau}_0\bar{\theta}}{\bar{U}}=\left(2+\frac{\Lambda}{6}\right)\left(\frac{37}{315}-\frac{\Lambda}{945}-\frac{\Lambda^2}{9072}\right)=f_2(K) \tag{4.34}$$

for the sake of brevity, and substituting $K$ and $\bar{\theta}^2$, together with $f_1(K)$and $f_2(K)$ from Eqs. (4.33) and (4.34), respectively, one obtains from the momentum equation Eq. (4.27) the relation

$$\bar{U}\frac{d\bar{\theta}^2}{d\bar{x}}=F(K) \tag{4.35}$$

where

$$F(K)=2f_2(K)-4K-2Kf_1(K)$$

It was pointed out by Walz that Eq. (4.35) can be reduced to a simple quadrature by the introduction of a further approximation without any appreciable loss of accuracy. Walz found that the function $F(K)$ can be approximated quite closely by the straight line

$$F(K)=0.470-6K$$

In this manner Eq. (4.35) is reduced to

$$\frac{d}{d\bar{x}}(\bar{U}\bar{\theta}^2)=0.470-5\bar{U}\bar{\theta}^2\frac{1}{\bar{U}}\frac{d\bar{U}}{d\bar{x}}$$

This differential equation for $\bar{U}\bar{\theta}^2$ can be integrated explicitly to

$$\bar{U}\bar{\theta}^2=\frac{0.470}{\bar{U}^5}\int_0^{\bar{x}}\bar{U}^5d\bar{x} \tag{4.36}$$

The functions $K(\Lambda)$, as well as $f_1(K)$, $f_2(K)$ are tabulated in Schlichting [38].

The variations of $\bar{\tau}_0$, $\bar{\delta}^*$ and $\bar{\theta}$ at the surface of the circular cylinder calculated by this procedure are shown in Figs. 4.34 (a) and (b). The comparisons between the results of the approximate calculation and those obtained with the aid of a Blasius series containing six terms (up to $\bar{x}^6$) are also shown in Figs. 4.32 (a), (b)

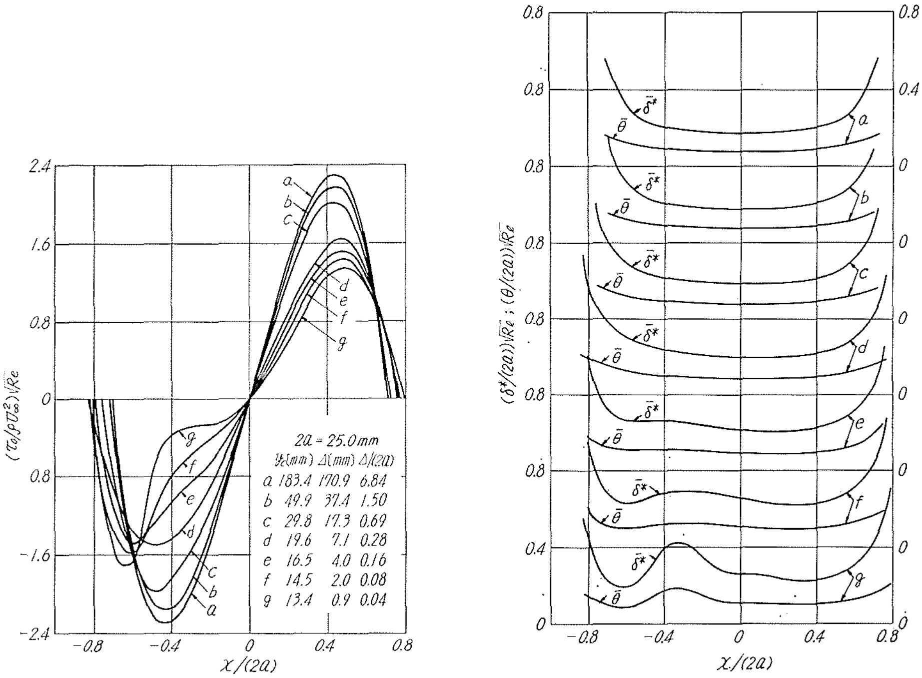

(a) (b)

**Fig. 4. 34.** Variation of (a) shearing stress and (b) displacement and momentum thicknesses on the circular cylinder.

and (c), and the agreement is not good for the case of $\Delta/(2a) = 0.080$. Since it has been shown by similar calculations (Schlichting [38]) that Pohlhausen's approximate method leads to very satisfactory results, one can say that the Blasius series for asymmetrical case does require many more terms (probably up to $\bar{x}^{11}$ in order to obtain more accurate values of $\bar\tau$, $\bar\delta^*$ and $\bar\theta$ for the case of a large asymmetry.

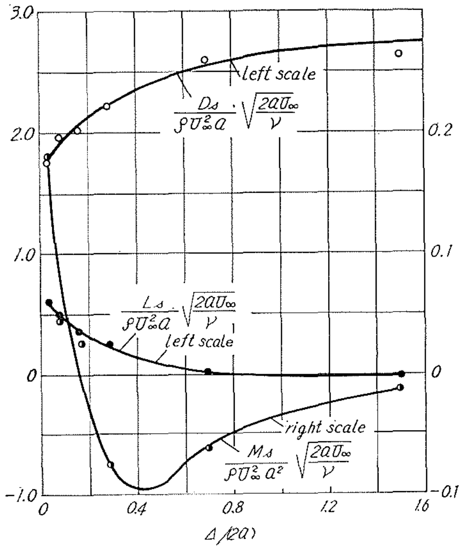

**Fig. 4. 35.** Variation of viscous lift and drag forces and torque acting on the circular cylinder.

Now it becomes possible to estimate the contribution of shearing stress to the lift and drag forces and the torque acting on the circular cylinder. The torque will exist since the distribution of shearing stress is asymmetrical on both sides of the stagnation point. The lift and drag coefficients, $C_{Ls}$ and $C_{Ds}$, and the coefficient of moment $C_{Ms}$ due to the viscous shearing stress can be computed as

$$C_{Ls} = \frac{L_s}{\rho U_\infty^2 a} = \frac{1}{\sqrt{R_e}}\int_{\theta_s^-}^{\theta_s^+} \bar\tau_0 \cos\Theta \, d\Theta$$

$$C_{Ds}=\frac{D_s}{\rho U_\infty^2 a}=\frac{1}{\sqrt{R_e}}\int_{\theta_s^-}^{\theta_s^+}\bar{\tau}_0\sin\Theta\, d\,\Theta$$

$$C_{Ms}=\frac{M_s}{\rho U_\infty^2 a}=\int_{\theta_s^-}^{\theta_s^+}\bar{\tau}_0 d\Theta$$

where $\theta_s^+$ and $\theta_s^-$ imply the points of separation on the sides of $\bar{x}>0$ and $\bar{x}<0$, respectively. The variations of $C_{Ls}\sqrt{R_e}$, $C_{Ds}\sqrt{R_e}$ and $C_{Ms}\sqrt{R_e}$ with respect to $\Delta/(2a)$ are shown in Fig. 4.35. The values of $C_{Ls}$ and $C_{Ds}$ are of a much smaller order of magnitude than those of $C_{Lp}$ and $C_{Dp}$, and $C_{Ms}$ is of a much smaller order of magnitude than $C_{Ls}$ and $C_{Ds}$. It is interesting to note that the variations of $C_{Ls}$ and $C_{Ds}$ with respect to $\Delta/(2a)$ have the same tendency as those of $C_{Lp}$ and $C_{Dp}$. The corrected values of the lift and drag coefficients are given in Table 4.3. The value of $C_D(=1.23)$ for $\Delta/(2a)=6.836$ is seen to agree quite well with that of the drag coefficient of a circular cylinder in an unbounded uniform flow.

The position of the point of separation can be found from the condition that the shearing stress must vanish there. The results of computation are listed in Table 4.4. It is seen from this table that the laminar boundary layer separates a little earlier on the upper side of the circular cylinder than on the lower one.

**Table 4. 3.** Lift and drag coefficients corrected for shearing stress.

| $\Delta/(2a)$ | $C_{Dp}$ | $C_{Lp}$ | $C_{Ds}$ | $C_{Ls}$ | $C_D$ | $C_L$ |
|---|---|---|---|---|---|---|
| 6.836 | 1.21 | 0.00 | 0.02 | 0.00 | 1.23 | 0.00 |
| 1.496 | 1.24 | 0.00 | 0.02 | 0.00 | 1.26 | 0.00 |
| 0.692 | 1.31 | 0.03 | 0.02 | 0.00 | 1.35 | 0.03 |
| 0.284 | 1.09 | 0.14 | 0.02 | 0.00 | 1.11 | 0.14 |
| 0.160 | 1.04 | 0.25 | 0.02 | 0.00 | 1.06 | 0.25 |
| 0.080 | 1.04 | 0.32 | 0.02 | 0.01 | 1.06 | 0.33 |
| 0.036 | 1.00 | 0.38 | 0.02 | 0.01 | 1.02 | 0.39 |

**Table 4. 4.** The position of separation of laminar boundary layer from the surface of the circular cylinder.

| $\Delta/(2a)$ | $\theta_s^-$ | $\theta_s^+$ | $\Theta_{\text{stag}}$ |
|---|---|---|---|
| 6.836 | −82.5° | 82.5° | 0.0° |
| 1.496 | −80.2° | 81·5° | 0.0° |
| 0.692 | −87.0° | 82.5° | − 0.5° |
| 0.284 | −94.0° | 87.0° | − 7.5° |
| 0.160 | −91.7° | 87.0° | − 7.5° |
| 0.080 | −91.7° | 88.2° | − 8.5° |
| 0.036 | −94.0° | 90.5° | −10.0° |

## 5. Turbulent Wake of a Circular Cylinder located in a Turbulent Boundary Layer

In the preceding chapters of this paper, the properties of flow about a circular cylinder placed in a turbulent boundary layer was described, together with the effect of a plane bounday wall located in the vicinity of the circular cylinder. In this chapter the far wake of the cylinder submerged in the same turbulent boundary layer as before was investigated.

### 5.1 Wake-producing Cylinders

Two circular cylinders of 1.2 mm and 3.2 mm diameters, respectively, were used as the wake-producing objects, and they were fixed in turn to the wind tunnel at the position $x_c = 219.8$ cm and $y_c = 30$ mm, where $x_c$ and $y_c$ denote the coordinates of the center of each cylinder. The span of each cylinder was 50 cm, so that it coincided with the width of the tunnel. As previously demonstrated, the turbulent boundary layer is fully developed at the section $x = 219.8$ cm and at successive downstream sections where the turbulent wake of the cylinders is to be developed.

The static pressure along the tunnel was found to be the same as that shown in Fig. 4.3.

### 5.2 Mean Velocity Distribution

The results of measurement of the mean velocity in the wake are shown in Figs. 5.1 and 5.2. The distributions of mean velocity far downstream in the cylinders are also plotted in Fig. 5.3 on nondimensional basis, i.e. $u/U_\infty - y/\delta^*$. It is seen from Fig. 5.3 that although the wake of the cylinder of 3.2 mm diameter produces a permanent change in the velocity profile of the disturbed turbulent boundary layer, that of the cylinder of 1.2 mm diameter does not produce this kind of distortion and the disturbed boundary layer recovers. This fact implies

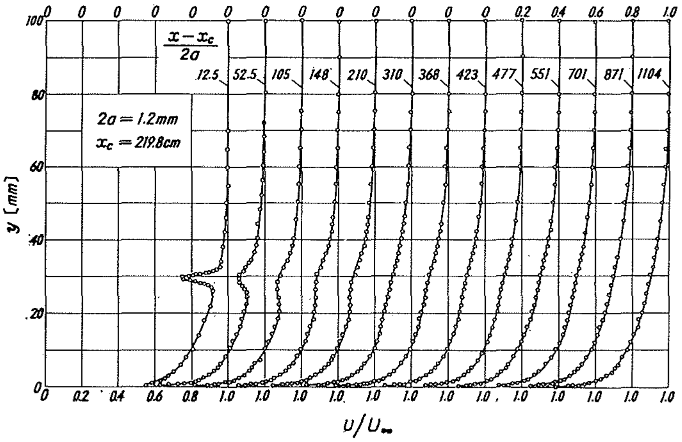

**Fig. 5.1.** Distribution of mean velocity in the wake of the circular cylinder of 1 mm diameter.

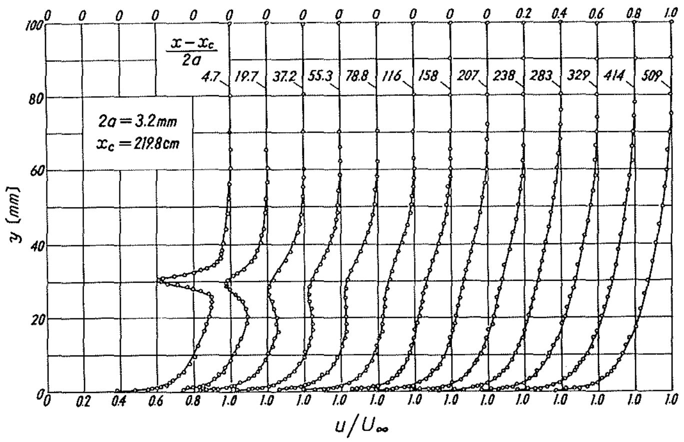

**Fig. 5. 2.** Distribution of mean velocity in the wake of the circular cylinder of 3.2 mm diameter.

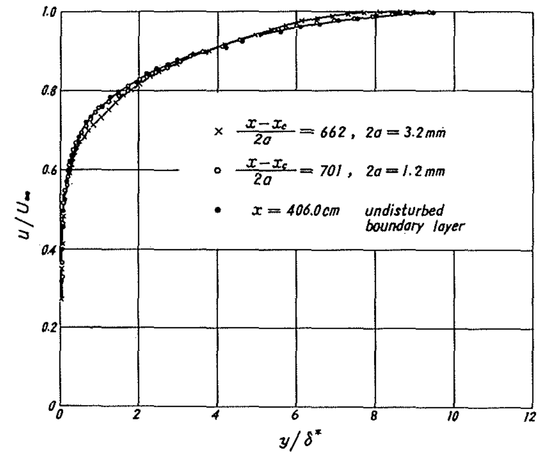

**Fig. 5. 3.** Nondimensional plot of mean velocity at a far downstream section of the turbulent boundary layer disturbed by the cylinders of 1.2 mm and 3.2 mm diameter, respectively.

that the disturbance introduced by the thinner cylinder is not large enough to permit an accurate determination of its drag force to be made from the momentum principle, since this principle gives the drag force as a residual value. Consequently the computation of drag force was made only for a cylinder of 3.2 mm diameter, and some of the required properties of the flow, i. e. the displacement and momentum thicknesses and the shearing stress are shown in Figs. 5. 4 (a) and (b). It is seen from Fig. 5. 4 (a) that the boundary layer is considerably thickened by the introduction of the cylinder, because a part of the energy of the boundary layer is diverted into an eddy motion in the wake. This phenomenon is also well represented by the decrease in the shearing stress at the wall, $\tau_w$, as will be seen

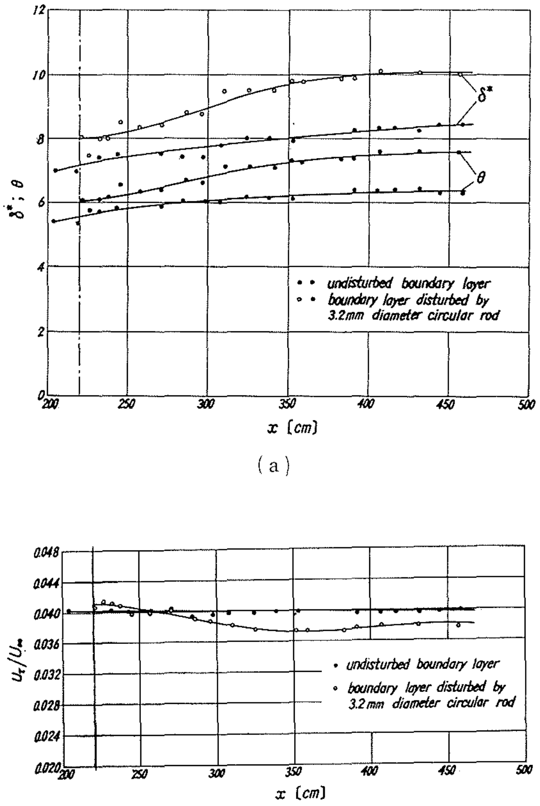

(a)

(b)

**Fig. 5. 4.** Variation of (a) displacement and momentum thicknesses and (b) shearing stress in the turbulent boundary layer disturbed by the circular cylinder of 3.2 mm diameter.

in Fig. 5. 4 (b).

The mean velocity is plotted in the non-dimensional form of $u/u_\tau$ against $yu_\tau/\nu$ in Fig. 5. 5. The law of the wall holds even in the turbulent boundary layer disturbed by the wake of the circular cylinder, and Clauser's law of the wall given by Eq. (4. 5 a) represents the measured data quite closely in this case as well. For large values of $yu_\tau/\nu$ the logarithmic velocity distribution deviates from the actual velocity distribution ; apparently it no longer holds in the outer region of the boundary layer where the distortion introduced by the wake of the cylinder is considerable. For that region it may be more appropriate to consider the velocity defect $(U_\infty - u)/u_\tau$ rather than $u/u_\tau$. The experimental results are plotted in this form in Fig. 5. 6, together with the velocity-defect law given by Eqs. (4. 6 a) and (4. 6 b), respectively. It should be noted that the experimental data show a good agreement with the velocity-defect law for the channel flow in the immediate downstream of the circular cylinder, while an increasing deviation from this law is seen as the lowest downstream section is approached. Finally, they

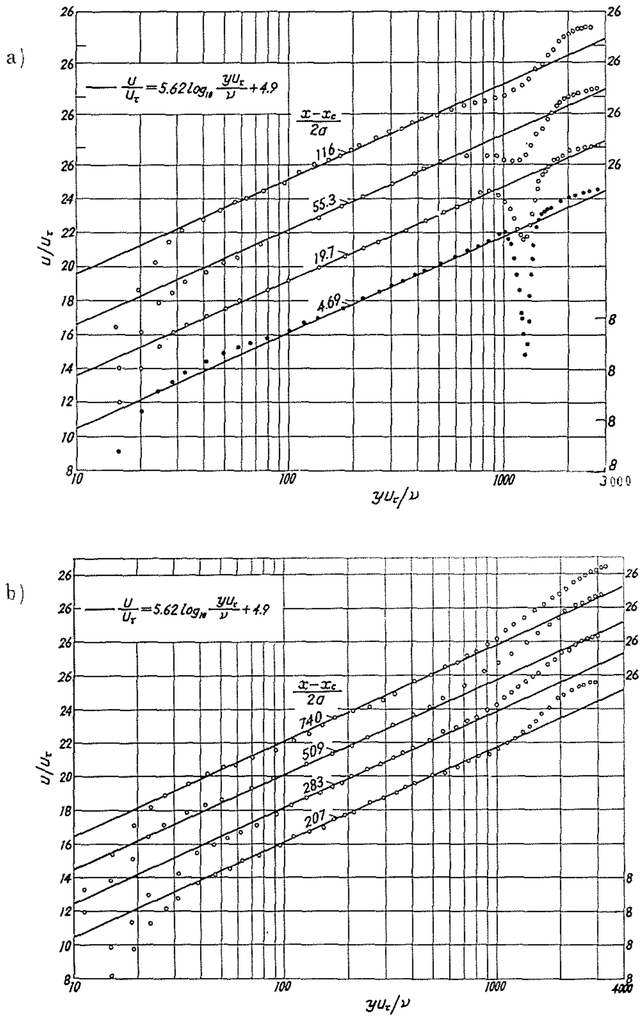

Fig. 5.5. Logarithmic law of mean velocity profile.

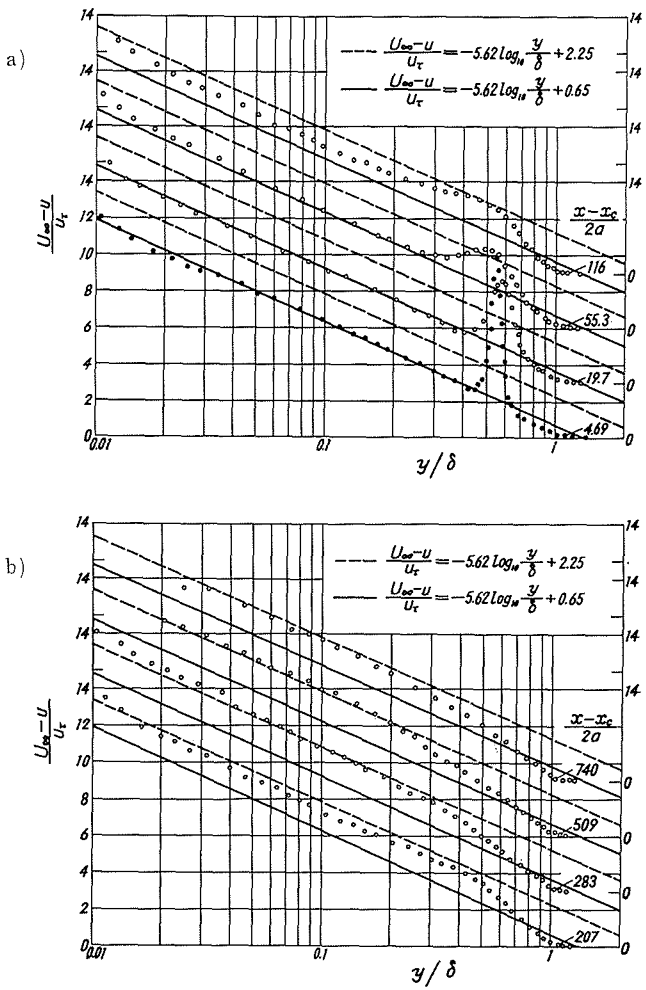

Fig. 5.6. Velocity-defect law of mean velocity.

eventually came to be represented quite closely by the velocity-defect law for the turbulent boundary layer with a zero pressure gradient. Namely, the boundary layer distorted by the wake of the cylinder may have the same dynamic structure as a fully-developed turbulent boundary layer over a smooth flat plate. This fact may be considered to give a clue to a new method of artificial thickening of the turbulent boundary layer.

### 5.3 Distribution of Turbulence

The values of $\sqrt{\overline{u'^2}}$, $\sqrt{\overline{v'^2}}$ and $\overline{u'v'}$ in the wake of the cylinder were measured by means of the single-hot-wire technique, and the results are shown in Figs. 5.7,

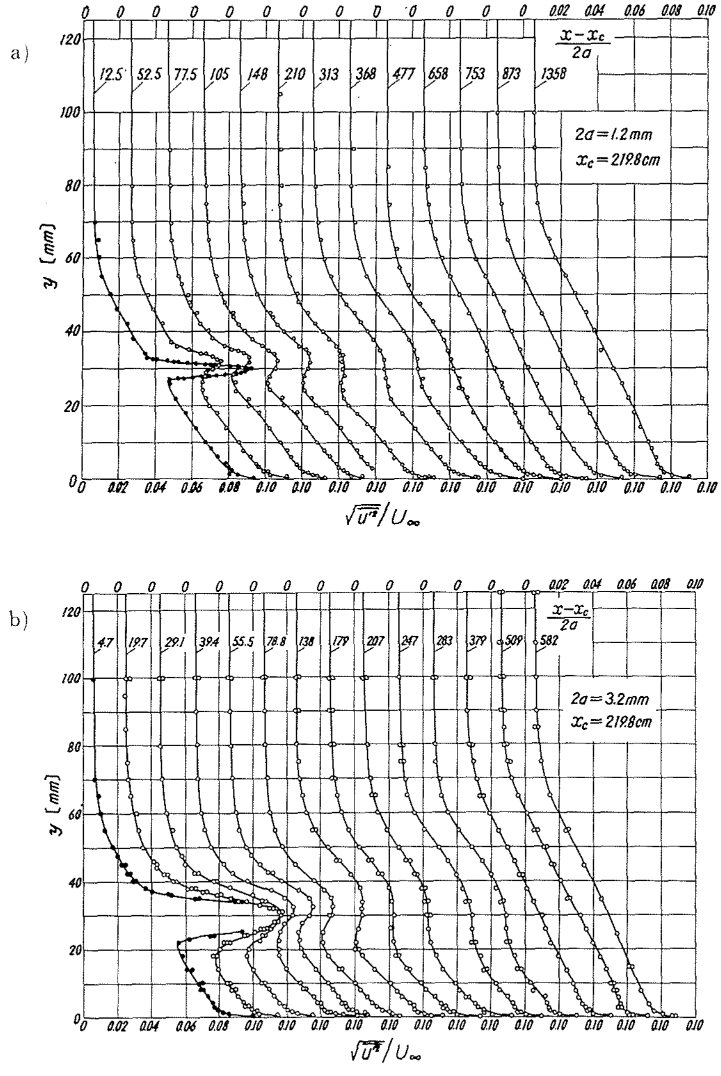

**Fig. 5.7.** Variation of $u$-component of turbulent fluctuation in the wake of the cylinders of (a) 1.2 mm and (b) 3.2 mm diameter, respectively.

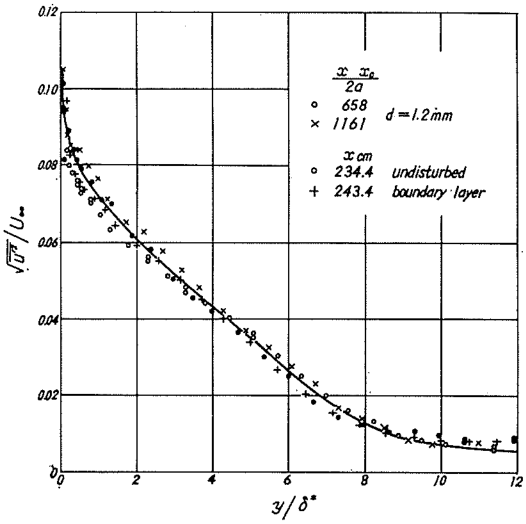

**Fig. 5. 8.** Variation of $u$-component of turbulent fluctuation in the turbulent boundary layer before and after the introduction of a 1.2 mm cylinder.

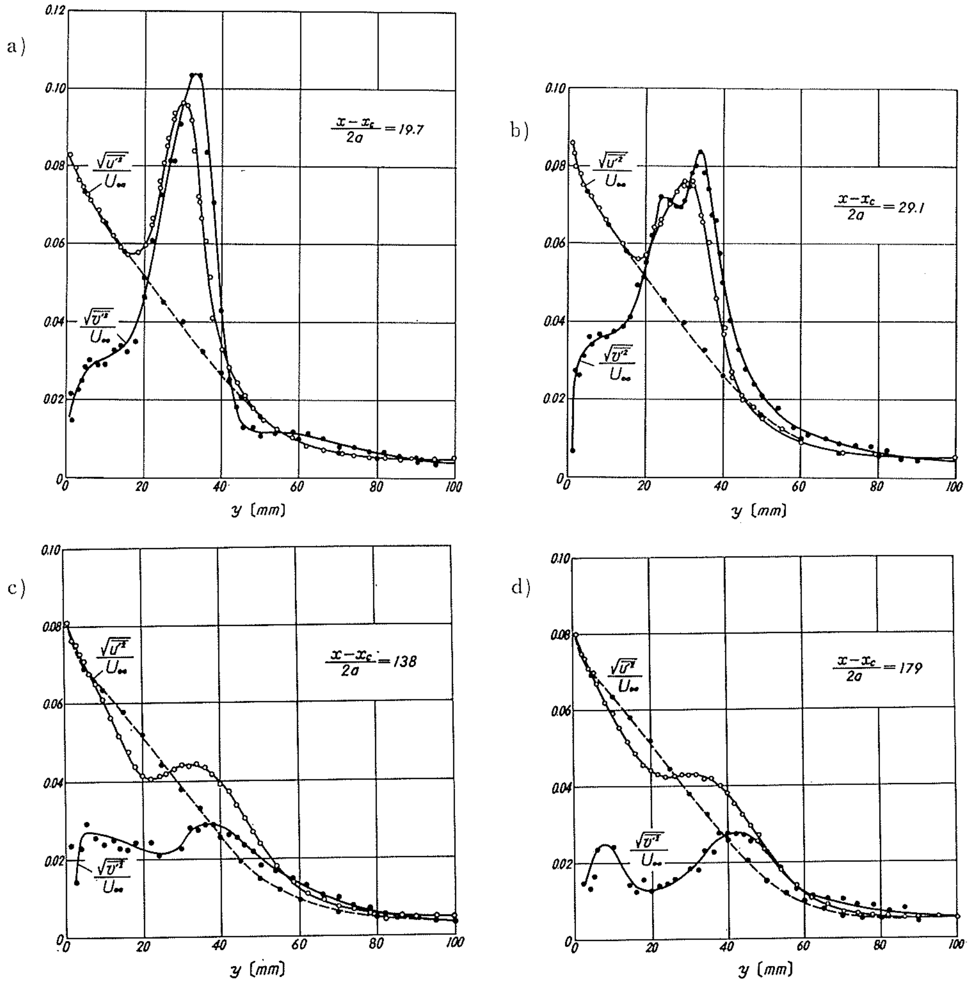

**Fig. 5. 9.** Variation of $\sqrt{\overline{u'^2}}$ and $\sqrt{\overline{v'^2}}$ across the wake: (a) $(x-x_c)/(2a)=19.7$, (b) 29.1, (c) 138, (d) 179

5.8, 5.9 and 5.10. Figs. 5.7(a) and (b) show the distribution of the intensity of the $u$-component of turbulence in the wake of the cylinder of either 1.2 mm or 3.2 mm diamenter, respectively, taking the nondimensional distance from the cylinder $(x-x_c)/d$ as a parameter. One can see from these figures the manner in which the turbulence in the wake of the cylinder spreads outwards and intermingles with the surrounding turbulence in the otherwise undisturbed turbulent boundary layer. It will also be seen that the effect of the cylinder seems to vanish at the downstream section $(x-x_c)/d=500\sim700$, which may be confirmed in turn by the mean velocity profile given in Figs. 5.1 and 5.2. According to the measurements of Townsend [39], the effect of the wake-producing object could be detected even at sections further down-

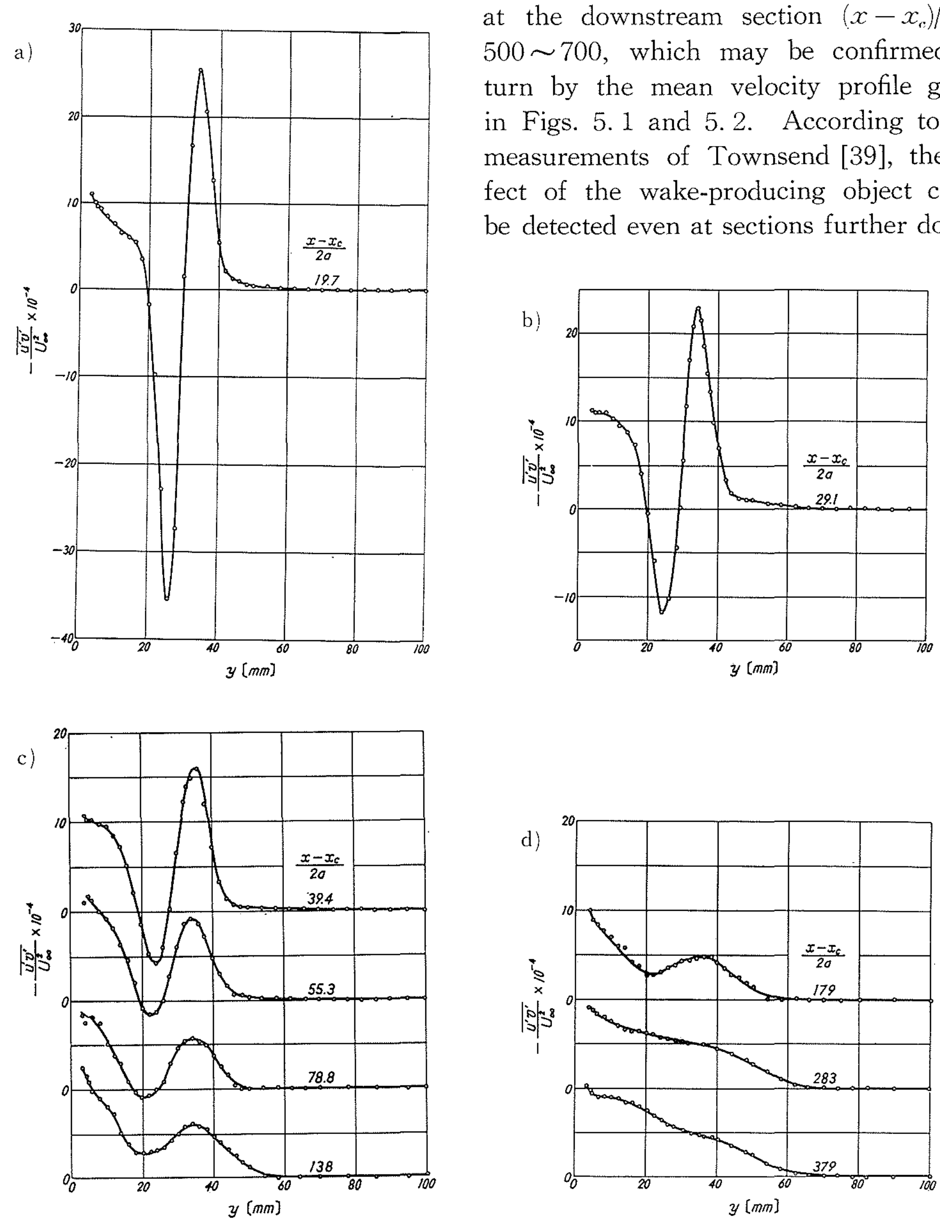

**Fig. 5.10.** Variation of $\overline{u'v'}$ across the wake: (a) $(x-x_c)/(2a)=19.7$, (b) 29.1, (c) 39.4, 55.3, 78.8, 138, (d) 179, 283, 379.

stream than $(x-x_c)/d=1000$ in the case of the unbounded uniform flow of low turbulence. Consequently it may be concluded that the spread and mixing of the wake are promoted by the action of the surrounding turbulence.

The distribution of $\sqrt{\overline{u'^2}}$ at the two sections far downstream of the 1.2 mm cylinder is shown in Fig. 5. 8, together with the values of $\sqrt{\overline{u'^2}}$ in the otherwise undisturbed turbulent boundary layer. The turbulence is seen to recover and return to its original distribution.

In Figs. 5. 9 and 5. 10, the variations of $\sqrt{\overline{v'^2}}$ and $\overline{u'v'}$ across the wake are represented at several sections downstream of the 3.2 mm cylinder, and these quantities clearly interpret the marked interaction between the wake and the surrounding turbulent boundary layer. It should be emphasized that although the values of $\sqrt{\overline{u'^2}}$ increase considerably at the immediate downstream of the cylinder as would intuitively be expected, those at further downstream sections (say $(x-x_c)/d \geqq 55.3$) are much less than the turbulence of the undisturbed turbulent boundary layer in the vicinity of the boundary wall. Some complex features of this interaction of the wake with the surrounding turbulent flow are also illustrated by the variation of $\sqrt{\overline{v'^2}}$ across the wake, but the detailed mechanism of the interaction still remains to be solved.

### 5. 4 Estimation of the drag force of the cylinder by momentum principle

The drag force acting on the cylinder can be estimated by considering the change in momentum flux between two vertical sections located upstream and downstream from the cylinder.

The Navier-Stokes equation in tensor notation is

$$\frac{\partial u_i}{\partial t}+u_k\frac{\partial u_i}{\partial x_k}=-\frac{1}{\rho}\frac{\partial p}{\partial x_i}+\nu\frac{\partial^2 u_i}{\partial x_k \partial x_k}$$

When the relations $u_i=U_i+u_i'$ and $p=P+p'$ are substituted, this equation becomes

$$\frac{\partial}{\partial t}(U_i+u_i')+(U_k+u_k')\frac{\partial}{\partial x_k}(U_i+u_i')=-\frac{1}{\rho}\frac{\partial(P+p')}{\partial x_i}+\nu\frac{\partial^2(U_i+u_k')}{\partial x_k \partial x_k}$$

where $U_i$ and $P$ represent the mean velocity and the mean piezometric pressure, respectively; $u_i'$ and $p'$ are the fluctuating components of velocity and pressure, respectively. Since $\overline{u_i'}=0$, $\partial U_k/\partial x_k=0$, $\overline{\partial u_k'/\partial x_k}=0$ and $\overline{p'}=0$, when one applies the averaging procedure, one obtains

$$\frac{\partial U_i}{\partial t}+U_k\frac{\partial U_i}{\partial x_k}+\overline{u_k'\frac{\partial u_i'}{\partial x_k}}=-\frac{1}{\rho}\frac{\partial P}{\partial x_i}+\nu\frac{\partial^2 U_i}{\partial x_k \partial x_k} \tag{5. 1}$$

This is called the Reynolds equation.

A volume integration of Eq. (5. 1) gives

$$\int\frac{\partial U_i}{\partial t}d\tilde{\omega}+\int U_k\frac{\partial U_i}{\partial x_k}d\tilde{\omega}+\int\overline{u_k'\frac{\partial u_i'}{\partial x_k}}d\tilde{\omega}=-\frac{1}{\rho}\int\frac{\partial P}{\partial x_i}d\tilde{\omega}+\nu\int\frac{\partial^2 U_i}{\partial x_k \partial x_k}d\tilde{\omega} \tag{5. 2}$$

where $d\tilde{\omega}$ denotes the volume element. Generally, Green's theorem states that

$$\int \frac{\partial G}{\partial x_i} d\tilde{\omega} = \int n_i \, G dS$$

in which $n_i$ are the direction cosines of a unit normal vector at the surface element $dS$ and the positive direction of the normal is understood to be outward from the surface ; $G$ is a function of $x_i$. Accordingly, Eq. (5. 2) takes the form

$$\int \frac{\partial U_i}{\partial t} d\tilde{\omega} + \int n_k U_k U_i dS + \int n_k \overline{u_k' u_i'} dS = -\frac{1}{\rho}\int n_i P dS + \nu \int n_k \frac{\partial U_i}{\partial x_k} dS$$

Since $\partial U_i / \partial t = 0$ for a steady flow, this equation may be reduced to

$$\int n_k U_k U_i dS + \int n_k \overline{u_k' u_i'} dS = -\frac{1}{\rho}\int n_i P dS + \nu \int n_k \frac{\partial U_i}{\partial x_k} dS \qquad (5.\,3)$$

This is the general equation of momentum for steady flow.

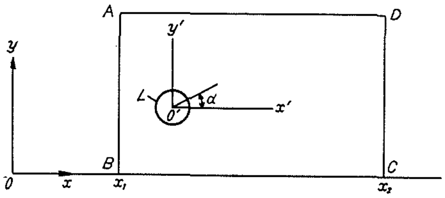

Fig. 5. 11. Control volume.

In order to obtain the drag force acting on the cylinder, Eq. (5. 3) will be applied to the control volume ABCD shown in Fig. 5. 11. Of course, BC denotes the boundary wall, and AD is taken parallel to BC. The coordinates of A and D are assumed to be $(x_1, H)$ and $(x_2, H)$, and the values of velocity and pressure at the two sections AB and DC are represented by the suffixes 1 and 2, respectively. Thus if one puts

$$M_1 = \int n_j U_j U_i dS\,, \qquad M_2 = \int n_j \overline{u_j' u_i'} dS$$

$$M_3 = -\frac{1}{\rho}\int n_i P dS\,, \qquad M_4 = \nu \int n_j \frac{\partial U_i}{\partial x_j} dS$$

these take the following forms at the surfaces of the control volume :

( i ) surface AB ;

$$M_1 = -\int_0^H U_1^2 dy\,, \qquad M_2 = -\int_0^H \overline{u_1'^2} dy$$

$$M_3 = \frac{1}{\rho}\int_0^H P_1 dy\,, \qquad M_4 = -\nu \int_0^H \frac{\partial U_1}{\partial x} dy$$

(ii) surfce CD ;

$$M_1 = \int_0^H U_2^2 dy\,, \qquad M_2 = \int_0^H \overline{u_2'^2} dy$$

$$M_3 = -\frac{1}{\rho}\int_0^H P_2 dy\,, \qquad M_4 = \nu \int_0^H \frac{\partial U_2}{\partial x} dy$$

(iii) surface BC ;

$$M_1 = -\int_{x_1}^{x_2} UV dx = 0\,, \qquad M_2 = -\int_{x_1}^{x_2} \overline{u'v'} dx = 0$$

$$M_3 = 0\,, \qquad M_4 = \nu\int_0^H \frac{\partial U_2}{\partial x}\,dy = -\frac{W_s}{\rho}$$

where

$$W_s = \int_{x_1}^{x_2} \tau_w\,dx$$

denotes the integral of shear stress at the wall.

(iv) surface AD ;

$$M_1 = \int_{x_1}^{x_2} (UV)_{\mathrm{AD}}\,dx\,, \qquad M_2 = \int_{x_1}^{x_2} \overline{u'v'}\,dx = 0$$

$$M_3 = 0\,, \qquad M_4 = \nu\int_{x_1}^{x_2} \frac{\partial U}{\partial y}\,dx = 0$$

since one takes the surface AD in the flow region outside of the boundary layer in which $U$ is independent of $y$.

(v) circle L ;

$$M_1 = 0\,, \qquad M_2 = 0\,, \qquad M_3 = -\frac{1}{\rho}\int n_1 P dS = -\frac{D_p}{\rho}$$

$$M_4 = \nu\int\left(n_1\frac{\partial U}{\partial x} + n_2\frac{\partial U}{\partial y}\right)dS = -\frac{D_s}{\rho}$$

wher $D_p$ and $D_s$ are the pressure and viscous drags of the cylinder, respectively, and are defined by

$$D_p = -\int_0^{2\pi} P\cos\alpha\,d\alpha$$

$$D_s = \mu\int_0^{2\pi}\left(\frac{\partial U}{\partial r}\right)_{r=a}\alpha\,d\alpha$$

The total drag $D$ acting on the cylinder is given by

$$D = D_p + D_s$$

Accordingly, the momentum equation Eq. (5. 3) becomes

$$\sum M_1 + \sum M_2 = \sum M_3 + \sum M_4$$

or, after rearranging the terms,

$$\begin{aligned}\frac{D}{\rho U_\infty^2 a} + \frac{W_s}{\rho U_\infty^2 a} = &\int_0^{H/a}\left(\frac{U_1^2}{U_\infty^2} - \frac{U_2^2}{U_\infty^2}\right)d\left(\frac{y}{a}\right) + \int_0^{H/a}\left(\frac{\overline{u_1'^2}}{U_\infty^2} - \frac{\overline{u_2'^2}}{U_\infty^2}\right)d\left(\frac{y}{a}\right)\\ &-\int_{x_1/a}^{x_2/a}\left(\frac{UV}{U_\infty^2}\right)_{\mathrm{AD}} d\left(\frac{x}{a}\right) + \int_0^{H/a}\left(\frac{P_1}{\rho U_\infty^2} - \frac{P_2}{\rho U_\infty^2}\right)d\left(\frac{y}{a}\right)\\ &-\frac{1}{R_a}\int_0^{H/a}\left\{\frac{\partial(U_1/U_\infty)}{\partial(x/a)} - \frac{\partial(U_2/U_\infty)}{\partial(x/a)}\right\}d\left(\frac{y}{a}\right) \qquad (5.\,3\,\mathrm{a})\end{aligned}$$

in which $U_\infty$ is the mean velocity at the edge of the boundary layer at the section $x = 219.8$ cm and $R_a$ denotes the Reynolds number based on $U_\infty$ and the radius of the cylinder and is equal to $1.5 \times 10^3$. The physical meanings of the terms in Eq. (5. 3 a) are self-evident from their forms.

On the other hand, when the test cylinder is absent, the shear force $W_s^*$ at the wall may be estimated from

$$\frac{W_s^*}{\rho U_\infty^2 a} = \int_0^{H/a}\left(\frac{U_1^2}{U_\infty^2} - \frac{U_2^2}{U_\infty^2}\right)^* d\left(\frac{y}{a}\right) + \int_0^{H/a}\left(\frac{\overline{u_1'^2}}{U_\infty^2} - \frac{\overline{u_2'^2}}{U_\infty^2}\right)^* d\left(\frac{y}{a}\right)$$
$$+ \int_0^{H/a}\left(\frac{P_1}{\rho U_\infty^2} - \frac{P_2}{\rho U_\infty^2}\right)^* d\left(\frac{y}{a}\right) - \int_{x_1/a}^{x_2/a}\left(\frac{UV}{U_\infty^2}\right)_{\mathrm{AD}}^* d\left(\frac{x}{a}\right)$$
$$-\frac{1}{R_a}\int_0^{H/a}\left\{\frac{\partial(U_1/U_\infty)}{\partial(x/a)} - \frac{\partial(U_2/U_\infty)}{\partial(x/a)}\right\}^* d\left(\frac{y}{a}\right) \tag{5. 4}$$

Subtracting Eq. (5. 4) from Eq. (5. 3 a), one obtains the relation

$$\frac{D}{\rho U_\infty^2 a} + \frac{W_s - W_s^*}{\rho U_\infty^2 a} = \int_0^{H/a}\left(\frac{U_1^2}{U_\infty^2} - \frac{U_2^2}{U_\infty^2}\right) d\left(\frac{y}{a}\right) - \int_0^{H/a}\left(\frac{U_1^2}{U_\infty^2} - \frac{U_2^2}{U_\infty^2}\right)^* d\left(\frac{y}{a}\right)$$
$$+ \int_0^{H/a}\left(\frac{P_1}{\rho U_\infty^2} - \frac{P_2}{\rho U_\infty^2}\right) d\left(\frac{y}{a}\right) - \int_0^{H/a}\left(\frac{P_1}{\rho U_\infty^2} - \frac{P_2}{\rho U_\infty^2}\right)^* d\left(\frac{y}{a}\right)$$
$$- \int_{x_1/a}^{x_2/a}\left(\frac{UV}{U_\infty^2}\right)_{\mathrm{AD}} d\left(\frac{x}{a}\right) + \int_{x_1/a}^{x_2/a}\left(\frac{UV}{U_\infty^2}\right)_{\mathrm{AD}}^* d\left(\frac{x}{a}\right) \tag{5. 5}$$

In Eq. (5. 4), the terms including the reciprocal of the Reynolds number and the turbulent fluctuating velocities have been neglected, since they are of an order of magnitude less than $10^{-3}$. As was already mentioned in 5. 2, the static pressure in the turbulent boundary layer is practically the same before and after the introduction of the cylinder, within a limit of experimental errors. So the third and fourth terms on the right-hand side of Eq. (5. 5) cancel out each other. If one takes the sections AB and CD immediate upstream and downstream of the cylinder, respectively, the fifth and sixth terms in Eq. (5. 5) may also cancel out each other and Eq. (5. 5) may be reduced to

$$\frac{D}{\rho U_\infty^2 a} + \frac{W_s - W_s^*}{\rho U_\infty^2 a} = \int_0^{H/a}\left\{\left(\frac{U_2^2}{U_\infty^2}\right)^* - \frac{U_2^2}{U_\infty^2}\right\} d\left(\frac{y}{a}\right) \tag{5. 6}$$

where the velocity $U_1$ immediately upstream of the cylinder is assumed to be the same.

The numerical calulations were performed with $x_1 = 219.5$ cm, $x = 221.3$ cm and $H = 245$ mm, by means of the measured data given in the foregoing sections. Since the experimental data are a little scattered in the vicinity of the selected sections, the probable four values of the right hand side of Eq. (5. 6) were estimated as 0.769, 0.785, 0.821 and 0.857. The mean value becomes 0.808 and the standard deviation amounts to 0.034. Accordingly, Eq. (5. 6) yields

$$\frac{D}{\rho U_\infty^2 a} + \frac{W_s - W_s^*}{\rho U_\infty^2 a} = 0.808 \pm 0.034 \tag{5. 7}$$

The value of $(W_s - W_s^*)/\rho U_\infty^2 a$ can be computed in terms of the shear velocity ;

$$\frac{W_s - W_s^*}{\rho U_\infty^2 a} = \int_{x_1/a}^{x_2/a}\left\{\frac{u_\tau^2}{U_\infty^2} - \left(\frac{u_\tau^2}{U_\infty^2}\right)^*\right\} d\left(\frac{x}{a}\right) = 0.001$$

where the values of $u_\tau$ presented in Fig. 5.4 have been used. Then, from Eq. (5.7), drag coefficient of the thin cylinder placed in the turbulent boundary layer may be estimated as

$$C_D = \frac{D}{\rho U_0^2 a} = \frac{D}{\rho U_\infty^2 a}\left(\frac{U_\infty}{U_0}\right)^2 = 0.95 \pm 0.04$$

since $D/\rho U_\infty^2 a = 0.808$, $U_\infty = 15.46$ m/sec and $U_0 = 14.22$ m/sec. The value of $C_D$ just obtained is practically equivalent to the drag coefficient of a circular cylinder in an unbounded uniform flow of the same Reynolds number as $U_0 a/\nu (= 1.5 \times 10^3)$. Consequently it may be said that a thin circular cylinder placed in a turbulent boundary layer experiences almost the same drag as that in an uniform flow, when the cylinder is not in the immediate neighborhood of the boundary wall.

### 5.5 Theoretical Consideration on the Two-Dimensional Wake in a Uniform Shear Flow

In order to clarify theoretically some of the experimental results obtained in the foregoing sections, the velocity distribution in the wake of a circular cylinder located in a turbulent boundary layer is derived on the basis of constant eddy viscosity. As well known, the mean velocity profile of a turbulent boundary layer has a form that is appoximated quite closely by the 1/7-th power law, but, for simplicity, it is assumed here that the approaching flow to the cylinder is an uniform shear flow with a constant vorticity. Since this flow model has a non-zero transverse velocity gradient as in the turbulent boundary layer, it may be expected that this model includes one of the most essential properties of the wake flow concerned.

*a) Mathematical Formulation of the Problem*

The fundamental equations governing the turbulent flow of an incompressible fluid are the Reynolds equation and the equation of continuity. For the two-dimensional case, these equations become

$$U_1\frac{\partial U_1}{\partial x_1} + U_2\frac{\partial U_1}{\partial x_2} = -\frac{1}{\rho}\frac{\partial P}{\partial x_1} + \nu\nabla^2 U_1 - \frac{\partial \overline{u_1'^2}}{\partial x_1} - \frac{\partial \overline{u_1'u_2'}}{\partial x_2} \tag{5.8}$$

$$U_1\frac{\partial U_2}{\partial x_1} + U_2\frac{\partial U_2}{\partial x_2} = -\frac{1}{\rho}\frac{\partial P}{\partial x_2} + \nu\nabla^2 U_2 - \frac{\partial \overline{u_1'u_2'}}{\partial x_1} - \frac{\partial \overline{u_2'^2}}{\partial x_2} \tag{5.9}$$

$$\frac{\partial U_1}{\partial x_1} + \frac{\partial U_2}{\partial x_2} = 0 \tag{5.10}$$

Let the center of the cylinder be located at the origin of the coordinate system $x_1x_2$, and the velocity profile of the approaching flow be described by

$$U_{1\infty} = U_0 + \omega x_2 \tag{5.11}$$

The configuration of the problem and the definition of symbols are illustrated in Fig. 5.12.

In Eqs. (5.8), (5.9) and (5.10), $U_1$, $U_2$ imply the components of mean velocity in the wake in the $x_1$ and $x_2$ directions, respectively, and $u_1'$, $u_2'$ are the corre-

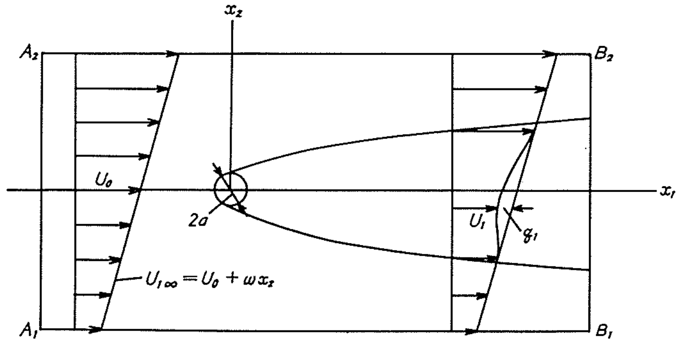

Fig. 5. 12. Definition sketch of the problem.

sponding components of the fluctuating velocity. Let the new variables $q_1$ and $q_2$ be defined by

$$q_1=(U_0+\omega x_2)-U_1 \tag{5. 12 a}$$

$$q_2=U_2 \tag{5. 12 b}$$

It is obvious from Fig. 5. 12 that $q_1$ means the amount of velocity defect in the wake. Substituting Eqs. (5.12) into Eqs. (5.8), (5.9) and (5.10) and making some reductions, one obtains

$$-(U_0+\omega x_2-q_1)\frac{\partial q_1}{\partial x_1}+q_2\left(\omega-\frac{\partial q_1}{\partial x_2}\right)=-\frac{1}{\rho}\frac{\partial P}{\partial x_1}-\frac{\partial \overline{u_1'^2}}{\partial x_1}-\frac{\partial \overline{u_1'u_2'}}{\partial x_2} \tag{5. 13}$$

$$(U_0+\omega x_2-q_1)\frac{\partial q_2}{\partial x_1}+q_2\frac{\partial q_2}{\partial x_2}=-\frac{1}{\rho}\frac{\partial P}{\partial x_2}-\frac{\partial \overline{u_1'u_2'}}{\partial x_1}-\frac{\partial \overline{u_2'^2}}{\partial x_2} \tag{5. 14}$$

$$-\frac{\partial q_1}{\partial x_1}+\frac{\partial q_2}{\partial x_2}=0 \tag{5. 15}$$

in which the viscous terms $\nu\nabla^2 U_1$, $\nu\nabla^2 U_2$ are neglected, since one assumes such a large Reynolds number that molecular effects are negligible with respect to the turbulent effects.

One introduces length scales $L_1$, $L_2$ for the $x_1$-and $x_2$-directions, respectively. Since the turbulent wake region is narrow in the $x_2$-direction in comparison with the $x_1$-direction, the length scales satisfy the relation

$$\frac{L_2}{L_1}\ll 1 \tag{5. 16}$$

Let $V_1$ be a suitable velocity scale for the main velocity $U_1$ ; one may conveniently take, for instance, the maximum velocity difference across a section perpendicular to the main-flow diretion. The magnitude of the velocity scale $V_2$ for the velocity component $U_2$ is no longer independent of the velocity scale $V_1$, because changes in the velocities in various directions are not independent on the ground of the equation of continuity. Hence, from Eq. (5. 15),

$$\frac{V_1}{L_1}\sim\frac{V_2}{L_2}\quad\text{or}\quad\frac{V_2}{V_1}\sim\frac{L_2}{L_1} \tag{5. 17}$$

The Reynolds equations of motion contain the turbulence Reynolds stresses $\rho\overline{u_i'u_j'}$, for which, too, one has to introduce a suitable scale. One knows from experience that, in anisotropic shear flows, the intensities $\overline{u_1'^2}$ and $\overline{u_2'^2}$ are of the same order of magnitude (Hinze [40]). So one may introduce the same scale $\overline{u'^2}$ for $\overline{u_1'^2}$ and $\overline{u_2'^2}$. The magnitude of the shear stress $\rho\overline{u_1'u_2'}$, compared with $\rho\overline{u_1'^2}$ and $\rho\overline{u_2'^2}$, depends on the magnitude of the correlation coefficient $R_{12}$. Thus one may assume

$$\overline{u_1'^2}\sim\overline{u_2'^2}\sim\overline{u'^2}$$

and

$$\overline{u_1'u_2'}\sim R_{12}\overline{u'^2} \tag{5. 18}$$

At a large distance behind the cylinder $q_1$ is small compared with $U_0$, so that one may put

$$\frac{U_0}{q_1}\gg 1 \tag{5. 19}$$

Now, it is possible to write down the equation of motion and, below each term, its relative order of magnitude with respect to the other terms, expressed in terms of the velocity and length scales. For the $x_1$-direction one obtains

$$\begin{array}{l}
-\left(U_0\dfrac{\partial q_1}{\partial x_1}+\omega x_2\dfrac{\partial q_1}{\partial x_1}-q_1\dfrac{\partial q_1}{\partial x_1}\right)+\left(\omega q_2-q_2\dfrac{\partial q_1}{\partial x_2}\right)\\
\qquad\dfrac{U_0}{q_1}\qquad\quad\dfrac{\omega L_2}{q_1}\qquad\quad 1\qquad\qquad\dfrac{\omega L_2}{q_1}\qquad 1\\
\quad=-\dfrac{1}{\rho}\dfrac{\partial P}{\partial x_1}-\dfrac{\partial\overline{u_1'^2}}{\partial x_1}-\dfrac{\partial\overline{u_1'u_2'}}{\partial x_2}\\
\qquad\quad\dfrac{\varDelta P_1}{\rho V_1^2}\qquad\dfrac{\overline{u_1'^2}}{V_1^2}\quad R_{12}\dfrac{\overline{u'^2}}{V_1^2}\dfrac{L_1}{L_2}
\end{array} \tag{5. 20}$$

where $\varDelta P_1$ means a change in pressure in the $x_1$-direction. For the equation of motion in the $x_2$-direction one obtains

$$\begin{array}{l}
\left(U_0\dfrac{\partial q_2}{\partial x_1}+\omega x_2\dfrac{\partial q_2}{\partial x_1}-q_1\dfrac{\partial q_2}{\partial x_1}\right)+q_2\dfrac{\partial q_2}{\partial x_2}\\
\quad\dfrac{U_0}{q_1}\qquad\quad\dfrac{\omega L_2}{q_1}\qquad\quad 1\qquad\quad 1\\
\quad=-\dfrac{1}{\rho}\dfrac{\partial P}{\partial x_2}-\dfrac{\partial\overline{u_1'u_2'}}{\partial x_1}-\dfrac{\partial\overline{u_2'^2}}{\partial x_2}\\
\qquad\quad\dfrac{\varDelta P_2}{\rho V_1^2}\quad R_{12}\dfrac{\overline{u'^2}}{V_1^2}\dfrac{L_1}{L_2}\quad\dfrac{\overline{u'^2}}{V_1^2}\dfrac{L_1^2}{L_2^2}
\end{array} \tag{5. 21}$$

On the grounds of the assumption that $U_0/q_1\gg 1$, the terms $q_1\partial q_1/\partial x_1$, $q_2\partial q_1/\partial x_2$, $q_1\partial q_2/\partial x_1$ and $q_2\partial q_2/\partial x_2$ on the left-hand side of Eqs. (5. 20) and (5. 21) are of a smaller order of magnitude. If it is assumed that the correlatio ncoefficient $R_{12}$ is not small compared with unity, $\partial\overline{u_1'^2}/\partial x_1$ in Eq. (5. 20) is small compared with $\partial \overline{u_1' u_2'}/\partial x_2$, and $\partial \overline{u_1' u_2'}/\partial x_1$ in Eq. (5.21) is small compared with another turbulence term.

Since at the most $\overline{u'^2}/U_1^2$ may be of the order 1, it follows from Eq. (5.20) that $U_0/q_1$ cannot be of a higher order of magnitude than $L_1/L_2$; in other words, $U_0/q_1$ must be of the same order of magnitude as $L_1/L_2$ (Hinze [40]). But, if this is so, the first term on the left-hand side of Eq. (5.21) also remains small compared with the turbulence term $\partial \overline{u_2'^2}/\partial x_2$. Hence the only other term that can balance these turbulence terms is the pressure term $\partial P/\rho \partial x_2$.

Consequently, if one retains only the terms of the highest order of magnitude, the equation of motion Eq. (5.21) may be reduced to

$$\frac{1}{\rho}\frac{\partial P}{\partial x_2}+\frac{\partial \overline{u_2'^2}}{\partial x_2}=0 \tag{5. 22 a}$$

or, after integration,

$$P+\rho \overline{u_2'^2}=P_0 \tag{5. 22 b}$$

where $P_0$ is the pressure at the same section but is outside of the turbulent wake region.

On the other hand Eq. (5.20) yields the two equations according to the order of magnitude of $\omega L_2/q_1$;

(Case 1)

$$U_0\frac{\partial q_1}{\partial x_1}=\frac{1}{\rho}\frac{\partial P}{\partial x_1}+\frac{\partial \overline{u_1' u_2'}}{\partial x_2} \tag{5. 23 a}$$

for

$$\frac{\omega L_2}{q_1}\sim 1 \quad \text{or} \quad \frac{\omega L_2}{q_1}\ll 1 \tag{5. 23 b}$$

(Case 2)

$$(U_0+\omega x_2)\frac{\partial q_1}{\partial x_1}-\omega q_2=\frac{1}{\rho}\frac{\partial P}{\partial x_1}+\frac{\partial \overline{u_1' u_2'}}{\partial x_2} \tag{5. 24 a}$$

for

$$\frac{\omega L_2}{q_1}\gg 1 \tag{5. 24 b}$$

The physical meaning of the conditions given by Eqs. (5.23 b) and (5.24 b) is illustrated in Fig. 5.13. In case 1, the flow in the wake can be treated as if there is no transverse velocity gradient in the approaching stream. So, in what follows, attention will be confined to case 2.

Eq. (5.24 a) can be solved if the function $\overline{u_1' u_2'}$ is known, or its relation to the distribution of $U_1$. From Eq. (5.22 b) one can calculate the pressure distribution. The turbulence term can be expressed in terms of the distribution of $U_1$ by introducing the eddy-diffusion coefficient $\varepsilon$, if it is assumed that the transport of momentum is due to the gradient type of diffusion :

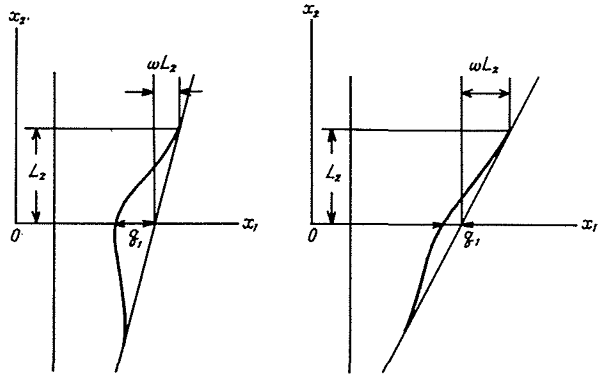

$\omega L_2/q_1 \sim 1$ or $\omega L_2/q_1 \ll 1$ $\omega L_2/q_1 \gg 1$

**Fig. 5. 13.** Illustration of the physical meaning of Eqs. (5. 23 b) and (5. 23 c).

$$-\rho\overline{u_1'u_2'} = \rho\varepsilon\frac{\partial U_1}{\partial x_2} = \rho\varepsilon\left(\omega - \frac{\partial q_1}{\partial x_1}\right) \tag{5. 25}$$

For the sake of simplicity, $\varepsilon$ is assumed a constant here, although it may take other forms according the various hypotheses proposed by Prandtl (the momentum transport), Taylor (the vorticity transport) and Kármán (the dynamical similarity hypothesis).

If one introduces the non-dimensional variables

$$\lambda = \omega d/U_0\,, \qquad \varepsilon_0 = \varepsilon/(U_0 d)$$
$$(\xi_1, \xi_2) = (x_1/d,\, x_2/d)\,, \qquad (\tilde{q}_1, \tilde{q}_2) = (q_1/U_0,\, q_2/U_0)$$
$$\tilde{p} = P/(\rho U_0^2)$$

Eqs. (5. 24 a) and (5. 15) can be rewritten as

$$(1+\lambda\xi_2)\frac{\partial\tilde{q}_1}{\partial\xi_1} - \lambda\tilde{q}_2 = \frac{\partial\tilde{p}}{\partial\xi_1} + \varepsilon_0\frac{\partial^2\tilde{q}_1}{\partial\xi_2^2} \tag{5. 26 a}$$

$$-\frac{\partial\tilde{q}_1}{\partial\xi_1} + \frac{\partial\tilde{q}_2}{\partial\xi_2} = 0 \tag{5. 26 b}$$

Eqs. (5. 26 a) and (5. 26 b) constitute the governing equations.

### *b) Perturbation Solution*

For such a moderate pressure gradient as involved in the present experiment, its effect on the wake development may be small enough to be neglected. Then omitting the pressure term in Eq. (5. 26 a), one obtains the following fundamental equations :

$$(1+\lambda\xi_2)\frac{\partial\tilde{q}_1}{\partial\xi_1} - \lambda\tilde{q}_2 = \varepsilon_0\frac{\partial^2\tilde{q}_1}{\partial\xi_2^2} \tag{5. 27 a}$$

$$-\frac{\partial\tilde{q}_1}{\partial\xi_1} + \frac{\partial\tilde{q}_2}{\partial\xi_2} = 0 \tag{5. 27 b}$$

Since $\lambda$ is of a smaller order of magnitude than unity, one assumes the perturbation solution

$$\tilde{q}_1 = q_1^{(0)} + \lambda q_1^{(1)} + \lambda^2 q_1^{(2)} + \cdots \tag{5. 28 a}$$

$$\tilde{q}_2 = q_2^{(0)} + \lambda q_2^{(1)} + \lambda^2 q_2^{(2)} + \cdots \tag{5. 28 b}$$

Inserting expressions (5. 28 a) and (5. 28 b) into Eqs. (5. 27 a) and (5. 27 b), and comparing the terms of the same power of $\lambda$, one obtains a system of simultaneous partial differential equations for the functions $q_1^{(0)}$, $q_1^{(1)}$, $\cdots$, $q_2^{(0)}$, $q_2^{(1)}$, $\cdots$ :

$$\frac{\partial q_1^{(0)}}{\partial \xi_1} = \varepsilon_0 \frac{\partial^2 q_1^{(0)}}{\partial \xi_2^2}, \qquad \frac{\partial q_1^{(0)}}{\partial \xi_1} = \frac{\partial q_2^{(0)}}{\partial \xi_2} \tag{5. 29 a, b}$$

$$\frac{\partial q_1^{(1)}}{\partial \xi_1} + \xi_2 \frac{\partial q_1^{(0)}}{\partial \xi_1} - q_2^{(0)} = \varepsilon_0 \frac{\partial^2 q_1^{(1)}}{\partial \xi_2^2}, \qquad \frac{\partial q_1^{(1)}}{\partial \xi_1} = \frac{\partial q_2^{(1)}}{\partial \xi_2} \tag{5. 30 a, b}$$

$$\frac{\partial q_1^{(2)}}{\partial \xi_1} + \xi_2 \frac{\partial q_1^{(1)}}{\partial \xi_1} - q_2^{(1)} = \varepsilon_0 \frac{\partial^2 q_1^{(2)}}{\partial \xi_2^2}, \qquad \frac{\partial q_1^{(2)}}{\partial \xi_1} = \frac{\partial q_2^{(2)}}{\partial \xi_2} \tag{5. 31 a, b}$$

..................................

$q_1^{(0)}$ and $q_2^{(0)}$ describe the wake of the cylinder placed in an unbounded uniform flow of which the velocity is unity, and is known to have the forms

$$q_1^{(0)} = \frac{A}{\sqrt{\xi_1}} \exp\left(-\frac{\eta^2}{4\varepsilon_0}\right) \tag{5. 32 a}$$

$$q_2^{(0)} = -\frac{A}{2\xi_1} \eta \exp\left(-\frac{\eta^2}{4\varepsilon_0}\right) \tag{5. 32 b}$$

where

$$\eta = \frac{\xi_2}{\sqrt{\xi_1}} \tag{5. 33}$$

$A$ is the constant of integration and, as will be derived later in 5. 5 (c), has the following relation to the drag coefficient $C_D$ ;

$$A = \frac{C_D}{\sqrt{4\pi\varepsilon_0}} \tag{5. 34}$$

According to the measurement of the wake behind a circular cylinder placed in an uniform flow, the value of $\varepsilon_0$ is about 0.016.

Substitution of Eqs. (5.32a) and (5.32b) into Eq. (5.30a) yields

$$\frac{\partial q_1^{(1)}}{\partial \xi_1} - \varepsilon_0 \frac{\partial^2 q_1^{(1)}}{\partial \xi_2^2} = -\frac{A}{4\varepsilon_0 \xi_1} \eta^3 \exp\left(-\frac{\eta^2}{4\varepsilon_0}\right) \tag{5. 35}$$

If one assumes the solution of the form

$$q_1^{(1)} = A f(\eta) \tag{5. 36}$$

and substitutes this into Eq. (5. 35), one obtains

$$\frac{d^2 f}{d\eta^2} + \frac{1}{2\varepsilon_0} \eta \frac{df}{d\eta} = \frac{\eta^3}{4\varepsilon_0^2} \exp\left(-\frac{\eta^2}{4\varepsilon_0}\right)$$

This equation can be easily integrated to

$$f(\eta)=\frac{1}{16\varepsilon_0^2}\int_{-\infty}^{\eta}\eta^4\exp\left(-\frac{\eta^2}{4\varepsilon_0}\right)d\eta+f'(0)\int_{-\infty}^{\eta}\exp\left(-\frac{\eta^2}{4\varepsilon_0}\right)d\eta$$

since $f\to 0$ as $\eta\to-\infty$. The value of $f'(0)$ can be obtained from the condition that $f\to 0$ as $\eta\to\infty$ ;

$$f'(0)=-\frac{1}{16\varepsilon_0^2}\int_{-\infty}^{\infty}\eta^4\exp\left(-\frac{\eta^2}{4\varepsilon_0}\right)d\eta\Big/\int_{-\infty}^{\infty}\exp\left(-\frac{\eta^2}{4\varepsilon_0}\right)d\eta=-\frac{3}{4}$$

Accordingly, the solution of Eq. (5. 35) becomes

$$q_1^{(1)}=Af(\eta)=A\int_{-\infty}^{\eta}\left(\frac{\eta^4}{16\varepsilon_0^2}-\frac{3}{4}\right)\exp\left(-\frac{\eta^2}{4\varepsilon_0}\right)d\eta \tag{5. 37}$$

$q_1^{(1)}$ means a first order correction of the velocity distribution in the wake. The corresponding component of velocity in the normal direction, $q_2^{(1)}$, can be computed from Eq. (5. 30 b) in terms of $q_1^{(1)}$ ;

$$q_2^{(1)}=\int\frac{\partial q_1^{(1)}}{\partial\xi_1}d\xi_2=\frac{A}{4\sqrt{\xi_1}}\left(5\varepsilon_0+2\eta^2+\frac{\eta^4}{4\varepsilon_0}\right)\exp\left(-\frac{\eta^2}{4\varepsilon_0}\right) \tag{5. 38}$$

An arbitrary function of $\xi_1$ may be added to the right-hand side of Eq. (5. 38), but, since there is no clue to determine this function, it will tentatively be put equal to zero.

In order to obtain a second order correction for the velocity distribution, Eqs. (5. 37) and (5. 38) are substituted into Eq. (5. 31 a). After some reductions one obtains

$$\frac{\partial q_1^{(2)}}{\partial\xi_1}-\varepsilon_0\frac{\partial^2 q_1^{(2)}}{\partial\xi_2^2}=\frac{A}{4\sqrt{\xi_1}}\left(5\varepsilon_0+\frac{\eta^2}{2}+\frac{\eta^4}{4\varepsilon_0}+\frac{\eta^6}{8\varepsilon_0^2}\right)\exp\left(-\frac{\eta^2}{4\varepsilon_0}\right)$$

If one assumes the solution of the form

$$q_1^{(2)}=A\sqrt{\xi_1}\,g(\eta) \tag{5. 39}$$

$g(\eta)$ must satisfy the following ordinary differential equation ;

$$\frac{d^2g}{d\eta^2}+\frac{\eta}{2\varepsilon_0}\frac{dg}{d\eta}-\frac{g}{2\varepsilon_0}=-\left(\frac{5}{4}+\frac{\eta^2}{8\varepsilon_0}+\frac{\eta^4}{16\varepsilon_0^2}+\frac{\eta^6}{32\varepsilon_0^3}\right)\exp\left(-\frac{\eta^2}{4\varepsilon_0}\right) \tag{5. 40}$$

Let the particular integral of Eq. (5. 40) be

$$g_p=\left(\varepsilon_0\delta+\alpha\eta^2+\frac{\beta\eta^4}{\varepsilon_0}+\frac{\gamma\eta^6}{\varepsilon_0^2}\right)\exp\left(-\frac{\eta^2}{4\varepsilon_0}\right)$$

where $\delta$, $\alpha$, $\beta$, and $\gamma$ are the constants to be determined. Substitution of this expression into the left-hand side of Eq. (5. 40) yields

$$\left\{(2\alpha-\delta)+\left(\frac{12\beta}{\varepsilon_0}-\frac{2\alpha}{\varepsilon_0}\right)\eta^2+\left(\frac{30\gamma}{\varepsilon_0^2}-\frac{3\beta}{\varepsilon_0^2}\right)\eta^4-\frac{4\gamma}{\varepsilon_0^3}\eta^6\right\}\exp\left(-\frac{\eta^2}{4\varepsilon_0}\right)$$
$$=-\left(\frac{5}{4}+\frac{\eta^2}{8\varepsilon_0}+\frac{\eta^4}{16\varepsilon_0^2}+\frac{\eta^6}{32\varepsilon_0^3}\right)\exp\left(-\frac{\eta^2}{4\varepsilon_0}\right)$$

By comparing the terms on each side of this equation, one obtains

$$\alpha=\frac{21}{31}, \qquad \beta=\frac{19}{192}, \qquad \gamma=\frac{1}{128}, \qquad \delta=\frac{41}{16}$$

Accordingly, the particular integral becomes

$$g_p=\left(\frac{41}{16}\varepsilon_0+\frac{21}{32}\eta^2+\frac{19}{192}\frac{\eta^4}{\varepsilon_0}+\frac{1}{128}\frac{\eta^6}{\varepsilon_0^2}\right)\exp\left(-\frac{\eta^2}{4\varepsilon_0}\right) \tag{5.41}$$

which tends to zero as $\eta \to +\infty$ and $-\infty$, respectively. The complementary function, $g_c$, of Eq. (5.40) is the solution of the equation

$$\frac{d^2 g}{d\eta^2}+\frac{\eta}{2\varepsilon_0}\frac{dg}{d\eta}-\frac{g}{2\varepsilon_0}=0$$

If one introduces the new variable $\tau$ defined by

$$\tau=\eta/\sqrt{2\varepsilon_0}$$

the above equation reduces to the form

$$\frac{d^2 g}{d\tau^2}+\tau\frac{dg}{d\tau}-g=0$$

This equation is a special case of the generalized Hermite's differential equation

$$\frac{d^2 G}{d\tau^2}+\tau\frac{dG}{d\tau}+(s+1)G=0 \tag{5.42}$$

with $s=-2$. The general solution of Eq. (5.42) is given by

$$G(\tau)=A_s\exp\left(-\frac{\tau^2}{4}\right)D_s(\tau)+B_s\exp\left(-\frac{\tau^2}{4}\right)D_{-s-1}(i\tau)$$

where $A_s$, $B_s$ are constants and $D_s(\tau)$ means the Weber function

$$\begin{aligned}D_s(\tau)=2^{\frac{s}{2}}\pi^{\frac{1}{2}}\exp\left(-\frac{\tau^2}{4}\right)&\left[\frac{1}{\Gamma\{(1-s)/2\}}F\left(-\frac{s}{2},\frac{1}{2};\frac{\tau^2}{2}\right)\right.\\&\left.-\frac{\sqrt{2}\,\tau}{\Gamma(-s/2)}F\left(\frac{1-s}{2},\frac{3}{2};\frac{\tau^2}{2}\right)\right]\end{aligned}$$

Consequently, the complementary function becomes

$$\begin{aligned}g_c&=A_{-2}\exp\left(-\frac{\tau^2}{4}\right)+B_{-2}\exp\left(-\frac{\tau^2}{4}\right)D_1(i\tau)\\&=A_{-2}\left[\exp\left(-\frac{\tau^2}{4}\right)-\sqrt{2\pi}\,\tau\left(1-\frac{1}{\sqrt{2\pi}}\int_{-\infty}^{\tau}\exp\left(-\frac{t^2}{2}\right)dt\right)\right]+B_{-2}i\tau\end{aligned}$$

Since $g_c$ must be a real function, it follows that $B_{-2}=0$. When $\tau \to +\infty$, $g_c$ certainly tends to zero, but it becomes $-\infty$ when $\tau \to -\infty$, which is never acceptable on physical grounds. Then $A_{-2}$ must also vanish, and the complementary function will not appear in the final solution.

Accordingly, a second order correction of the longitudinal component of velocity, $q_1^{(2)}$, becomes

$$q_1^{(2)}=A\sqrt{\xi_1}\,g_p(\eta) \tag{5.43}$$

The velocity component in the $x_2$ direction is obtained from Eq. (5. 31 b):

$$q_2^{(2)}-q_2^{(2)}(-\infty)=\frac{A}{2}\int_{-\infty}^{\eta}\left(g_p-\eta\frac{dg_p}{d\eta}\right)d\eta$$

$$=\frac{A}{2}\int_{-\infty}^{\eta}\left(\frac{41\varepsilon_0}{16}+\frac{5\eta^2}{8}+\frac{\eta^4}{32\varepsilon_0}+\frac{\eta^6}{96\varepsilon_0^2}+\frac{\eta^8}{256\varepsilon_0^3}\right)\exp\left(-\frac{\eta^2}{4\varepsilon_0}\right)d\eta \qquad (5.\ 44)$$

Since the right-hand side of this equation tends to nonzero value (say, $\alpha$) when $\eta\rightarrow+\infty$, one obtains the relation

$$q_2^{(2)}(\infty)-q_2^{(2)}(-\infty)=\alpha \qquad (5.\ 45)$$

Eq. (5. 45) shows that the direction of the velocity vector at each edge of the wake is not parallel to the main flow direction, and may be understood to represent the spread of the wake in the transverse direction. However, one has no clue to obtain on a theoretical basis the possible values of $q_2^{(2)}(\infty)$ and $q_2^{(2)}(-\infty)$, respectively, and these remain undetermined. Since the same kind of indeterminacy necessarily appears when one calculates the higher order corrections, it will be meaningless to extend the calculation to higher order terms. Thus the perturbation solution of the form of Eqs. (5. 28 a) and (5. 28 b) may be said to give the correct longitudinal component of velocity up to the first three terms.

*c) Drag Force Acting on the Cylinder*

By means of the momentum principle one can calculate the drag force acting on the cylinder from the velocity profile in the wake. In order to determine the momentum-flux balance one assumes a set of imaginary control planes at large distances from the cylinder (see Fig. 5.12). Through the set of planes $A_1A_2$ and $B_1B_2$ there is a flux of momentum in the $x_1$ direction:

$$\rho h\int_{-\infty}^{+\infty}\left\{(U_0+\omega x_2)^2-(U_0+\omega x_2-q_1)^2\right\}dx_2$$

$$\fallingdotseq 2\rho h\int_{-\infty}^{\infty}(U_0+\omega x_2)\,q_1\,dx_2$$

where $h$ is the depth of the control volume. Through the same control planes $A_1A_2$ and $B_1B_2$ there is a defect in mass flow equal to

$$\rho h\int_{-\infty}^{\infty}\left\{(U_0+\omega x_2)-(U_0+\omega x_2-q_1)\right\}dx=\rho h\int_{-\infty}^{\infty}q_1\,dx_2$$

This is balanced by an efflux of an equal amount through the set of control planes $A_1B_1$ and $A_2B_2$, causing a loss in momentum flux in the $x_1$-direction. Upon remembering that the flow outside the wake is uniformly sheared, one may write this loss in momentum flux in th form

$$-\rho h\,U_0\int_{-\infty}^{\infty}q_1\,dx_2$$

The sum of these momentum fluxes must be equal to the drag $D$ of the cylinder:

$$D=\rho h\int_{-\infty}^{\infty}(U_0+2\omega x_2)\,q_1\,dx_2$$

Accordingly, the drag coefficient becomes

$$C_D = 2\int_{-\infty}^{\infty} (1+2\lambda\xi_2)\,\tilde{q}_1\,d\xi_2 \tag{5. 55}$$

Subsituting Eq. (5. 28 a) into Eq. (5. 55), one obtains

$$C_D = 2\int_{-\infty}^{\infty} q_1^{(0)}\,d\xi_2 + 2\lambda\int_{-\infty}^{\infty} (2\xi_2 q_1^{(0)} + q_1^{(1)})\,d\xi_2 + \cdots$$

Since, as is easily seen in Eqs. (5. 32 a) and (5. 37), the functions $q_1^{(0)}$ and $q_1^{(1)}$ are even and odd functions of $\xi_2$, respectively, the second integral of the above expression is identically zero. Thus one obtains

$$C_D = 2\int_{-\infty}^{\infty} q_1^{(0)}\,d\xi_2 = A\sqrt{4\pi\varepsilon_0} \tag{5. 55 a}$$

or

$$A = \frac{C_D}{\sqrt{4\pi\varepsilon_0}} \tag{5. 56 b}$$

Eq. (5. 55 a) shows that the effect of the transverse velocity gradient of the oncoming flow on the drag coefficient of the cylinder is of a higher order of magnitude than the first power of $\omega d/U_0$.

*d) A Comparison with Experiments*

The longitudinal velocity component in the wake is calculated for several sections downstream of the cylinder, the values of constants being taken as $\varepsilon_0 = 0.016$ and $\lambda = 0.05$. The results are presented in Fig. 5. 14 in the form of $\tilde{q}_1/(C_D/\sqrt{4\pi\varepsilon_0})$ against $\xi_2/\sqrt{\varepsilon_0\xi_1}$. It will be seen from this figure that the spread of the wake is greater towards the side of the smaller velocity than on the side of the larger one as would physically be expected, and that the degree of asymmetry of the wake on both sides of the center line ($x_1$-axis) increases as further downstream sections are approached. For the sake of reference, the relation between the diameter of the cylinder and the inclination of the velocity profile is illustrated in Fig. 5. 15 for two values of $\lambda$, i. e. $\lambda = 0.05$ and $\lambda = 0.1$.

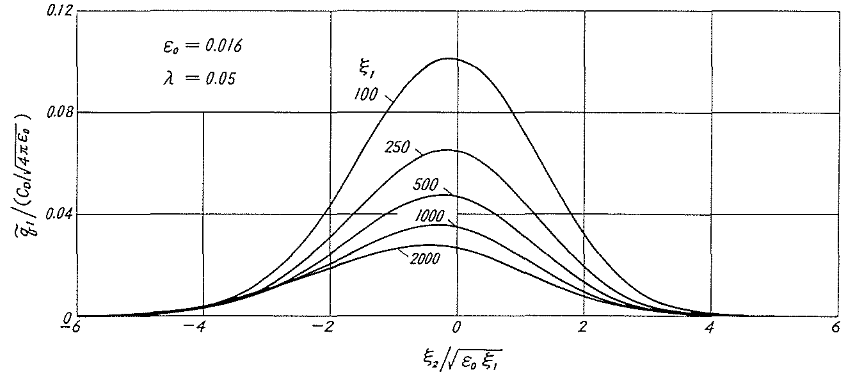

**Fig. 5. 14.** Distribution of longitudinal component of velocity in the wake (Theory).

The mean velocity profiles in the wake of 1.2 mm cylinder are shown in Fig. 5. 16 for several downstream sections, together with the one in the undisturbed turbulent boundary layer. As was previously stated, the center of the cylinder was located at a position 30 mm apart from the boundary wall. Since, as will be seen in Figs. 5. 16, the flow outside the wake is considerably accelerated especially in the sections $(x-x_c)/d=51.7$, 105 and 148, it is difficult to define the amount of velocity defect in the wake. Thus the dotted lines in the figures are tentatively chosen as the reference velocity to compute the velocity defect. The results at the two sections, i. e. $(x-x_c)/d=105$ and 148, respectively, are shown in Fig. 5. 17 in terms of $\tilde{q}_1$ and $\xi_2$. It is clearly seen that the wake spreads more rapidly on the side of lower velocity than on the

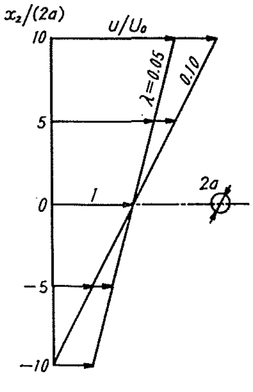

**Fig. 5. 15.** Geometrical relation between the diameter of cylinder and the inclination of velocity profile.

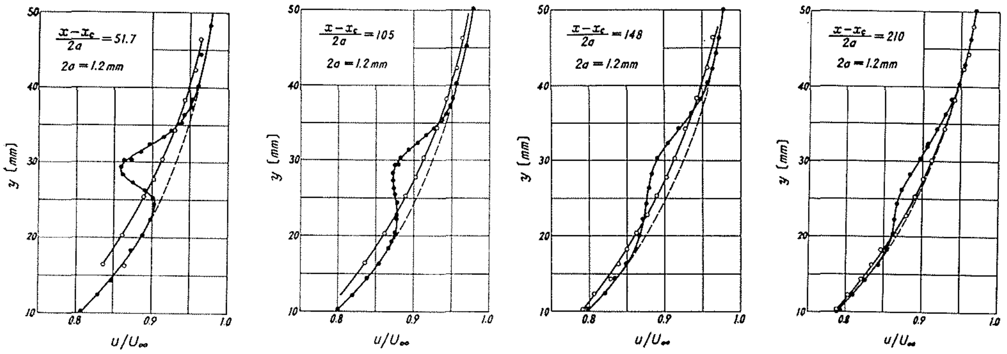

(a) (b) (c) (d)

**Fig. 5. 16.** Velocity distribution in the wake of 1.2 mm cylinder: (a) $(x-x_c)/(2a)=51.7$, (b) 105, (c) 148, (d) 210.

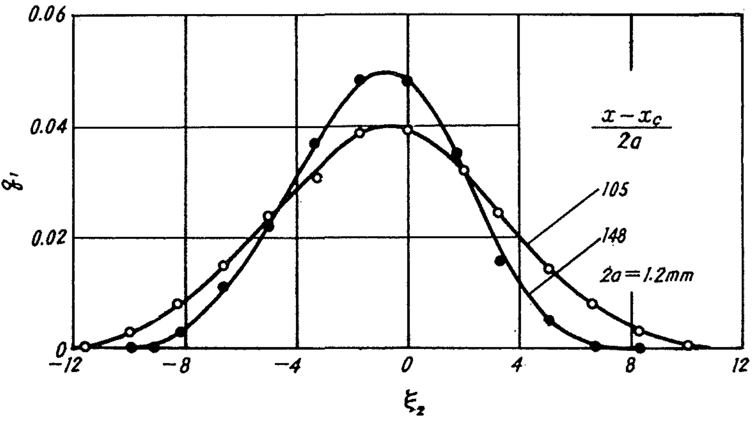

**Fig. 5. 17.** Velocity defect in the wake of 1.2 mm cylinder.

side of the larger one, which confirms qualitatively the theoretical prediction.

It was shown in the last section that the drag force of the cylinder will not be affected by the presence of the transverse velocity gradient of the approaching stream, at least to the first order of magnitude of the coefficient $\omega d/U_0$. This fact may be verified experimentally by the result of section 5. 4.

## 6. Concluding Remarks

This study describes a two-dimensional flow past a circular cylinder placed in a turbulent boundary layer, with special reference to the drag and lift forces acting on the cylinder. A theoretical analysis of the flow was made for a hypothetical inviscid shear flow with a linearly varying velocity profile, and experiments were performed with a circular cylinder placed in an artificially produced shear flow and in a turbulent boundary layer, respectively.

The primary results of these investigations will be summarized in what follows.

In order to simulate theoretically the flow across a two-dimensional body in a turbulent boundary layer, an analytical method of determining the simple shear flow past two circular cylinders was devised by the use of bipolar coordinates. The result includes as a special case of solutions of a uniform flow past two cylinders that were previously obtained by Lagally [19] and Müller [20], and therefore constitutes an extension of their problem. By making the radius of the lower cylinder infinitely large, one can establish the simple shear flow past a circular cylinder subjected to an interference of a plane wall by means of the stream function :

$$\frac{\phi}{U_0 a}=(1-\lambda)\sinh\alpha\phi^{(0)}+\frac{\lambda}{2}\sinh\alpha\tanh\alpha\phi^{(1)}$$

where

$$\phi^{(0)}=\frac{\sinh\eta}{\cosh\eta-\cos\xi}-4\sum_{n=1}^{\infty}\frac{\sinh n\eta\cos n\xi}{e^{2n\alpha}-1}$$

$$\phi^{(1)}=\left(\frac{\sinh\eta}{\cosh\eta-\cos\xi}\right)^2-4\sum_{n=1}^{\infty}\frac{\coth\alpha+n}{e^{2n\alpha}-1}\sinh n\eta\cos n\xi$$

The corresponding pressure coefficient on the circular cylinder is found to be

$$\frac{p-p_0}{\frac{1}{2}\rho U_0^2}=1-\lambda(2-\lambda)(1-\tanh\alpha)-\left(\frac{q_c}{U_0}\right)^2$$

A numerical calculation of the pressure coefficient was performed in some detail in order to clarify the combined effect of both the approaching velocity gradient and the plane boundary wall on the pressure distribution of the cylinder. The stagnation pressure decreases as the distance between the cylinder and the plane wall decreases, while in the case of uniform flow the stagnation pressure coefficient is always unity. In both cases, the pressure distribution becomes asymmetrical on the upper and lower surfaces of the cylinder, respectively, and this fact suggests that a lift force will act on the cylinder. The lift force is calculated by numerically integrating the pressure on the surface of the cylinder, and is found to be negative in the vicinity of the plane wall so far as $\omega=0$ that means the case of a uniform flow. However, the lift force becomes positive when there exists a certain amount of velocity gradiedt in the vertical diection of flow, which is similar to the case of a practical boundary layer that develops along a stationary boundary wall.

In order to check the theoretical predictions, an experiment was made with a cylinder in a uniform shear flow artificially produced by arranging a grid of rods over an entire section of a wind tunnel. It was found that an acceptable agreement between the theory and experiment was obtained concerning the stagnation pressure and the position of stagnation point, respectively, provided that the clearance between the cylinder and the plane wall is not too small. The experimental value of lift coefficient increases when the cylinder approaches the plane wall, which is the qualitative agreement with the theory.

Klebanoff and Diehl [25] have reported that it is possible to thicken substantially a fully developed turbulent boundary layer on a flat plate by placing appropriate tripping devices in contact with the surface, However, it was found from preliminary measurements that their method was not effective when the boundary layer to be thickened was alreardy turbulent at the section of tripping objects. After trial and error, the turbulent boundary layer along the tunnel wall was successfully thickened by cementing a circular cylinder of 19 mm diameter onto the tunnel wall in the manner as is shown in Fig. 4. 12. The layer so formed becomes almost characteristic of that developed from the beginning on a smooth flat plate after passing over the required length of a smooth surface.

Four cylinders of different diameter are mounted in turns in the artificially thickened turbulent boundary layer of about 60 mm in thickness at the section where the test cylinder is mounted. The pressure distribution on the cylinder is measured to be integrated for the evaluation of the lift and drag forces. It is found that the drag and lift coefficients plotted against the ratio $\Delta/(2a)$, where $\Delta$ is the clearance between the cylinder and the boundary wall and $a$ is the radius of the cylinder, are represented respectively by a single curve within an acceptable experimental errors, the Reynolds number being in a range of $(0.99\sim3.78)\times10^4$. The lift and drag coefficients and the Reynolds number have been formed in terms of the approaching velocity at the center of the cylinder and the diameter of the cylinder. With $\Delta/(2a)$ decreasing, the lift coefficient is found to increase monotonically from 0 to a moximum value of about 0.8 at $\Delta/(2a)=0$, and on the contrary the drag coefficient decreases from 1.2 to a minimum value of about 0.95 after passing the maximum value of about 1.3 in the vicinity of $\Delta/(2a)=0.16$. The positive value of lift coefficient implies that the cylinder in the turbulent boundary layer acquires a transverse force that tends to move it from the boundary wall, as is predicted qualitatively by the theoretical analysis of a uniform shear flow.

In order to estimate the contribution of viscous shear stress to the lift and drag coefficients, the laminar boundary layer that develops along the surface of the cylinder is calculated in detail by the use of asymmetrical Blasius series and Pohlhausen's approximate method. It is clarified that, as the distance between the cylinder and the boundary wall decreases, the distribution of shearing stress becomes more and more asymmetrical on the upper and lower surfaces of the cylinder, and accordingly a torque acts on the cylinder. Moreover, it becomes obvious that the laminar boundary layer separates from the surface a little earlier (about 4° at most when measured from the stagnation point) on the upper side than on the lower one. The contribution of shearing stress to the lift and drag coefficients is found to be 2% at most of the total value in the Reynolds number range $(0.99 \sim 3.78) \times 10^4$, in accordance with the case of uniform flow.

When the diameter of cylinder becomes very small compared with the thickness of the boundary layer, it becomes difficult in practice to estimate the drag force by the measurement of pressure distribution on the cylinder, and use must be made of the momentum principle. Two cylinders of 1.2 mm and 3.2 mm diameter, respectively, are placed in turns in the turbulent boundary layer of 60 mm in thickness and 30 mm apart from the boundary wall to measure the variations of mean velocity, turbulence and the static pressure in the wake. The drag coefficient of the 3.2 mm cylinder computed from the momentum principle is found, within a limit of experimental errors, to be the same as that when it is placed in the unbounded uniform flow, provided that the Reynolds numbers for both cases are the same. Hence it may be said that the normal velocity gradient of the boundary layer exerts little effect on the drag coefficient of a thin circular cylinder, when it is not in the immediate vicinity of the boundary wall. It also becomes evident that the spread of the wake is greater towards the side of the smaller velocity than on the side of larger one.

In an attempt to investigate these facts theoretically, the velocity profile in the wake is derived for the case of uniform shear flow that simulates the velocity profile of the turbulent boundary layer in which the cylinder is placed, the eddy viscosity being assumed to be a constant. It is found from the analysis that the effect of the transverse velocity gradient of the approaching flow on the drag coefficient of the cylinder is of a higher order of magnitude than the first power of $2a\omega/U_0$, where $\omega$ denotes the velocity gradient. It is also found theoretically that the spread of the wake is greater on the side of lower velocity. Thus the experimental results are well interpreted by the theory.

# Appendix

## The Stability of Asymmetrical Double Rows of Vortices in a Uniform Shear Flow

### A 1. Configuration of Vortex Rows

For a two-dimensional flow behind a bluff symmetrical obstacle at a Reynolds number above a certain critical value (about 40), the well known Kármán vortex street is formed behind the obstacle. The regular pattern of vortices is in most cases evident at a distance of four or five diameters behind a solid body. However, in suitable circumstances the trail of vortices persists for a considerable distance behind the body. For theoretical purposes the system far downstream was considered by Kármán [41] to be composed of isolated rectilinear vortices in two parallel rows. Von Kármán's study was followed by a widespread and lasting series of investigations of the subject. For the most part these concerned themselves with experimental comparisons of real vortex streets with Kármán's idealized model, calculations, etc. Rosenhead [42] studied the effect of the walls of a channel on the characteristics and stability of a symmetrically situated vortex street. Levy and Hooker [43] showed that a vortex-street is unstable for the two-dimensional infinitesimal disturbances considered by Kármán if the undisturbed velocity is not uniform but is greatest along the middle of the street.

In the present analytical and experimental studies on the shear flow past a circular cylinder, the Reynolds number of the flow concerned was of the order of magnitude between $10^3$ and $10^4$. For the flow of lower Reynolds number, a vortex system akin to the Kármán vortex street may be originated even in the wake of a two-dimensional bluff obstacle in a shear flow. In this appendix, a flow model of the vortex system which would be formed behind the solid body in a simple shear flow $u=\omega y+U$ is presented, together with a discussion on the stability of the vortex system concenrned.

As a vortex street in a simple shear flow, one takes the configuration illustrated in Fig. A. 1. $l$ and $h$ denote the distance between consecutive vortices in the same row and the lateral spacing between the rows, respectively. The circulation of vortices in the upper row is denoted by $\Gamma_1 (\Gamma_1 > 0)$, while that in the lower

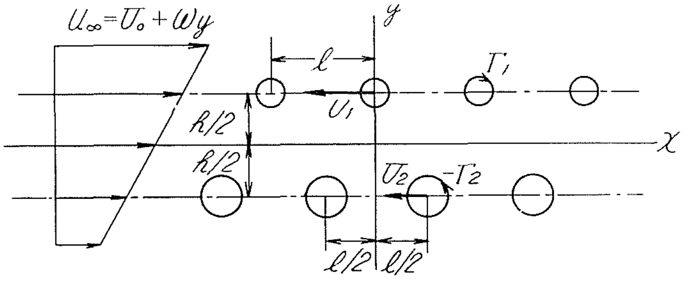

**Fig. A. 1.** Configuration of a vortex-street in a uniform shear flow.

one by $-\Gamma_2 (\Gamma_2 > 0)$. This flow model can be reduced to the Kármán vortex street when $\Gamma_1 = \Gamma_2 = \Gamma$.

It is noted here that for each single infinite row of equidistant vortices, each of a strength of $\Gamma_1$ and $-\Gamma_2$, at distances $l$ apart, with the origin shown in Fig. A. 1 and the axis of $x$ along the row, the complex flow potentials produced by each row are

$$W_1 = \frac{i\Gamma_1}{2\pi} \log \sin \frac{\pi}{l}\left(z - i\frac{h}{2}\right) \tag{A. 1}$$

$$W_2 = -\frac{i\Gamma_2}{2\pi} \log \cos \frac{\pi}{l}\left(z + i\frac{h}{2}\right) \tag{A. 2}$$

where

$$z = x + iy$$

Then the total flow field induced by the two rows of vortices can be described by the sum of $W_1$ and $W_2$:

$$W = W_1 + W_2 = \frac{i\Gamma_1}{2\pi} \log \sin \frac{\pi}{l}\left(z - i\frac{h}{2}\right) - \frac{i\Gamma_2}{2\pi} \log \cos \frac{\pi}{l}\left(z + i\frac{h}{2}\right) \tag{A. 3}$$

It follows easily that when there are two parallel rows of equidistant vortices, the strength being $\Gamma_1$ for the upper and $-\Gamma_2$ for the lower row, as indicated in Fig. A. 1, each row of vortices will move towards the negative $x$ direction with the velocity induced by the vortices in the opposite row. The velocities of advance of the upper and lower rows are given by

$$U_1 = \left(\frac{dW_2}{dz}\right)_{z = ih/2} = -\frac{\Gamma_2}{2l} \tanh \frac{\pi h}{l} \tag{A. 4}$$

$$U_2 = \left(\frac{dW_1}{dz}\right)_{z = -i(h/2) + (l/2)} = -\frac{\Gamma_1}{2l} \tanh \frac{\pi h}{l} \tag{A. 5}$$

respectively. Since $\Gamma_1 \doteqdot \Gamma_2$ in general, the two velocities $U_1$ and $U_2$ are not equal, and consequently the configuration of vortices shown in Fig. A. 1 cannot persist in itself. However, if one superposes a uniform shear flow $u = \omega y + U$ on the system, each row of vortices can be made to move with the same velocity. The condition for this requirement is written as

$$\frac{\omega h}{2} + U + U_1 = -\frac{\omega h}{2} + U + U_2$$

or

$$\omega h = \frac{\Gamma_2 - \Gamma_1}{2l} \tanh \frac{\pi h}{l} \tag{A. 6}$$

Without loss in generality one can put $\omega > 0$. Then $\Gamma_2 > \Gamma_1$, that is, the strength of the vortices in the lower row must be larger than that in the upper row for the vortex system to exist.

## A 2. Equations of Motion of Vortices

When there are $n$ vortices of circulation $\Gamma_k (k=1, 2, \cdots, n)$ at the position $z_k = x_k + iy_k$, the complex flow potential $W$ induced at any point $z = x + iy$ is given by

$$W = \sum_{k=1}^{n} \frac{-i\Gamma_k}{2\pi} \log(z - z_k)$$

Then the induced velocity at the same point becomes

$$u - iv = \frac{dW}{dz} = -\sum_{k=1}^{n} \frac{\Gamma_k}{2\pi} \frac{1}{z - z_k}$$

or, after separating into real and imaginary parts,

$$u = -\sum_{k=1}^{n} \frac{\Gamma_k}{2\pi} \frac{y - y_k}{r_k^2}, \qquad v = \sum_{k=1}^{n} \frac{\Gamma_k}{2\pi} \frac{x - x_k}{r_k^2}$$

where

$$r_k = \left[(x - x_k)^2 + (y - y_k)^2\right]^{1/2}$$

If $z$ coincides with the location $z_m$ of the $m$th vortex, the velocity induced on this vortex by the remaining $(n-1)$ vortices can be written as

$$u_m = -\sum_{k=1}^{n}{}' \frac{\Gamma_k}{2\pi} \frac{y_m - y_k}{r_{mk}^2}, \qquad v_m = \sum_{k=1}^{n}{}' \frac{\Gamma_k}{2\pi} \frac{x_m - x_k}{r_{mk}^2} \tag{A. 7, 8}$$

$$r_{mk} = \left[(x_m - x_k)^2 + (y_m - y_k)^2\right]^{1/2} \tag{A. 9}$$

where $\sum'$ denotes summation over all possible integral values of $k$, excluding $k=m$.

Let the vortices initially on the line $y = h/2$ be subject to a slight displacement so that the coordinates of the $m$th vortex are $(ml + x_m, (h/2) + y_m)$ where one considers the vortex initially at the point $(0, h/2)$ to correspond to $m=0$. Also let the vortices on the line $y = -h/2$ be subject to a slight displacement so that the coordinates of the $n$th vortex are $\left\{\left(n+\frac{1}{2}\right)l + x'_n, -\frac{h}{2} + y'_n\right\}$, and the

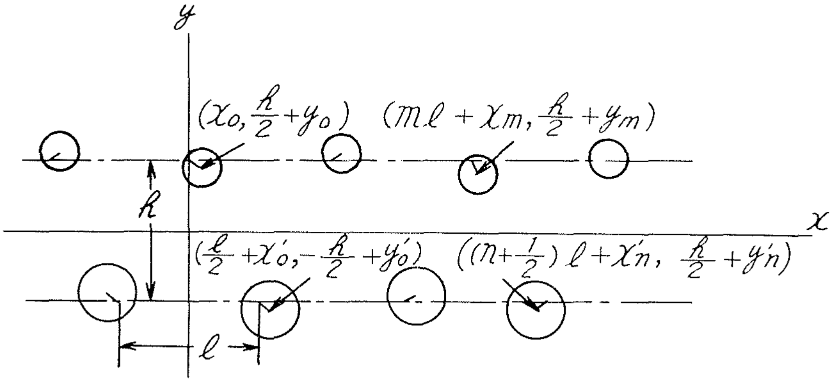

Fig. A. 2. Configuration of slightly displaced vortices.

vortex initially at $(l/2, -h/2)$ is considered to correspond to $n=0$ (Fig. A.2). Let $u_i$ and $v_i$ be the components of velocity of the vortex initially at $(0, h/2)$ induced by all other vortices that are displaced slightly from their equilibrium position. From Eqs. (A. 7), (A. 8) and (A. 9), $u_i$ and $v_i$ are seen to take the forms

$$u_i = \sum_{m=-\infty}^{\infty}{}' \frac{\Gamma_1}{2\pi} \frac{y_0-y_m}{r_{2m}^2} - \sum_{n=-\infty}^{\infty} \frac{\Gamma_2}{2\pi} \frac{y_0-y_n'+h}{r_{0n}^2}$$

$$v_i = -\sum_{m=-\infty}^{\infty} \frac{\Gamma_1}{2\pi} \frac{x_0-x_m-ml}{r_{0m}^2} - \sum_{n=-\infty}^{\infty} \frac{\Gamma_2}{2\pi} \frac{x_0-x_n'-\left(n+\frac{1}{2}\right)l}{r_{0n}^2}$$

where

$$r_{0m}^2 = (x-x_m-ml)^2+(y_0-y_m)^2$$

$$r_{0n}^2 = \left\{x_0-x_n'-\left(n+\frac{1}{2}\right)l\right\}^2+(y_0-y_n'+h)^2$$

In the same manner, the components of velocity $u_i'$, $v_i'$ induced on the vortex initially located at $(l/2, -h/2)$ by all other displaced vortices become

$$u_i' = \sum_{m=-\infty}^{\infty} \frac{\Gamma_1}{2\pi} \frac{y_0'-y_m-h}{r_{0m}'^2} - \sum_{n=-\infty}^{\infty}{}' \frac{\Gamma_2}{2\pi} \frac{y_0'-y_n'}{r_{0n}'^2}$$

$$v_i' = -\sum_{m=-\infty}^{\infty} \frac{\Gamma_1}{2\pi} \frac{x_0'-x_m-\left(m-\frac{1}{2}\right)l}{r_{0m}'^2} + \sum_{n=-\infty}^{\infty} \frac{\Gamma_2}{2\pi} \frac{x_0'-x_n'-nl}{r_{0n}'^2}$$

in which

$$r_{0n}'^2 = \left\{x_0'-x_m-\left(m-\frac{1}{2}\right)l\right\}^2+(y_0'-y_m-l)^2$$

$$r_{0m}'^2 = (x_0'-x_n'-nl)^2+(y_0'-y_n')^2$$

Expanding $1/r_{0m}^2$, $1/r_{0n}^2$, $\cdots$ by the binomial theorem and retaining only the first powers of $x_m$, $y_m$, $x_n'$ and $y_n'$, one obtains

$$\frac{1}{r_{0m}^2} = \frac{1}{m^2 l^2}\left\{1+\frac{2(x_0-x_m)}{ml}\right\},$$

$$\frac{1}{r_{0n}^2} = \frac{1}{\left(n+\frac{1}{2}\right)^2 l^2+h^2}\left\{1+\frac{2\left(n+\frac{1}{2}\right)l}{\left(n+\frac{1}{2}\right)^2 l^2+h^2}(x_0-x_n')-\frac{2h}{\left(n+\frac{1}{2}\right)^2 l^2+h^2}(y-y_n')\right\}$$

$$\cdots\cdots\cdots\cdots\cdots\cdots\cdots\cdots\cdots\cdots\cdots$$

Upon substituting these relations into the expressions for $u_i$, $v_i$ and $u_i'$. $v_i'$ and making a small reduction, one obtains

$$u_i = \sum_{m=-\infty}^{\infty}{}' \frac{\Gamma_1}{2\pi} \frac{y_0-y_m}{m^2 l^2} - \sum_{n=-\infty}^{\infty} \frac{\Gamma_2}{2\pi} \frac{h}{\left(n+\frac{1}{2}\right)^2 l^2+h^2}$$

$$- \sum_{n=-\infty}^{\infty} \frac{\Gamma_2}{2\pi} \frac{2\left(n+\frac{1}{2}\right)lh}{\left\{\left(n+\frac{1}{2}\right)^2 l^2+h^2\right\}^2}(x_0-x_n') - \sum_{n=-\infty}^{\infty} \frac{\Gamma_2}{2\pi} \frac{\left(n+\frac{1}{2}\right)^2 l^2-h^2}{\left\{\left(n+\frac{1}{2}\right)^2 l^2+h^2\right\}^2}(y_0-y_n'),$$

$$v_i=\sum_{m=-\infty}^{\infty}\frac{\Gamma_1}{2\pi}\frac{x_0-x_m}{m^2l^2}+\sum_{n=-\infty}^{\infty}\frac{\Gamma_2}{2\pi}\frac{-\left(n+\frac{1}{2}\right)^2l^2+h^2}{\left\{\left(n+\frac{1}{2}\right)^2l^2+h^2\right\}^2}(x_0-x'_n)$$

$$+\sum_{n=-\infty}^{\infty}\frac{\Gamma_2}{2\pi}\frac{2\left(n+\frac{1}{2}\right)lh}{\left\{\left(n+\frac{1}{2}\right)^2l^2+h^2\right\}^2}(y_0-y'_n)\,;$$

$$u'_i=-\sum_{m=-\infty}^{\infty}\frac{\Gamma_1}{2\pi}\frac{h}{\left(m-\frac{1}{2}\right)^2l^2+h^2}-\sum_{m=-\infty}^{\infty}\frac{\Gamma_1}{2\pi}\frac{2\left(m-\frac{1}{2}\right)lh}{\left\{\left(m-\frac{1}{2}\right)^2l^2+h^2\right\}^2}(x'_0-x_m)$$

$$+\sum_{m=-\infty}^{\infty}\frac{\Gamma_1}{2\pi}\frac{\left(m-\frac{1}{2}\right)^2l^2-h^2}{\left\{\left(m-\frac{1}{2}\right)^2l^2+h^2\right\}^2}(y'_0-y_m)-\sum_{n=-\infty}^{\infty}{}'\,\frac{\Gamma_2}{2\pi}\frac{y'_0-y'_n}{n^2l^2}$$

$$v'_i=\sum_{m=-\infty}^{\infty}\frac{\Gamma_1}{2\pi}\frac{\left(m-\frac{1}{2}\right)^2l^2-h^2}{\left\{\left(m-\frac{1}{2}\right)^2l^2+h^2\right\}^2}(x'_0-x_m)$$

$$+\sum_{m=-\infty}^{\infty}\frac{\Gamma_1}{2\pi}\frac{2\left(m-\frac{1}{2}\right)lh}{\left\{\left(m-\frac{1}{2}\right)^2l^2+h^2\right\}^2}(y'_0-y_m)-\sum_{n=-\infty}^{\infty}{}'\,\frac{\Gamma_2}{2\pi}\frac{x'_0-x'_n}{n^2l^2}$$

Now, the equations of motion of the vortices at $(x_0,\ h/2+y_0)$ and $(l/2+x'_0,\ -h/2+y'_0)$, respectively, are

$$\frac{dx_0}{dt}=\left\{\omega\left(\frac{h}{2}+y_0\right)+U+u_i\right\}-\left(\omega\frac{h}{2}+U+U_1\right)$$

$$\frac{dy_0}{dt}=v_i$$

$$\frac{dx'_0}{dt}=\left\{\omega\left(-\frac{h}{2}+y'_0\right)+U+u'_i\right\}-\left(-\omega\frac{h}{2}+U+U_2\right)$$

$$\frac{dy'_0}{dt}=v'_i$$

Since it is known that

$$\sum_{n=-\infty}^{\infty}\frac{\Gamma_2}{2\pi}\frac{h}{\left(n+\frac{1}{2}\right)^2l^2+h^2}=\frac{\Gamma_2}{2l}\tanh\frac{\pi h}{l}=-U_1$$

$$\sum_{m=-\infty}^{\infty}\frac{\Gamma_1}{2\pi}\frac{h}{\left(m-\frac{1}{2}\right)^2l^2+h^2}=\frac{\Gamma_1}{2l}\tanh\frac{\pi h}{l}=-U_2$$

the velocities of displacement of the vortices $dx_0/dt$, $dy_0/dt$, $\cdots$ become

$$\frac{dx_0}{dt}=\omega y_0+\sum_{m=-\infty}^{\infty}{}' \frac{\Gamma_1}{2\pi}\frac{y_0-y_m}{m^2l^2}-\sum_{n=-\infty}^{\infty}\frac{\Gamma_2}{2\pi}\frac{2\left(n+\frac{1}{2}\right)lh}{\left\{\left(n+\frac{1}{2}\right)^2l^2+h^2\right\}^2}(x_0-x_n')$$
$$-\sum_{n=-\infty}^{\infty}\frac{\Gamma_2}{2\pi}\frac{\left(n+\frac{1}{2}\right)^2l^2-h^2}{\left\{\left(n+\frac{1}{2}\right)^2l^2+h^2\right\}^2}(y_0-y_n') \tag{A. 10}$$

$$\frac{dy_0}{dt}=\sum_{m=-\infty}^{\infty}{}' \frac{\Gamma_1}{2\pi}\frac{x_0-x_m}{m^2l^2}-\sum_{n=-\infty}^{\infty}\frac{\Gamma_2}{2\pi}\frac{\left(n+\frac{1}{2}\right)^2l^2-h^2}{\left\{\left(n+\frac{1}{2}\right)^2l^2+h^2\right\}^2}(x_0-x_n')$$
$$+\sum_{n=-\infty}^{\infty}\frac{\Gamma_2}{2\pi}\frac{2\left(n+\frac{1}{2}\right)lh}{\left\{\left(n+\frac{1}{2}\right)^2l^2+h^2\right\}^2}(y_0-y_n') \tag{A. 11}$$

$$\frac{dx_0'}{dt}=\omega y_0'-\sum_{m=-\infty}^{\infty}\frac{\Gamma_1}{2\pi}\frac{2\left(m-\frac{1}{2}\right)lh}{\left\{\left(m-\frac{1}{2}\right)^2l^2+h^2\right\}^2}(x_0'-x_m)$$
$$+\sum_{m=-\infty}^{\infty}\frac{\Gamma_1}{2\pi}\frac{\left(m-\frac{1}{2}\right)^2l^2-h^2}{\left\{\left(m-\frac{1}{2}\right)^2l^2+h^2\right\}^2}(y_0'-y_m)-\sum_{n=-\infty}^{\infty}{}' \frac{\Gamma_2}{2\pi}\frac{y_0'-y_n'}{n^2l^2} \tag{A. 12}$$

$$\frac{dy_0'}{dt}=\sum_{m=-\infty}^{\infty}\frac{\Gamma_1}{2\pi}\frac{\left(m-\frac{1}{2}\right)^2l^2-h^2}{\left\{\left(m-\frac{1}{2}\right)^2l^2+h^2\right\}^2}(x_0'-x_m)$$
$$+\sum_{m=-\infty}^{\infty}\frac{\Gamma_1}{2\pi}\frac{2\left(m-\frac{1}{2}\right)lh}{\left\{\left(m-\frac{1}{2}\right)^2l^2+h^2\right\}^2}(y_0'-y_m)-\sum_{n=-\infty}^{\infty}{}' \frac{\Gamma_2}{2\pi}\frac{x_0'-x_n'}{n^2l^2} \tag{A. 13}$$

### A 3. Condition of Stability

There are an infinite number of such equations but they are reduced to two if one puts

$$\left.\begin{aligned} x_m&=\alpha\cos m\phi\,, & y_m&=\beta\cos m\phi\\ x_n'&=\alpha'\cos\left(n+\frac{1}{2}\right)\phi\,, & y_n'&=\beta'\cos\left(n+\frac{1}{2}\right)\phi \end{aligned}\right\} \tag{A. 14}$$

$\alpha$, $\beta$, $\alpha'$ and $\beta'$ are functions of the time and $\phi$ is a real constant such that $0\leqq\phi\leqq\pi$. The factors $\cos m\phi$ and $\cos\left(n+\frac{1}{2}\right)\phi$ introduce a periodicity depending upon position into the displacements of the vortices; the wave length of this disturbance being $2\pi l/\phi$ (Rosenhead [42]).

Substitution of Eq. (A. 14) into Eqs. (A. 10) and (A. 11) yields

$$\frac{d\alpha}{dt}=\left(\omega+\frac{\Gamma_1}{2\pi l^2}A-\frac{\Gamma_2}{2\pi l^2}B\right)\beta+\beta'\frac{\Gamma_2}{2\pi l^2}C \tag{A. 15}$$

$$\frac{d\beta}{dt}=\left(\frac{\Gamma_1}{2\pi l^2}A-\frac{\Gamma_2}{2\pi l^2}B\right)\alpha+\alpha'\frac{\Gamma_2}{2\pi l^2}C \tag{A. 16}$$

where

$$A=\sum_{m=-\infty}^{\infty}\frac{1-\cos m\phi}{m^2}=\frac{1}{2}\phi(2\pi-\phi)$$

$$B=\sum_{n=-\infty}^{\infty}\frac{\left(n+\frac{1}{2}\right)^2-k^2}{\left\{\left(n+\frac{1}{2}\right)^2+k^2\right\}^2}=\frac{\pi}{\cosh^2 k\pi}$$

$$C=\sum_{n=-\infty}^{\infty}\frac{\left(n+\frac{1}{2}\right)^2-k^2}{\left\{\left(n+\frac{1}{2}\right)^2+k^2\right\}^2}\cos\left(n+\frac{1}{2}\right)\phi$$

$$=\frac{\pi^2\cosh k\phi}{\cosh^2 k\pi}-\frac{\pi\phi\cosh k(\pi-\phi)}{\cosh k\pi}$$

$$k=\frac{l}{h}$$

To deduce the equations relating to the lower row one has merely to replace $\Gamma_1$ and $\Gamma_2$ with $-\Gamma_2$ and $-\Gamma_1$, respectively, and interchange accented and unaccented letters. Hence

$$\frac{d\alpha'}{dt}=\left(\omega-\frac{\Gamma_2}{2\pi l^2}A+\frac{\Gamma_1}{2\pi l^2}B\right)\beta'-\beta\frac{\Gamma_1}{2\pi l^2}C \tag{A. 17}$$

$$\frac{d\beta'}{dt}=\left(-\frac{\Gamma_2}{2\pi l^2}A+\frac{\Gamma_1}{2\pi l^2}B\right)\alpha'-\alpha\frac{\Gamma_1}{2\pi l^2}C \tag{A. 18}$$

Putting

$$\alpha=\alpha_0e^{\lambda t}, \qquad \beta=\beta_0e^{\lambda t}, \qquad \alpha'=\alpha_0'e^{\lambda t}, \qquad \beta'=\beta_0'e^{\lambda t}$$

in Eqs. (A. 15) and (A. 16), one obtains

$$-\alpha_0\lambda+\left(\omega+\frac{\Gamma_1}{2\pi l^2}A-\frac{\Gamma_2}{2\pi l^2}B\right)\beta_0+\beta_0'\frac{\Gamma_2}{2\pi l^2}C=0$$

$$\left(\frac{\Gamma_1}{2\pi l^2}A-\frac{\Gamma_2}{2\pi l^2}B\right)\alpha_0-\beta_0\lambda+\alpha_0'\frac{\Gamma_2}{2\pi l^2}C=0$$

$$-\beta_0\frac{\Gamma_1}{2\pi l^2}C-\alpha_0'\lambda+\left(\omega-\frac{\Gamma_2}{2\pi l^2}A+\frac{\Gamma_1}{2\pi l^2}B\right)\beta_0'=0$$

$$-\alpha_0\frac{\Gamma_1}{2\pi l^2}C+\left(-\frac{\Gamma_2}{2\pi l^2}A+\frac{\Gamma_1}{2\pi l^2}B\right)\alpha_0'-\beta_0'\lambda=0$$

These four homogenous equations for $\alpha_0$, $\beta_0$, $\alpha_0'$ and $\beta_0'$ lead to the condition

$$\begin{vmatrix} -\lambda & \omega+\frac{\Gamma_1}{2\pi l^2}A-\frac{\Gamma_2}{2\pi l^2}B & 0 & \frac{\Gamma_2}{2\pi l^2}C \\ \frac{\Gamma_1}{2\pi l^2}A-\frac{\Gamma_2}{2\pi l^2}B & -\lambda & \frac{\Gamma_2}{2\pi l^2}C & 0 \\ 0 & -\frac{\Gamma_1}{2\pi l^2}C & -\lambda & \omega-\frac{\Gamma_2}{2\pi l^2}A+\frac{\Gamma_1}{2\pi l^2}B \\ -\frac{\Gamma_1}{2\pi l^2}C & 0 & -\frac{\Gamma_2}{2\pi l^2}A+\frac{\Gamma_1}{2\pi l^2}B & -\lambda \end{vmatrix}=0$$

or, in expanded form

$$\lambda^4+a\lambda^2+b=0 \tag{A. 19}$$

where

$$a=\frac{\Gamma_1\Gamma_2}{4\pi^2 l^4}C^2+\omega\frac{\Gamma_2-\Gamma_1}{2\pi l^2}(A+B)-\frac{\Gamma_1^2+\Gamma_2^2}{4\pi^2 l^4}(A^2+B^2)+\frac{\Gamma_1\Gamma_2}{\pi^2 l^4}AB$$

$$\begin{aligned} b=&\left\{\omega^2-\omega\frac{\Gamma_2-\Gamma_1}{2\pi l^2}(A+B)+\frac{\Gamma_1\Gamma_2}{4\pi^2 l^4}(C^2-A^2-B^2)+\frac{\Gamma_1^2+\Gamma_2^2}{4\pi^2 l^4}AB\right\} \\ &\times\left\{\frac{\Gamma_1\Gamma_2}{4\pi^2 l^4}(C^2-A^2-B^2)+\frac{\Gamma_1^2+\Gamma_2^2}{4\pi^2 l^4}AB\right\} \end{aligned}$$

The solutions of Eq. (A. 19) are

$$\lambda=\pm\frac{1}{\sqrt{2}}\sqrt{-a+\sqrt{a^2-4b}}\,, \qquad \lambda=\pm\frac{1}{\sqrt{2}}\sqrt{-a-\sqrt{a^2-4b}}$$

For stability therefore one must have $-a+\sqrt{a^2-4b}$ and $-a-\sqrt{a^2-4b}$ either negative or zero in the range $0\leqq\phi\leqq\pi$. Hence

$$-a+\sqrt{a^2-4b}\leqq 0 \quad \text{and} \quad -a-\sqrt{a^2-4b}\leqq 0$$

which are equivalent to the inequalities

$$a\geqq 0\,, \qquad b\geqq 0\,, \qquad a^2-4b\geqq 0 \tag{A. 20}$$

For the sake of simplicity, one puts

$$\Gamma_1/\Gamma_2=\gamma\,, \qquad p=k\pi\,, \qquad x=k(\pi-\phi)$$

Hence, by taking into account the relation

$$\omega=\frac{\Gamma_2-\Gamma_1}{2lh}\tanh\frac{\pi h}{l}=\frac{\pi\Gamma_1}{2l^2}(\gamma-1)\frac{\tanh p}{p} \tag{A. 21}$$

$a$, $b$ and $a^2-4b$ on the left-hand side of Eq. (A. 20) can be written in terms of $p$, $\gamma$ and $x$;

$$\begin{aligned} \frac{4\pi^2 l^4}{\Gamma_1^2}k^4 a=&\frac{2\gamma}{\cosh^4 p}(p^2\sinh p\sinh x-px\cosh p\cosh x)^2 \\ &+(\gamma-1)^2 p\tanh p\left(-\frac{x^2}{2}+\frac{p^2}{2}+\frac{p^2}{\cosh^2 p}\right) \\ &-(\gamma^2+1)\left\{\left(\frac{x^2}{2}-\frac{p^2}{2}\right)^2+\frac{p^4}{\cosh^4 p}\right\}+\frac{4\gamma p^2}{\cosh^2 p}\left(\frac{x^2}{2}-\frac{p^2}{2}\right) \end{aligned} \tag{A. 22}$$

$$\begin{aligned}\left(\frac{4\pi^2 l^4}{\Gamma_1^2}\right)^2 k^8 b =& \Bigg[(\gamma-1)^2 p^2 \tanh^2 p-(\gamma-1)^2 p \tanh p\left(-\frac{x^2}{2}+\frac{p^2}{2}+\frac{p^2}{\cosh^2 p}\right)\\ &+\gamma\left\{\frac{1}{\cosh^4 p}\,(p^2\sinh p \sinh x-px\cosh p\cosh x)-\left(\frac{x^2}{2}-\frac{p^2}{2}\right)^2-\frac{p^4}{\cosh^4 p}\right\}\\ &+(\gamma^2+1)\left(-\frac{x^2}{2}+\frac{p^2}{2}\right)\frac{p^2}{\cosh^2 p}\Bigg]\Bigg[\gamma\left\{\frac{(p^2\sinh p\sinh x-px\cosh p\cosh x)^2}{\cosh^4 p}\right.\\ &\left.-\left(\frac{x^2}{2}-\frac{p^2}{2}\right)^2-\frac{p^4}{\cosh^4 p}\right\}-(\gamma^2+1)\left(-\frac{x^2}{2}+\frac{p^2}{2}\right)\frac{p^2}{\cosh^2 p}\Bigg] \qquad \text{(A. 23)}\end{aligned}$$

$$\begin{aligned}\left(\frac{4\pi^2 l^4}{\Gamma_1^2}\right)^2 k^8(a^2-4b) =& \Bigg[(\gamma+1)^2\left(\frac{p^2}{2}-\frac{x^2}{2}-\frac{p^2}{\cosh^2 p}\right)^2\\ &-\frac{4\gamma}{\cosh^4 p}\,(p^2\sinh p\sinh x-px\cosh p\cosh x)^2\Bigg]\\ &\times(\gamma-1)^2\left\{p\tanh p-\left(-\frac{x^2}{2}+\frac{p^2}{2}+\frac{p^2}{\cosh^2 p}\right)\right\}^2 \qquad \text{(A. 24)}\end{aligned}$$

where $x$ can vary in the range $0\leqq x\leqq p$. If one substitutes any value of $x$ in this range into Eqs. (A.22), (A.23) and (A.24), one can easily obtain the value of $p$ which satisfies the equations $a=0$, $b=0$ and $a^2-4b=0$, respectively, since the left-hand sides of these equations are polynomials of the second degree of $\gamma$. In this manner the curves $a=0$, $b=0$ and $a^2-4b=0$ are plotted in the $\gamma p$-plane and the area which satisfies the condition Eq. (A. 20) is determined for each value of $x$. It is found from this procedure that the area corresponding to $x=0$ (i.e. $\phi=\pi$) satisfies the condition Eq. (A. 20) for all other values of $x$, and consequently is the required area of stability for the vortex system to be stable against disturbances of any wave-length. This stable area is given by

$$\begin{aligned}&(\gamma-1)^2\,\frac{\tanh p}{p}\left[\frac{\tanh p}{p}-\frac{1}{2}-(1-\tanh^2 p)\right]\\ &-\gamma\left[\frac{1}{4}+(1-\tanh^2 p)^2\right]+\frac{\gamma^2+1}{2}\,(1-\tanh^2 p)\geqq 0 \qquad \text{(A. 25)}\end{aligned}$$

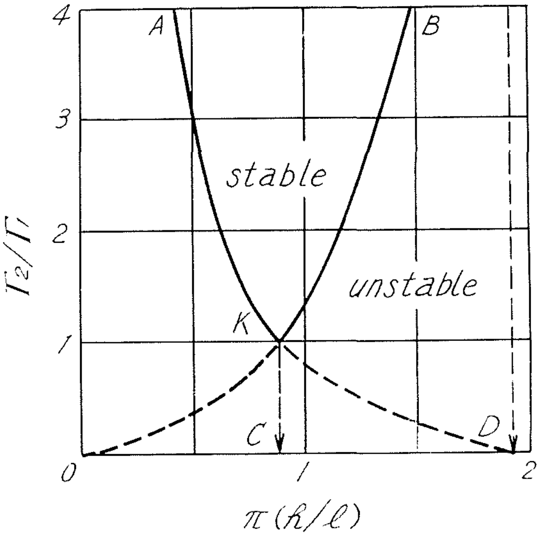

**Fig. A. 3.** Stable area of the vortex system.

and is shown in Fig. A. 3. The point denoted by $K$ corresponds to the point of stability of the ordinary Kármán vortex street. Since the boundary curve of the stability area has an asymptote $p=1.916$, i.e. $h/l=0.610$, the vortex system with $h/l$ more than 0.610 cannot exist at least on theoretical grounds.

### A 4. The Average Drag

If one considers the double vortex trail behind a cylinder to extend without distortion to an infinite distance downstream, then by considerations of momentum one can obtain a formula for the average drag force per unit length of the cylinder.

As previously mentioned in section A 1., the entire vortex street may be considered to be moving with the velocity

$$U_v = \frac{1}{2}\omega h + U - \frac{\Gamma_2}{2l}\tanh\frac{\pi h}{l} \tag{A. 25 a}$$

$$= -\frac{1}{2}\omega h + U - \frac{\Gamma_1}{2l}\tanh\frac{\pi h}{l} \tag{A. 25 b}$$

in the positive $x$ direction. Since the vortices are continuously shed from the cylinder at interval $\tau$, the period of the motion will be $\tau$, and one obtains

$$\tau = l/U_v \tag{A. 26}$$

One takes the $x$-axis midway between the rows and in the direction of advance. One also considers a rectangle ABCD of dimensions which are larger as compared with those of the cylinder and $h$, $l$, the side AB being coincident with the axis $y$, which is so chosen that the origin is at the center of the parallelogram whose vertices are the four vortices nearest to the origin (see Fig. A. 4.). The control volume ABCD is assumed to be moving with the velocity $U_v$. Then the fluid in ABCD is acted upon by the force $-D'$ by the cylinder, and by the pressure over the external boundary of ABCD. According to Euler's momentum theorem and the theorem of Blasius, the drag force $D'$ experienced by the cylinder is given by

$$D' = \frac{\partial M_x}{\partial t} + \Re\left\{\frac{1}{2}i\rho\int_{(S)}\left(\frac{dW}{dz}\right)^2 dz\right\} \tag{A. 27}$$

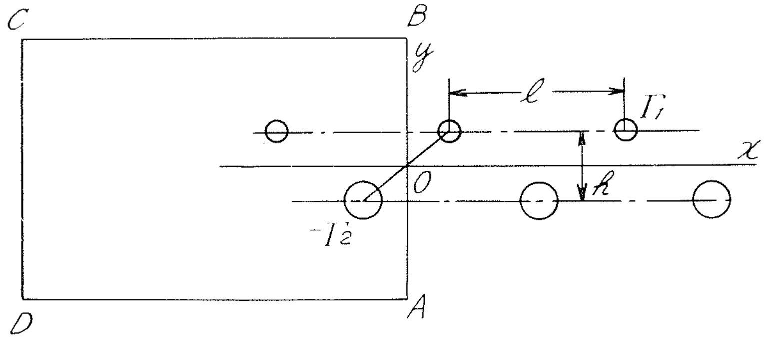

Fig. A. 4. Control volume for the evaluation of drag force.

where $M_x$ denotes the $x$-component of the momentum of fluid within ABCD, $S$ denotes the contour of the rectangle ABCD, and $W$ is the complex flow potential of the form

$$W=\frac{i\Gamma_1}{2\pi}\log\sin\frac{\pi}{l}(z-z_0)-\frac{i\Gamma_2}{2\pi}\log\sin\frac{\pi}{l}(z+z_0) \tag{A. 28}$$

$$z_0=\frac{l}{4}+i\frac{h}{2}$$

Since the velocities on BC, CD and DA are of an order of $1/r$ $(r=(x^2+y^2)^{1/2})$, Eq. (A. 27) can also be written in the form

$$D'=\frac{\partial M_x}{\partial t}+\Re\left\{\frac{1}{2}i\rho\lim_{L\to\infty}\int_{-iL/2}^{iL/2}\left(\frac{dW}{dz}\right)^2dz\right\} \tag{A. 29}$$

where $L$ implies the distance between A and B.

Since the motion is peroidic with period $\tau$, one obtains the mean drag force $D$ by integrating Eq. (A. 29) from 0 to $\tau$ with respect to time $t$;

$$D=\frac{(M_x)_\tau-(M_x)_0}{\tau}+\Re\left\{\frac{1}{2}i\rho\lim_{L\to\infty}\int_{-iL/2}^{iL/2}\left(\frac{dW}{dz}\right)^2dz\right\} \tag{A. 30}$$

The first term on the right-hand side indicates the increase in $x$-momentum due to the appearance of two new vortices within the contour in the interval $\tau$, and is given by

$$\frac{(M_x)_\tau-(M_x)_0}{\tau}=\frac{\rho h}{\tau}\left(\frac{\Gamma_1+\Gamma_2}{2}\right) \tag{A. 31}$$

To evaluate the integral in Eq. (A. 30), one has, from Eq. (A. 28),

$$\frac{dW}{dz}=\frac{i\Gamma_1}{2l}\cot\frac{\pi}{l}(z-z_0)-\frac{i\Gamma_2}{2l}\cot\frac{\pi}{l}(z+z_0)$$

and therefore

$$\begin{aligned}\int_{-iL/2}^{iL/2}\left(\frac{dW}{dz}\right)^2dz=&-\frac{\Gamma_1^2}{4l^2}\int_{-iL/2}^{iL/2}\cot^2\frac{\pi}{l}(z-z_0)\,dz\\&-\frac{\Gamma_2^2}{4l^2}\int_{-iL/2}^{iL/2}\cot^2(z+z_0)\,dz\\&+\frac{\Gamma_1\Gamma_2}{2l^2}\int_{-iL/2}^{iL/2}\cot\frac{\pi}{l}(z-z_0)\cot\frac{\pi}{l}(z+z_0)\,dz\\=&-\frac{\Gamma_1^2}{4l^2}\cdot i\left(\frac{2l}{\pi}-L\right)-\frac{\Gamma_2^2}{4l^2}\cdot i\left(\frac{2l}{\pi}-L\right)\\&+\frac{\Gamma_1\Gamma_2}{2l^2}\left\{i\left(2h\tanh\frac{\pi h}{l}-L\right)+l\tanh\frac{\pi h}{l}\right\}\end{aligned}$$

Substitution of this expression into Eq. (A. 30) together with Eq. (A. 31) yields

$$D=\frac{\rho}{2}(\Gamma_1+\Gamma_2)\frac{h}{l}U_v+\frac{\rho(\Gamma_1^2+\Gamma_2^2)}{4\pi l}-\frac{\rho h\Gamma_1\Gamma_2}{2l^2}\tanh\frac{\pi h}{l}-\lim_{L\to\infty}\frac{(\Gamma_1-\Gamma_2)^2}{8l^2}L$$

or, omitting the last term, one obtains

$$D=\frac{\rho}{2}(\Gamma_1+\Gamma_2)\frac{h}{l}U_v+\frac{\rho(\Gamma_1^2+\Gamma_2^2)}{4\pi l}-\frac{\rho h\Gamma_1\Gamma_2}{2l^2}\tanh\frac{\pi h}{l} \tag{A. 32}$$

If one puts

$$\omega=0\,,\qquad \Gamma_1=\Gamma_2=\Gamma$$

$$U_s=\frac{\Gamma}{2l}\tanh\frac{\pi h}{l} \tag{A. 33}$$

Eq. (A. 32) reduces to the well known Kármán's formula for the drag force, i. e.

$$D_K=\frac{\rho\Gamma^2}{2\pi l}+\frac{\rho h\Gamma}{l}(U-2U_s) \tag{A. 34}$$

Also if one puts

$$\Gamma_1=\Gamma(1-\varepsilon)\,,\qquad \Gamma_2=\Gamma(1+\varepsilon)$$

where $\varepsilon$ is a small positive constant, one obtains from Eq. (A. 32)

$$D=D_K+\varepsilon^2\left(\frac{\rho\Gamma^2}{2\pi l}+\frac{\rho h\Gamma}{l}U_s\right) \tag{A. 35}$$

This formula shows that an additional drag force

$$\varepsilon^2\left(\frac{\rho\Gamma^2}{2\pi l}+\frac{\rho h\Gamma}{l}U_s\right)$$

will act on the cylinder placed in a shear flow. However, if the velocity gradient of the oncoming stream is not too large, the additional term will make but little contribution to the drag, because the contribution is of a second order of magnitude compared with $D_K$. Accordingly the cylinder placed in a shear flow with a moderate normal velocity gradient will be acted upon by the same drag force as that of the cylinder in a uniform flow, if the approaching velocity to the center of the cylinder is the same in both cases. This result corresponds to the conclusion obtained in chapter 5 for a shear flow of a larger Reynolds number.

## Acknowledgements

The author is grateful to Professor M. Arie for his helpful discussions and encouragements during the progress of this work and especially for his critical comments on the preparation of the manuscript. The author is also indebted to the staff of the Laboratory of Fluid Mechanics for the construction of the experimental apparatus and for the reproduction of some parts of drawings. The author wishes to add that this paper was prepared for print after the kind encouragement of Dr. Arie.

## References

[1] Welschof, G. N.: VDI-Forschungsheft 492 Ausgabe 2, Band 28 (1962).
[2] Dryden, H. L.: Ind. Eng. Chem., 31 (1936), 416.
[3] Corrin, S. and Uberoi, M. S.: NACA Tech. Rep. No. 1040 (1951).
[4] Hinze, J. O. and van der Hegge Zijnen, B. G.: General discussion on heat transfer, Institute of Mechanical Engineering, London (1951), 188.
[5] v. Sanden, H.: Z. Math. Phys., 61 (1912), 225.
[6] Tsien, Hsue-Shen: Quart. appl. Math., 1 (1943), 130.
[7] Jones, E. E.: Z. AMM, Band 37 (1957), 362.
[8] Kotansky, D. R.: Thin airfoils in rotational flow, Sc. D. Thesis, Dept. of Mechanical Engineering, M. I. T. (1965).
[9] Arie, M.: Trans. JSME, Vol. 22, No. 117 (1956), 365.
[10] Hall, I. M.: J. Fluid Mech., 1 (1956), 142.
[11] Lighthill, M. J.: J. Fluid Mech., 2 (1957), 493.
[12] Young, A. D. and Maas, J. M.: Rep. Mem. Aeron. Res. Coun., London, No. 1770 (1938).
[13] Davies, P. O. A. L.: J. Fluid Mech., 2 (1958), 441.
[14] Bretherton, F. P.: J. Fluid Mech., 14 (1962), 284.
[15] Saffman, P. G.: J. Fluid Mech., 14 (1961), 385.
[16] Kiya, M.: Study on shear flow past a sphere and a circular cylinder, Master Thesis, Faculty of Engineering, Hokkaido University (1964).
[17] Segre, G. and Silberberg, A.: J. Fluid Mech., 14 (1962), 115.
[18] Eichhorn, R. and Small, S.: J. Fluid Mech., 20 (1964), 513.
[19] Lagally, M.: Z. AMM, 9-4 (1929), 299.
[20] Müller, W.: Z. AMM, 9-3 (1929), 200.
[21] Owen, P. R. and Zienkiewicz, H. K.: J. Fluid Mech., 2 (1957), 521.
[22] Wieghardt, K. E. G.: Aeron. Quart., 4 (1953), 186.
[23] Fage, A. and Falkner, V. M.: Rep. Mem. Aeron. Res. Coun., London, No. 1369 (1931)
[24] MacMillan, F. A.: Rep. Mem. Aeron. Res. Coun., London, No. 2310 (1956).
[25] Klebanoff, P. S. and Diehl, Z. W.: NACA Rep., No. 1110 (1952).
[26] Clauser, F. H.: Advances in Applied Mechanics, 4 (1956).
[27] Coles, D.: J. Fluid Mech., 1 (1956), 191.
[28] Laufer, J.: NACATM, No. 2123 (1950).
[29] Dönch, F.: Forsch, Geb. Ing.-Wesen, Heft 282 (1926).
[30] Arie, M.: Memoirs of the Faculty of Engineering, Hokkaido University, Vol. 10, No. 2 (1956), 211.
[31] Li, T. Y.: J. Aeron. Sci., 23-12 (1956), 1128.
[32] Ting, Lu: Phys. Fluids, 3 (1960), 78.
[33] Murray, J. D.: J. Fluid Mech., 11 (1961), 309.
[34] Devan, L.: Phys. Fluids, 8 (1965), 2211.
[35] Arie, M. and Iida, S.: Preprint of the 753th lecture meeting of JSME (1966), 61.
[36] Pohlhausen, K.: Z. AMM, 1 (1921), 252.
[37] Walz, A.: Lilienthal-Bericht 141 (1941), 8.
[38] Schlichting, H.: Grenzschicht-Theorie, Verlag G. Braun., Karlsruhe (1965).
[39] Townsend, A. A.: Proc. Roy. Soc. Lond., 190 A (1947), 551.
[40] Hinze, J. O.: Turbulence, An introduction to its mechanism and theory, McGraw-Hill Book Co., Inc. (1959).
[41] Kármán, Th. von and Rubach, H., Phys. Zeit., 8 (1912).
[42] Rosenhead, L.: Phil. Trans. Roy. Soc. Lond., 228 (1929).
[43] Levy, H. and Hooker, S. G.: Phil. Mag., Vol. 9, No. 57 (1930), 489.